PREPARATION AND RHEOLOGICAL CHARACTERIZATION OF CALCIUM SILICATE/ALUMINATE BASED CEMENTITIOUS INKS

A Thesis Submitted to
the Graduate School of Engineering and Sciences of
İzmir Institute of Technology
in Partial Fulfillment of the Requirements for the Degree of

MASTER OF SCIENCE

in Chemical Engineering

by
Pelin KELEŞ

December, 2023
İZMİR

ACKNOWLEDGEMENTS

I would like to express my gratefulness to my advisor Prof. Dr. Muhsin ÇİFTÇİOĞLU for his guidance, motivation, support, and encouragement during my M.Sc. Thesis.

I would like to thank to my co-advisor, Assist. Prof. Dr. Erdem Şahin for his support, encouragement, and assistance during this study.

I am also grateful to my laboratory colleagues, Gözde GÖZEL, Özgür Enes TAYTAŞ, Kıymet Miray ÖZTÜRK, Sevgi SEZGİN, Simay ÖZEL and Şıvga Şengül AKTAŞ for their support, friendship, and assistance to my work.

I would like to thank İzmir Institute of Technology Center for Materials Research (IZTECH MAM) for providing technical support and help.

This thesis work was conducted as a MSc. Scholar and supported by TÜBİTAK within the context of 119N523 project.

Finally, I express my sincere thanks to my family Fikriye TURAN, Öykü KELEŞ and Gökdeniz KELEŞ for their love, support, encouragement, and patience throughout my education.

ABSTRACT

PREPARATION AND RHEOLOGICAL CHARACTERIZATION OF CALCIUM SILICATE/ALUMINATE BASED CEMENTITIOUS INKS

Increasing number of bone tissue transplant operations conducted every year has increased the use of bone grafts and bone replacement materials. The commonly employed treatment methods however have several disadvantages. Bone tissue engineering scientists has been conducting intensive research on 3D scaffolds to overcome these disadvantages. Although different materials such as hydrogels, polymers, and metals are heavily used for scaffolds the most suitable material is agreed to have a ceramic/inorganic structure since they have a similar composition to the natural bone. The perfect material for 3D scaffolds formation however has not been found due to the rheological limits of inks/suspensions used in this versatile consolidation technique.

Tricalcium aluminate (C3A) and tricalcium silicate (C3S) cement powders were produced with three different marble dust sources and two different silica sources in this work. The produced powders were combined with additives such as magnesium sulfate (MgSO4), hydroxyethyl cellulose (HEC), gluconic acid (GA), polyethylene glycol (PEG), trisodium sulfate (TSC) and sodium dodecyl sulfate (SDS) for the optimization of 3D printing cementitious inks/suspensions through the investigation of their rheological properties. The optimum firing temperature for C3A powder was determined to be 1300^{o}C with 2 hours hold period while it was found to be 1400^{o}C for 4 hours for C3S powder preparation with rapid cooling to room temperature. The use of C3A suspensions in 3D printers necessitate the presence of 1M $MgSO_4$ which acts as a retarder; 2% HEC and 1% PEG for increasing stability; and finally, 10% marble dust and silica. C3S suspensions should contain 1M gluconic acid, 2.5% HEC, 1% PEG, 0.1M trisodium citrate and 0.1M sodium dodecyl sulfate. Capillary rheometer results are compatible with oscillating rheometer results and have been the subject of a preliminary study for 3D printers in this thesis work.

ÖZET

KALSİYUM SİLİKAT ALÜMİNAT ESASLI ÇİMENTO MÜREKKEPLERİNİN İŞLENMESİ VE REOLOJİK KARAKTERİZASYONU

Her geçen yıl artan kemik doku nakilleri kemik greftleri ve kemik ikame malzemelerinin kullanımı arttırmıştır. Fakat yaygın olarak kullanılan tedavi yöntemlerinin dezavantajları bulunmaktadır. Bu dezavantajların üstünden gelmek için kemik doku mühendisliği 3D yapı iskeletleri üzerine birçok araştırma yapmaktadır. Yapı iskeleti için hidrojel, polimer ve metal gibi farklı malzemeler kullanılsa da en uygun malzeme kemikle aynı kompozisyona sahip olduğu için seramiklerdir. Buna rağmen yapı iskeletleri için mükemmel malzeme reolojik limitler yüzünden bulunamamıştır.

Bu çalışmada, trikalsiyum alüminat (C3A) ve trikalsiyum silikat (C3S) çimentolarının üç farklı mermer tozu kaynağı ve iki farklı silika kaynağı ile üretimi yapıldı. Daha sonrasında üretilen tozlar magnezyum sülfat ($MgSO_4$), hidroksietil selüloz (HEC), glukonik asit (GA), polietilen glikol (PEG), trisodyum sülfat (TSC) ve sodyum dodesil sülfat (SDS) gibi katkı maddeleri ile birleştirilerek reolojik özellikleri incelenmiştir. C3A için en uygun fırınlanma sıcaklığı 1300 °C ve 2 saat iken C3S için 1400 °C 4 saat olarak bulunmuştur. C3A süspansiyonlarının 3D yazıcılarda kullanılabilmesi için geciktirici görev gören 1M $MgSO_4$, stabiliteyi arttıran %2 HEC ve %1 PEG ve son olarak ta %10 mermer tozu ve silika içermelidir. C3S süspansiyonlarında ise 1M glukonik asit, %2.5 HEC, %1 PEG, 0.1M trisodyum sitrat ve 0.1M sodyum dodesil sülfat bulunmalıdır. Kapiler reometre sonuçları salınımlı reometre sonuçları ile uyumlu olup 3D yazıcılar için ön çalışma olmuştur.

TABLE OF CONTENTS

LIST OF FIGURES

Figure **Page**

Figure **Page**

Figure **Page**

Figure **Page**

Figure **Page**

Figure **Page**

LIST OF TABLES

Table **Page**

CHAPTER 1

INTRODUCTION

1.1. Introduction

Bone is a complex tissue composed of hydroxyapatite, organic compounds composed mostly of collagen, and water. The human body contains 206 bones (Brydone, Meek, and Maclaine 2010). They provide structural support and protection, allow movement, trap dangerous minerals such as lead, and, most importantly, self-repair. The healing process takes place in three stages. In the first stage, a hematoma develops, and inflammatory cells provide the necessary nutrients and oxygen. Fibroblasts start to create stroma to promote vascular development in the second stage. The bone continues to heal during the last stage until it reverts to its initial size, form, and mechanical strength. The body cannot however heal bone defects when they exceed a critical size and surgical intervention may be required (Kalfas 2001).

Bone is the second commonly transplanted tissue globally with at least 4 million surgical procedures conducted annually. There are four different traditional treatment methods each with some significant drawbacks. Autograft involves the transplantation of one's own tissue from one region to another and is known to be the most applied method. This method however may cause problems such as pain, bleeding, infection, and it is also not suitable for large or multiple disorders as it allows a limited amount of tissue transfer. Allograft tissues that can be obtained from both a cadaver and a living donor have the possibility of disease transmission in the second method. They also lack a cellular component that would aid in regeneration. Stress-related bone thinning and wear over time may occur if metalwork is used for bone transplantation. Non-invasive treatments such as ultrasound therapy which are currently used as final method is limited to adult patients with stable and reduced fractures. Emphasis recently has been given to bone tissue engineering and especially on 3D scaffolds research due to the limitations and shortcomings of traditional treatment methods. The application of 3D scaffolds to clinical studies however has been very limited since techniques for the preparation of suitable scaffold materials could not be developed (Turnbull 2017).

The production and rheological characterization of calcium silicate and aluminate-based cementitious inks suitable for 3D scaffold consolidation/printing were conducted in this thesis work. The calcium silicate/aluminate (C3S and C3A) powders were synthesized by using various calcium carbonate, silica (silica fume) and alumina(boehmite) sources at high temperatures. The rheological properties of the prepared inks were determined by using oscillating rotational and capillary rheometers for the determination of suitable ink formulations for 3D printing.

1.2. Ideal Scaffolds

Scaffolds are used as templates for bone regeneration in bone tissue engineering, facilitating cell interaction and supporting newly produced tissue. Scaffolds must meet many criteria, such as biocompatibility, biodegradability, bioactivity, structural and mechanical properties so that they can provide cell interaction and function.

Scaffolds and their components must be biocompatible in order not to cause toxicity to cells, to be easily excreted from the body, and not to activate the immune system. Controlled biodegradability is also a crucial factor in scaffold applications. Controlled biodegradability is related to the rate of degradation. If the implanted scaffold degrades too quickly, it may break as it cannot support the mechanical load. Inflammatory reaction may occur hindering tissue regeneration conversely if it degrades too slowly. The bioactivity of a scaffold increases when it interacts with cells and the bound living tissues. The scaffold's osteoconductive and osteoinductive capabilities will be enhanced as bioactivity increases.

Scaffold porosity is a very important structural property and both microporosity and macroporosity which are the two commonly present types of porosity each have unique functions in the body. Micropores enable cell-to-scaffold interaction whereas macropores facilitate cell migration. The pore size is also a parameter to be considered for cell migration and attachment. The ideal pore size for bone regeneration has been determined to be approximately 100μm (Karageorgiou and Kaplan 2005). Pore size and porosity content are very important structural parameters in bone regeneration which also directly affect the scaffold mechanical properties. There is an inverse relationship between porosity and mechanical properties. The mechanical properties of the scaffold include Young's modulus which (also known as the elastic modulus) is a criterion of

stiffness along with the compressive strength (the capacity to withstand load) and tensile strength which is the maximum stress that it can withstand without breaking. The ideal scaffold should have the following properties: a porosity of 60%-90%, a pore size of more than 150 microns, a compressive strength of 100-230 MPa, a Young's modulus of 7-30 GPa, and a tensile strength of 50-151 MPa (Turnbull 2017).

1.3. Materials for BTE and Scaffolds

Metals, polymers, hydrogels, and ceramics are mostly used in bone tissue engineering and scaffolds. Due to their outstanding biocompatibility and high strength, metal alloys like zirconium, titanium, and stainless steel are employed in a variety of applications, including joint replacement and implants. Their applications in bone tissue engineering however are restricted due to their poor biodegradation properties. Surgical removal of the scaffold is frequently necessary when metal alloys are used in BTE applications. There is also a potential risk of toxicity with the release of metal ions (Staiger, Pietak, Huadmai and Dias 2006).

Polymers are preferred materials for bone tissue engineering due to their design flexibility, biocompatibility, and biodegradability. They also include components that can help cell functions. Polymers however do not provide the necessary mechanical and structural properties for scaffolds and may contain pathogenic contaminants (Liu and Ma 2004).

Hydrogels are formed by cross-linking hydrophilic polymer chain networks. They can support cell growth and permit the flow of oxygen, nutrients, and other substances due to their hydrophilic properties. This makes hydrogels a suitable material for tissue engineering. They however like polymeric equivalents are not suitable materials for scaffolding even if their mechanical properties may be increased by crosslinking (Zhu and Marchant 2011).

Inorganic materials like ceramics have a great potential for BTE due to their high mechanical strength and bioactivity. Ceramic structures formed from calcium phosphates, hydroxyapatites (HA), and tricalcium phosphates (TCP) are already used in scaffolds. The inorganic/mineral component of bone (about 70% by mass) has a close similarity to ceramic structures. This accelerates the formation of new bone by making strong bonds with cells. HA is frequently used in BTE applications due to its biocompatibility and lack

of toxicity whereas mechanical properties and degradation rate are also two other important factors. HA is the slowest-degrading calcium phosphate phase. This both causes the scaffold to be fragile and limits its applicability to individual fractures (Kumar, Kargozar, Baino and Han 2019). TCP is the most common of the BTE materials used commercially. Injectable Beta-TCP was studied by Matsuno et al. to produce 3D scaffolds for bone tissue engineering applications. Despite its biocompatible and biodegradable properties, it is difficult to shape beta-TCP particles for the surgical site (Matsuno et al. 2008). Bioactive cement materials such as tricalcium aluminate (C3A) and tricalcium silicate (C3S) among a series of probable ceramic phases are already being used for scaffold preparation. C3A is a major cement phase with a chemical formula of $3CaOAl_2O_3$. The reason for its potential in scaffold studies is its high calcium content. Alumina (Al_2O_3) has been also used for a long time in joint replacements due to its mechanical strength, low coefficient of friction, and bio-inert characteristics (Oh, Finones, Jin, Choi and Kim 2004). There are various C_3A production methods such as solid-state reaction, polymeric pechini and solvent based methods. The solid-state reaction method is however the most widely used method because it is simple, low-cost, and suitable for large scale production (Jamal, Xu, Shao and Abdiryim 2013). Tricalcium silicate ($3CaOSiO_2$) which is commonly expressed as C_3S is the major phase responsible for cement initial setting and strength. Silicon is an element found in the early stages of bone formation. Silicon in soluble form plays a role in the synthesis of collagen type I in the bone structure. C3S is commonly believed to be an appropriate candidate for scaffold investigations. Although C3S has a variety of manufacturing techniques, the solid-state reaction technique is the most beneficial (Ding, Shie and Wang 2009).

Ceramic materials/structures although may have a significant promise in scaffold preparation in BTE applications due to their mechanical properties and biocompatibility there is still a need for research and development for improving current formation/shaping methods towards the preparation of bulk structures which has a less brittle nature. The development of these qualities is anticipated to be obtained by 3D scaffold fabrication techniques.

1.4. Scaffold Fabrication Techniques

Scaffolds can be prepared by using various techniques. The control of the pore structure (pore size, shape, and connectivity) is quite challenging and very hard by using traditional forming methods. Recent research is focused on the development of computer-aided 3D methods for the preparation of scaffolds with satisfactory structural and mechanical properties. The development of successful 3D printing methods may bring a unique solution to the problems related with the various disadvantages like the use of organic solvents, the difficulties in controlling pore size and shape, the necessity of the use of high pressures, restricted thicknesses, and inadequate cell incorporation of traditional manufacturing techniques such as solvent casting (Liao et al. 2001), gas foaming (Dehghani and Annabi 2011), freeze-drying (Whang, Thomas and Healy 1995), and electrospinning (Huang et al. 2013).

The most popular and straightforward 3D manufacturing technique is direct ink writing (DIW) which is commonly referred to as robocasting. The substance runs through the nozzle and starts to form a 3D picture on a plate during the direct ink writing process. Research on the use of ceramic powders by this technology have been conducted in recent years. The nozzle diameter for ceramic materials is typically between 100 and 1000 microns. Hardness is influenced by the setting time of inks in direct writing and variables like setting time and rheological characteristics must be optimized. The choice of the right printer structure and the utilization of additives like dispersants and retarders is necessary for this optimization. The rheological characteristics of the cement paste should be taken into consideration while determining the printer structure. There are two distinct pressure application mechanisms which basically depends on the rheological characteristics of the paste in direct writing systems. These two application mechanisms where a piston is used to apply normal tension and the use of a screw mechanism to apply shear stress is schematically shown in Figure 1 (Balani et al. 2021).

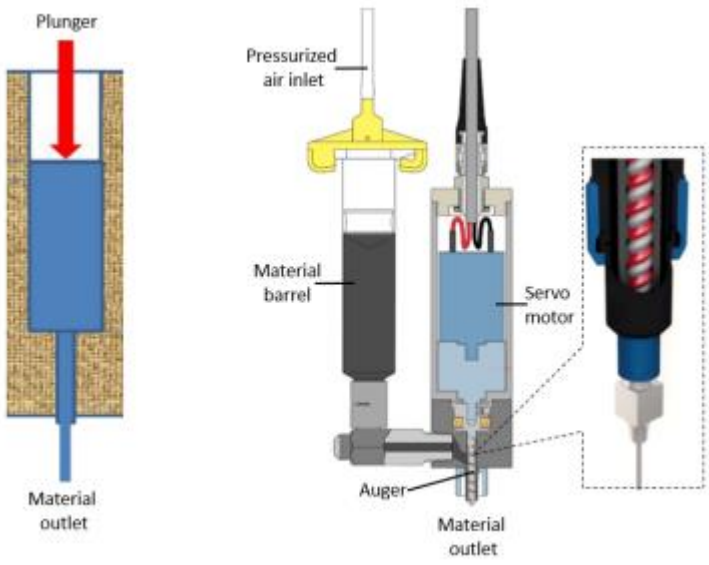

Figure 1. Plunger type and screw type of printers
(Source: Li, Armani, Leu and Landers, 2015).

1.5. Rheology

The science of rheology examines how a material flows and deforms. Materials can be classified in two major groups depending on their flow behavior. Viscosity is solely affected by temperature and not by shear rate as dictated by Newton's principles and water is the most common example given for the Newtonian fluids. The remaining fluids can be called as non-Newtonian fluids where shear thinning behavior is observed, which indicates that viscosity reduces as shear rate increases. Ceramic and cement suspensions are known to be Non-Newtonian fluids. Viscosity increases with increasing shear rate for Non-Newtonian fluids/suspensions with shear thickening behaviour.

Suspensions of ceramic and cement powders may experience issues like sedimentation or phase separation during direct writing. The initial rheological characteristics as well as the injectability characteristics should be investigated for the solution of these issues. Initial setting, final setting, and open-time direct writing method are the main rheological properties that need to be examined. The initial setting time is the first time the suspension begins to harden after mixing. The final setting time, on the other hand, is the point at which solidification is complete and the fluidity of the suspension ends (Figure 2). While the suspension has high fluidity at the initial setting time point, its fluidity drops considerably at the final point. These properties are not solely

sufficient for assessing printability although may show how the suspension behaves over time. The open time which represents the printable time of the suspension therefore is an important parameter. The open time must be long enough to allow for both the flow of existing material and the addition of new material. A short open time will result in the substance solidifying in the chamber and obstructing flow. These properties can be improved by examining rheological properties such as loss (G") and storage (G') modulus using an oscillatory rheometer and by using suspension-modifying additives (Balani et al. 2021).

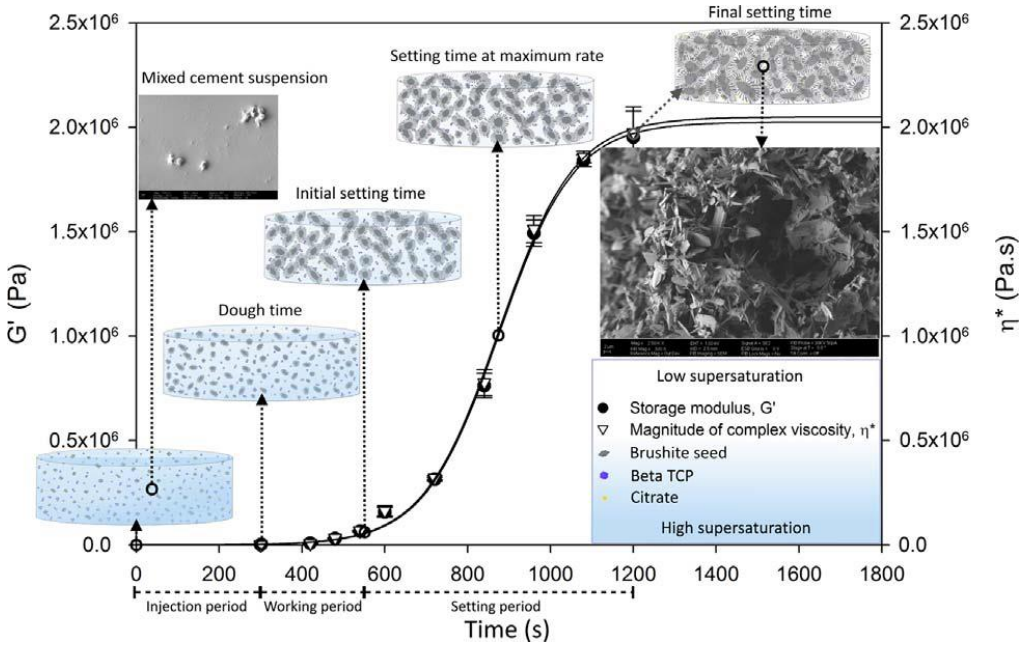

Figure 2. Cement setting kinetics with respect to time
(Source: Şahin & Kalyon, 2017).

Another feature that needs to be developed is injectability. Phase separation is one of the biggest problems in injecting cementitious powder suspensions. Phase separation occurs when the liquid in suspension moves faster than the solid in the nozzle generating an undesirable variation between the liquid and solid phases. This causes a decrease in viscosity, an increase in setting time, and a decrease in the mechanical properties of the material if the liquid ratio is higher than the solid ratio. Powder agglomerates form in the nozzle and the nozzle becomes clogged on the contrary due to a fast-setting time (Balani et al. 2021). Nozzle diameter/length and extrusion speed combinations must be determined for achieving optimum injectability.

CHAPTER 2

LITERATURE SURVEY

2.1. Synthesis of C3A and C3S

There are three major methods for tricalcium aluminate (C3A) powder synthesis which are known as the Polymeric Pechini, solid state reaction, and organic solvent approach. The solid-state reaction is the mostly used method since it is straightforward and affordable.

Mohamed and Sharp (2002) investigated C3A formation kinetics by using solid-state reaction method by using two different alumina sources. Calcite and alpha alumina or gibbsite were mixed with distilled water in a molar ratio of 3:1 and the suspension was filtered and further dried at 110°C. Dried powder pellets about 1 g in weight with a diameter of 12.5 mm was formed by uniaxial pressing at 326 MPa. The pellets were first calcined at 850 °C for 1 hour for carbon dioxide removal through calcite decomposition. The calcined powder was further heat treated at 1150 to 1350 °C for 24 hours tricalcium aluminate phase formation and the phase structures of the final powders were finally investigated. The C12A7 and CA phases were identified to be the precursor phases of C3A formation reaction (Figure 3). Highly pure C3A phase containing powders were obtained and the C12A7 and CA phase contents decreased with increasing calcination temperature as shown in Figure 4.

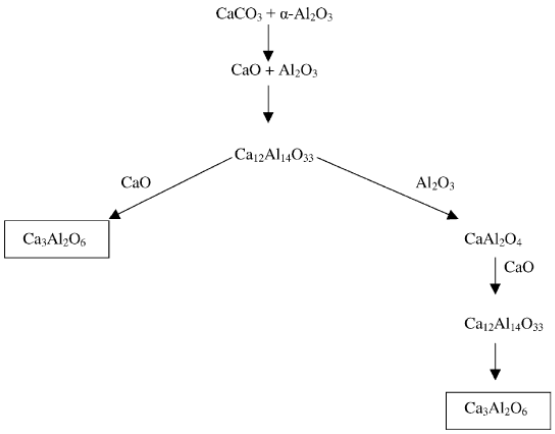

Figure 3. Reaction kinetics of C3A
(Source: Mohamed and Sharp, 2002).

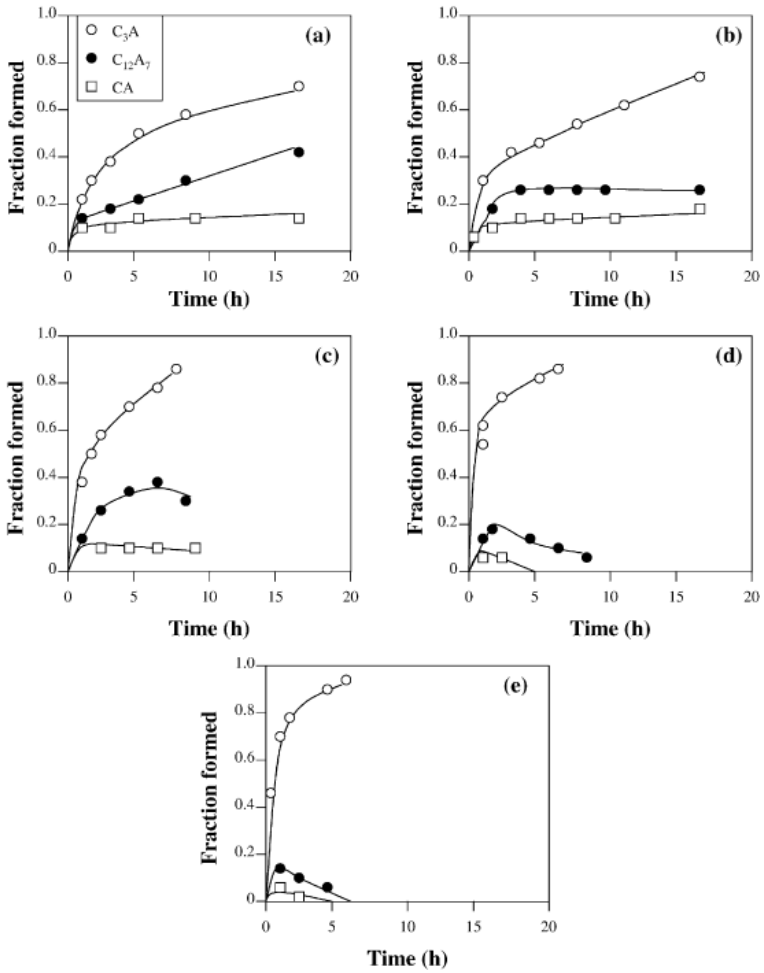

Figure 4. Fraction of produced C3A at a)1150°C b)1200°C c)1250°C d)1300°C e)1350°C (Source: Mohamed and Sharp 2002).

Solid-state reactions are also used in the production of tricalcium silicate. Li, Ouzia, and Scrivener (2018) investigated the effects of different temperatures and times on C3S production using calcium carbonate and fumed silica and investigated the optimum conditions C3S production in relatively high amounts in the laboratory environment. Distilled water, fumed silica, and CaCO3 were placed in a grinding jar with zirconium balls in the initial step of the powder synthesis. The balls were separated from the suspension which was then dried in the oven after the grinding process. The dried powders were held at 1450 and 1600 degrees with different heat treatment hold times at the peak temperatures C3S production. The C3S production process is schematically given in Figure 5. The purity of C3S powders produced in different processes with various parameters are given in Table 1. It was observed that the purity of C3S increased as the heat treatment temperature and hold time increased.

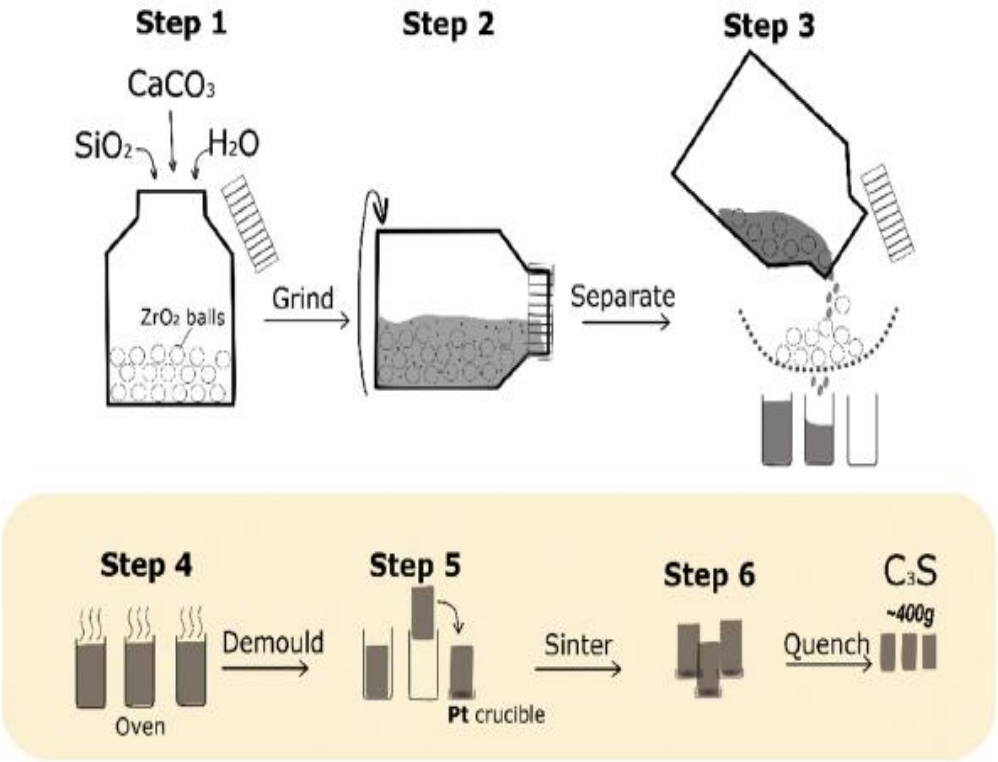

Figure 5. Process flow of C3S production
(Source: Li, Ouzia, and Scrivener, 2018).

Table 1. Summary of parameters for synthesis of C3S (Source: Li, Ouzia, and Scrivener, 2018).

Temperature	Resistance time	Sample status	Speed, notes	C_3S	β-C_2S	free-CaO
°C	hours	–	°C/min	wt%		
1450	2.5	Piece[a]	5	81.8	14.5	3.7
1450	5.0	Piece	5	94.2	4.8	1.1
1450	10.0	Piece	5	96.1	3.4	0.5
1450	20.0	Piece	5	96.5	3.2	0.3
1500	2.5	Piece	5	94.3	4.9	0.7
1500	5.0	Piece	5	95.6	3.8	0.6
1500	10.0	Cylinder, average[b]	5	96.5 ± 0.4	3.2 ± 0.3	0.3 ± 0.04
1500	15.0	Cylinder, average	5	96.4 ± 0.3	3.3 ± 0.3	0.3 ± 0.01
1550	2.5	Piece	5	95.0	4.5	0.5
1550	5.0	Piece	5	96.1	3.5	0.3
1550	10.0	Piece	5	95.9	3.8	0.3
1550	15.0	Piece	5	96.3	3.3	0.4
1600	2.5	Piece	5	96.4	3.2	0.4
1600	5.0	Piece	5	96.3	3.3	0.3
1600	8.0	Piece	5	96.9	2.8	0.3
1600	10.0	Cylinder, average	5	97.3 ± 0.2	2.5 ± 0.4	0.2 ± 0.01
1550	5.0	Cylinder, average	7	96.3	3.3	0.4
1600	3	Piece, C_3S 0.2 μm	7	96.4	3.2	0.4
1600	6	Piece, C_3S 0.2 μm	7	96.5	3.2	0.3

2.2. Rheological Behaviour of Cements

Mansoutre, Colompet, and Damme investigated the rheological properties of C3S cement powder suspensions. Suspensions were prepared with a w/s ratio between 0.7 and 0.43. The prepared suspensions were placed on parallel plates with a diameter of 4 cm with a gap of 1.5 mm. Two different measurement techniques were used. One is the static mode, which shows the flow behavior of the suspension, and the other is the dynamic mode, which shows the viscoelastic behavior. The internal structure of the suspension deteriorates in static mode while it is preserved in dynamic mode without exceeding the critical value. The dynamic mode is widely used when studying cement rheology. The flow curve of the C3S suspension with w/s of 50 is given Figure 6. Since the C3S suspension does not exceed the critical stress value at first, it exhibits plastic behavior (1) and shear thinning (2) after the value is exceeded (Mansoutre, Colompet, and Damme 1999).

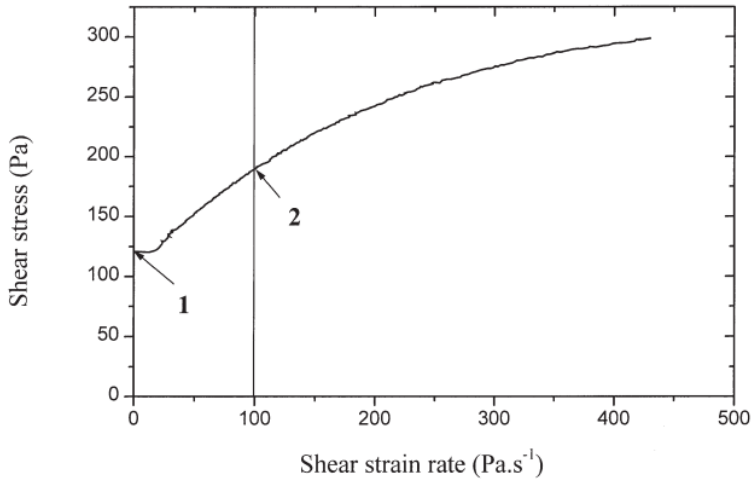

Figure 6. Flow curve of C3S with w/s of 50
(Source: Mansoutre, Colompet, and Damme, 1999).

While the internal structure is preserved in the static mode, the internal structure of the material deteriorates after the critical value is exceeded in the dynamic mode. In dynamic mode, elastic modulus (G') and loss modulus (G") are functions of strain. During dynamic rheology tests, the frequency was kept constant at 1 Hz, and the strain value was increased from 10^{-5} to $10^{\wedge 5}$. As seen in Figure 7, the critical strain value for C3S suspension is between 10^{-5} and 10^{-4} since G' starts to decrease in this range. The critical

strain value of cement suspensions is quite low. C3S suspension also showed the same behavior as Portland cement (Mansoutre, Colompet, and Damme 1999).

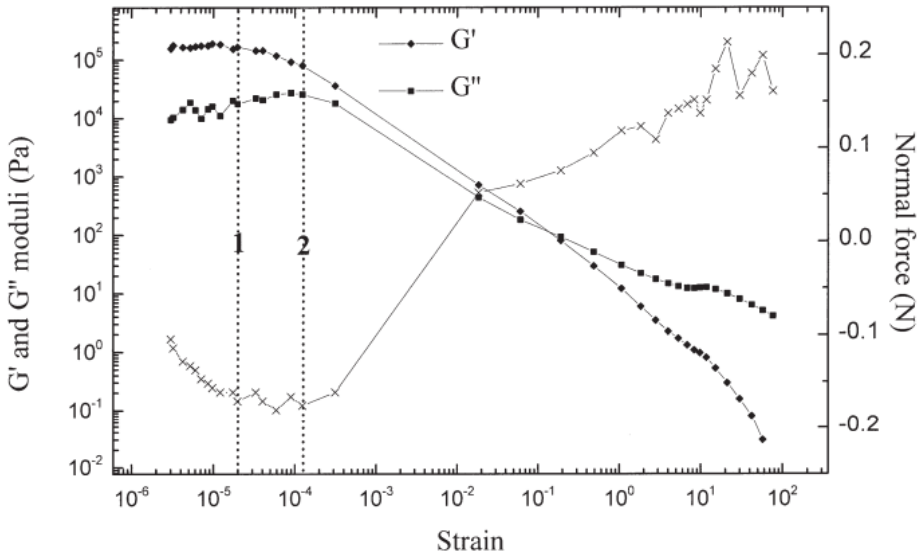

Figure 7. Dynamic rheology measurement of C3S with w/s 50
(Source: Mansoutre, Colompet, and Damme, 1999).

Since phosphate cements are important in BTE applications, their rheological properties have been extensively investigated. Liu et al. (2006) investigated the rheological properties of injectable calcium phosphate cement. Figure 8 shows the strain sweep results to determine the linear viscoelastic region of the calcium phosphate suspension. As mentioned before, because the critical strain value of cement suspensions is very low, a value could not be determined here. The critical value for the frequency test was determined as 1%. Figure 9 shows the frequency sweep results. While the loss modulus, storage modulus, and viscosity increase at low frequencies, they begin to deform and decrease after passing the critical value. Figure 10 shows the setting kinetics of phosphate cement. While the strength is low between 0 and a region, the strength starts to increase between a and b regions and then increases exponentially (Liu et al. 2006).

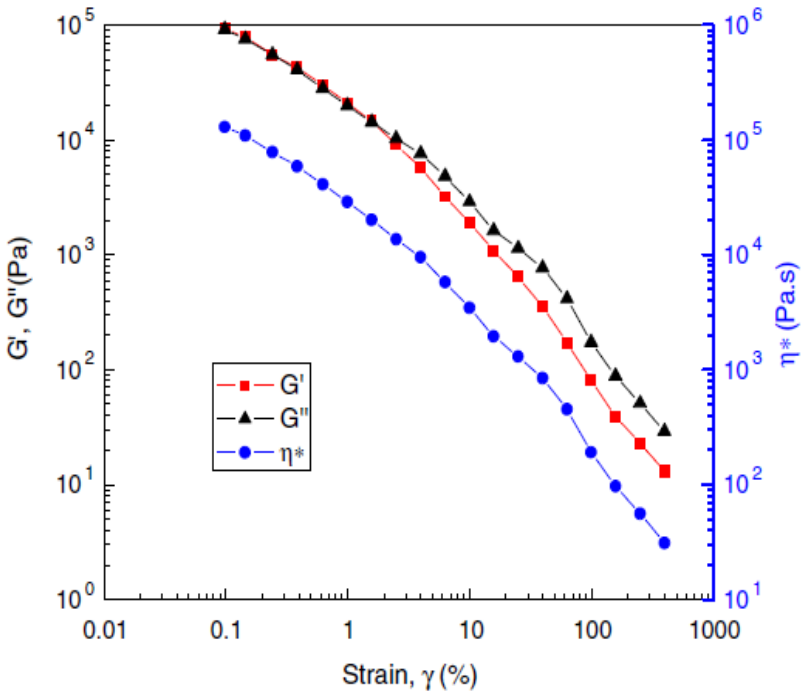

Figure 8. Strain sweep for linear viscoelastic region
(Source: Liu et al. 2006).

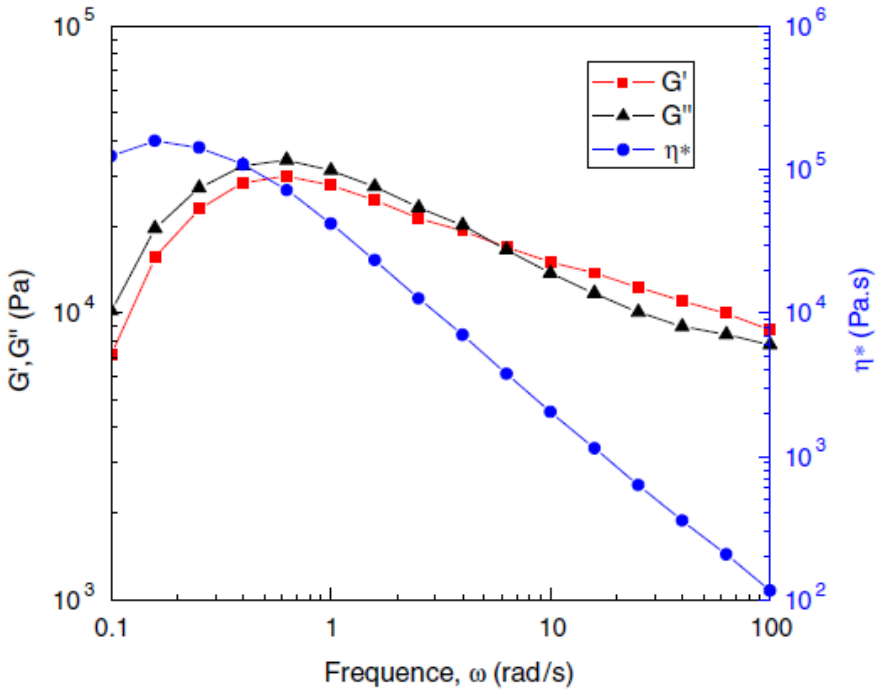

Figure 9. Frequency sweep
(Source: Liu et al. 2006).

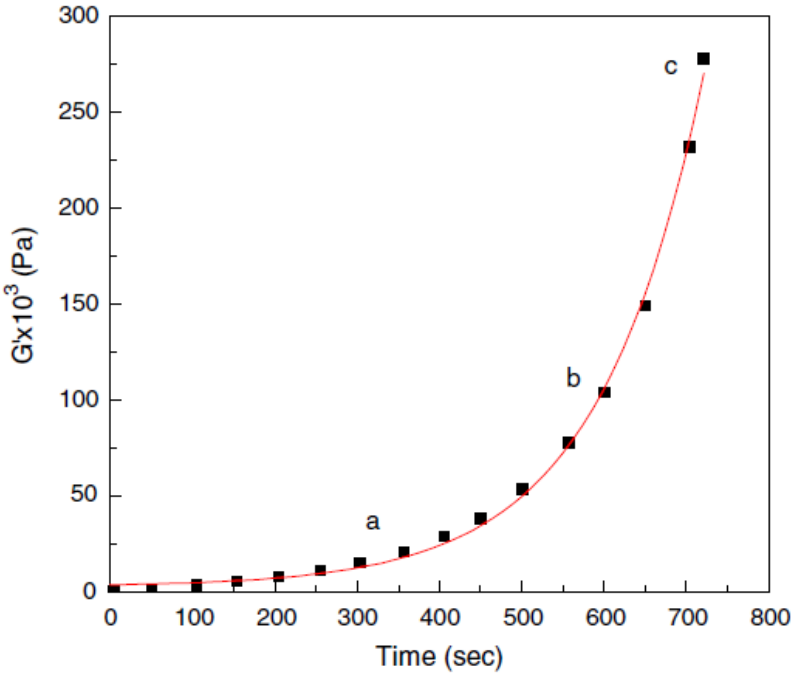

Figure 10. Setting kinetics of phosphate cement
(Source: Liu et al. 2006).

CHAPTER 3

EXPERIMENTAL

3.1. Materials and Methods

Calcite powder 1 ($CaCO_3$, Marble powder Egemin), commercial calcite powder 2 ($CaCO_3$, Marble powder Tekkim), commercial calcite powder 3 ($CaCO_3$, AFG Bio), quartz powder (SiO_2) with 10μm particle size produced in Muğla Yatağan quartz mine, colloidal silica (Aerosil 200), ethanol (Absolute Merck) and Boehmite (AlOOH, Disperal P2 Sasol) were used to synthesize tricalcium aluminate (C3A) and tricalcium silicate (C3S) powders in this work.

Magnesium sulfate heptahydrate (MgSO4.7H2O, 99.5%, Tekkim), Hydroxyethyl-cellulose (HEC, Sigma-Aldrich), Gluconic acid (GA, C6H12O7, Sigma-Aldrich), Trisodium citrate (TSC, Na3C6H5O7, Tekkim), Polyethylene glycol (PEG, Merck), Sodium dodecyl sulfate (SDS, NaC12H25SO4, Sigma-Aldrich), and marble powder (Egemin) were mixed with the individual C3A and C3S powders to prepare suspensions that were then used to analyze the rheological characteristics of the C3A and C3S cementitious inks/suspensions which may be used in 3D printing of scaffolds.

RETSCH PM100 planetary ball mill and Telemecanique Altivar 28 rotary ball mill were used to reduce the particle size of the produced powders and to obtain a homogeneous precursor mixture before high temperature heat treatments. These homogeneous multi-phase precursor powder mixtures (final phases C3A and C3S) were heat treated by using Carbolite CWF 1300 and Carbolite RHF 16/3 high temperature furnaces to form the desired phases through solid-state reactions. HAAKE^{TM} MARS^{TM} Rheometer was used to characterize the rheological behavior of the prepared suspensions/inks. A 35-mm parallel plate and 1-mm gap spacing were used in the rheological behavior characterization experiments.

Testometric testing machine was used by adding a capillary rheometer apparatus. Capillary rheometer apparatus was made of stainless steel with high dimensional accuracy. The capillary sleeve seen in Figure 11 is attached to the compression apparatus of the extensiometric mechanical test device and applies pressure on the vertical axis to

the fluid placed inside. Pressure and extension changes during the flow of the fluid through the capillary channels (Figure 12) placed at the end of the barrel chamber were monitored by computer. Different nozzle diameters, lengths, and injection speeds were used in the tests.

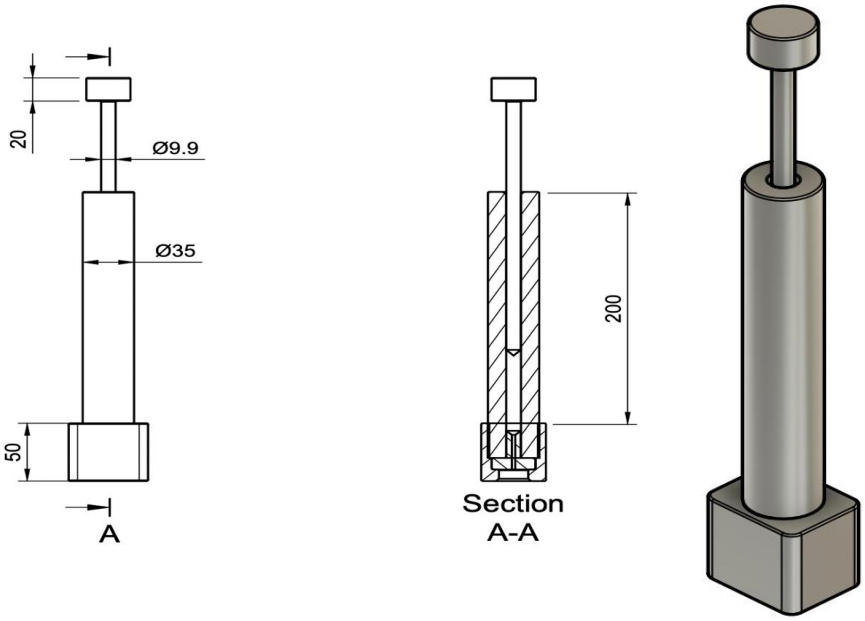

Figure 11. Capillary rheometer parts technical drawings and isometric three-dimensional visualization.

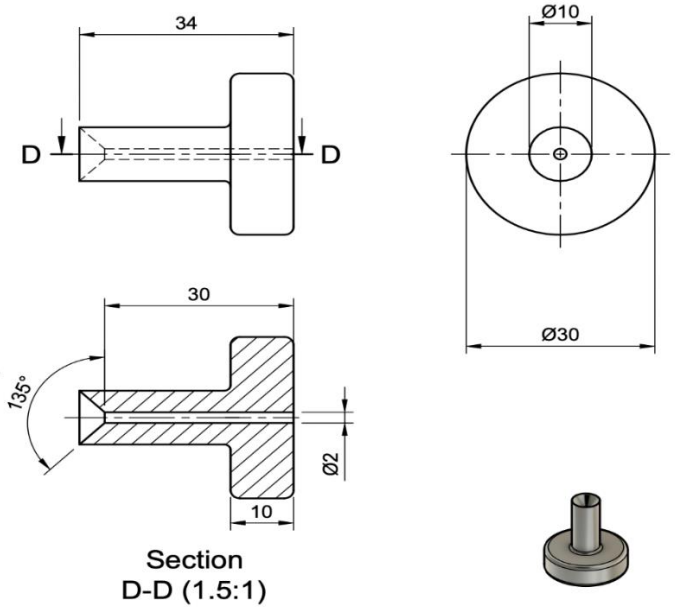

Figure 12. Extruder mold technical and isometric three-dimensional drawings used in cement measurements.

3.2. Preparation of Cementitious Powders

3.2.1. Synthesis of C3A

Two different calcite sources (marble powder) and boehmite were used for the synthesis of C3A. The powder mixtures were heat treated at temperatures of 1200°C, 1300°C and 1350°C degrees for 2 and 4 hours to synthesize phase pure C3A.

3.2.1.1. C3AB-12004/13002/13004:

Calcite (marble powder 1 Egemin) and boehmite powders were mixed with a mole ratio of 3:2 with sufficient distilled water for 4 hours by ball milling to prepare 50 grams of final C3A powder. The slurry was subsequently dried in an oven at 100 °C for 24 hours and calcined in a furnace at 1300 °C for 2 hours and 1200 °C and 1300 °C for 4 hours as schematically given in Figure 13.

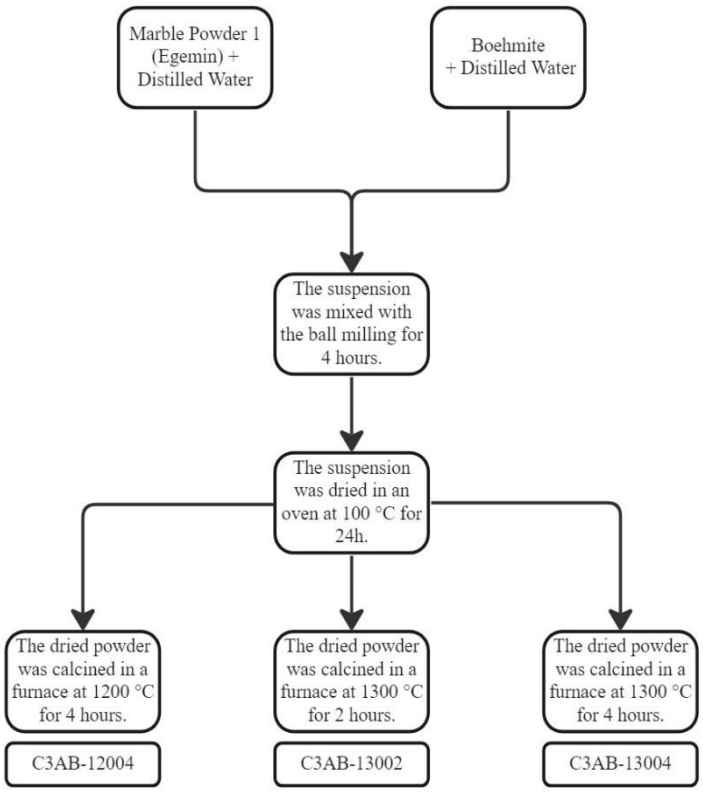

Figure 13. Processing flowsheet of C3AB-12004/13002/13004 powders.

3.2.1.2. EC3A-13002/13004/13504:

Calcite (Marble powder 1 Egemin) and boehmite powder suspensions in distilled water were separately prepared with the help of a magnetic stirrer until homogeneous mixtures were obtained and then they were combined and mixed. The produced mixture was kept in an oven at 100 °C for a day before being calcined at 1300 °C for 2 and 4 hours and 1350 °C for 4 hours as schematically shown in Figure 14.

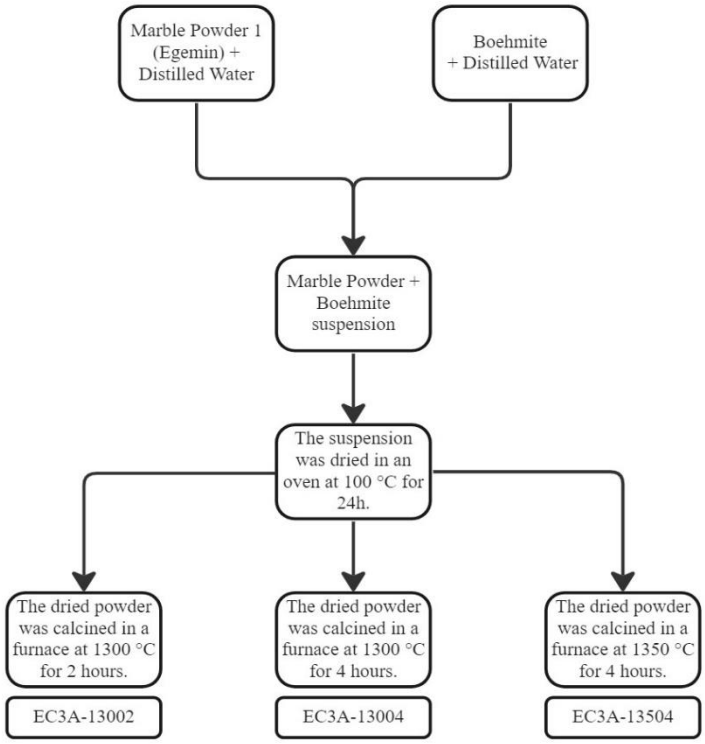

Figure 14. Processing flowsheet of EC3A-13002/13004/13504 powders.

3.2.1.3. C3AETB-12004/13002/13004

Marble powder 1 (Egemin), Boehmite, and ethanol were mixed homogeneously for 4 hours with the help of a ball mill. After being dried in an oven at 100 °C for a day, the final mixtures were calcined at 1200 °C for 4 hours and at 1300 °C for both 2 and 4 hours as shown schematically in Figure 15.

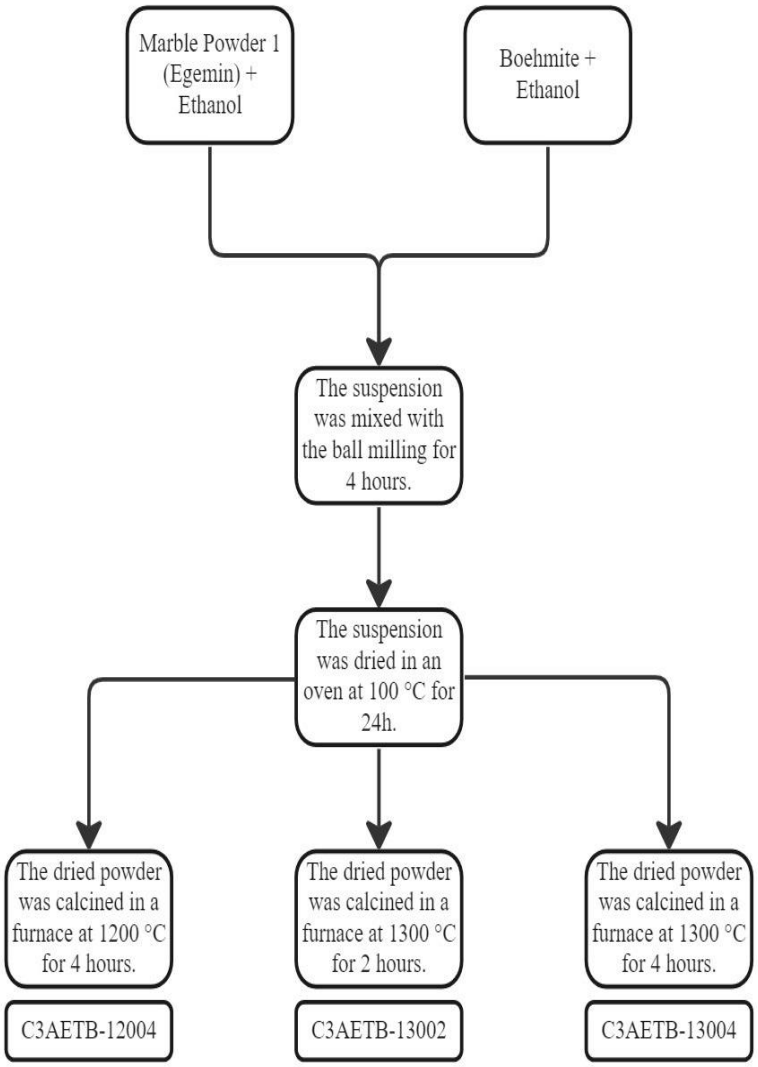

Figure 15. Processing flowsheet of C3AETB-12004/13002/13004 powders.

3.2.1.4. C3ATB-13002:

Commercial marble powder 2 (Tekkim), boehmite powder and distilled water were mixed in ball milling for 4 hours until homogeneous mixtures were obtained. The produced mixture was kept in an oven at 100 °C for a day before being calcined at 1300 °C for 2 hours as schematically shown in Figure 16.

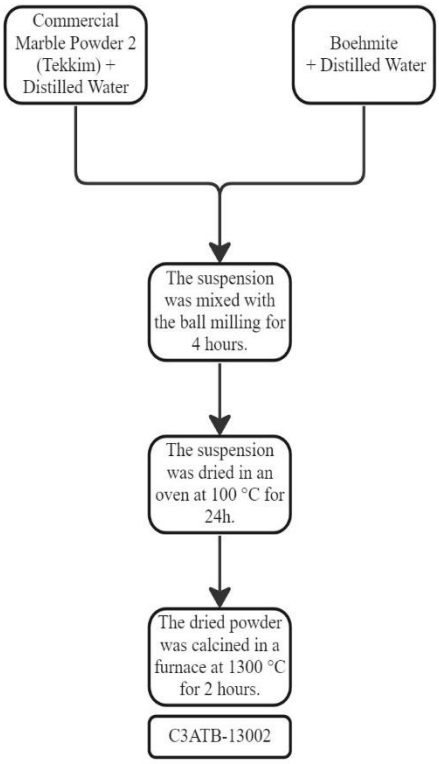

Figure 16. Processing flowsheet of C3ATB-13002 powder.

3.2.2. Synthesis of C3S

Two different sources of silica, marble powder 1 (Egemin) and commercial marble powder 3 (AFG Bio) were used for the synthesis of C3S. Different mixtures were heat treated at temperatures 1300°C and 14000°C degrees for 2 and 4 hours to produce C3S.

3.2.2.1. ST-13002/14002/14004:

10 μm quartz and marble powder 1 (Egemin) were prepared as separate suspensions with distilled water using a magnetic stirrer. The prepared suspensions were combined with continuous mixing. They were dried in an oven at 100 °C for a day when a homogeneous mixture was obtained. The dried powder mixtures were further heat treated at two different temperatures and residence times as shown schematically in Figure 17.

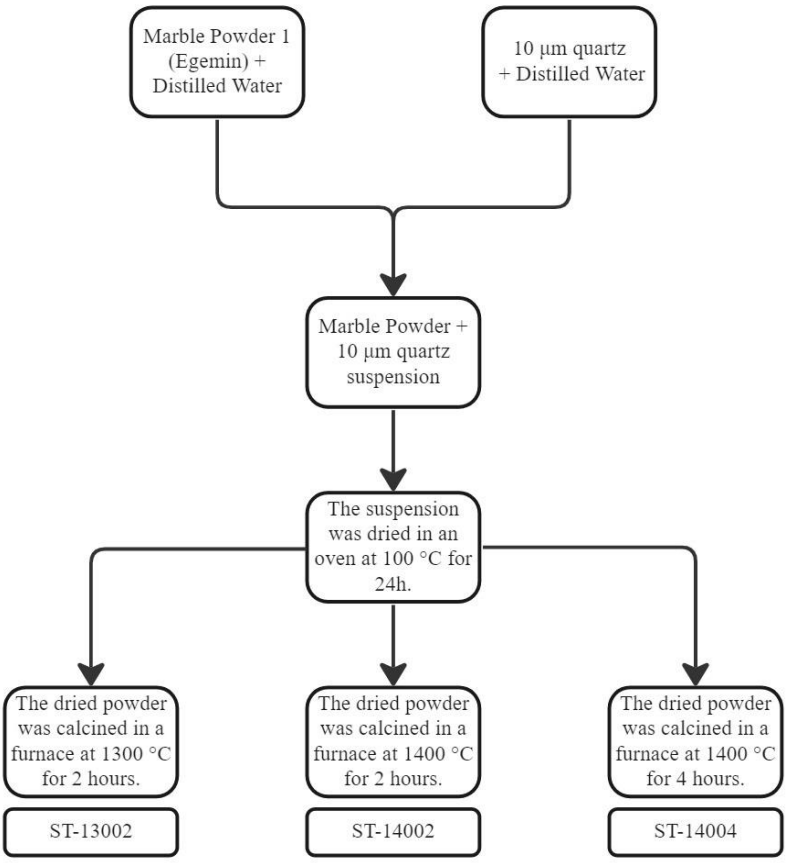

Figure 17. Processing flowsheet of ST-13002/14002/14004 powders.

3.2.2.2. SF-13002/14002/14004:

Colloidal (fume) silica and marble powder 1 (Egemin) were prepared as separate suspensions with distilled water using a magnetic stirrer. The prepared suspensions were combined with continuous mixing. They were dried in an oven at 100 °C overnight upon the successful preparation of a homogeneous suspension. The oven dried powder mixtures were heat treated at two temperatures for 2 to 4 hours as shown schematically in Figure 18 for the solid-state synthesis of the desired C3S phase. The crucibles containing the reaction products were taken out from the furnace quickly and air quenched for the stabilization of the high temperature C3S phase for the prevention of the C3S decomposition to the C2S phase.

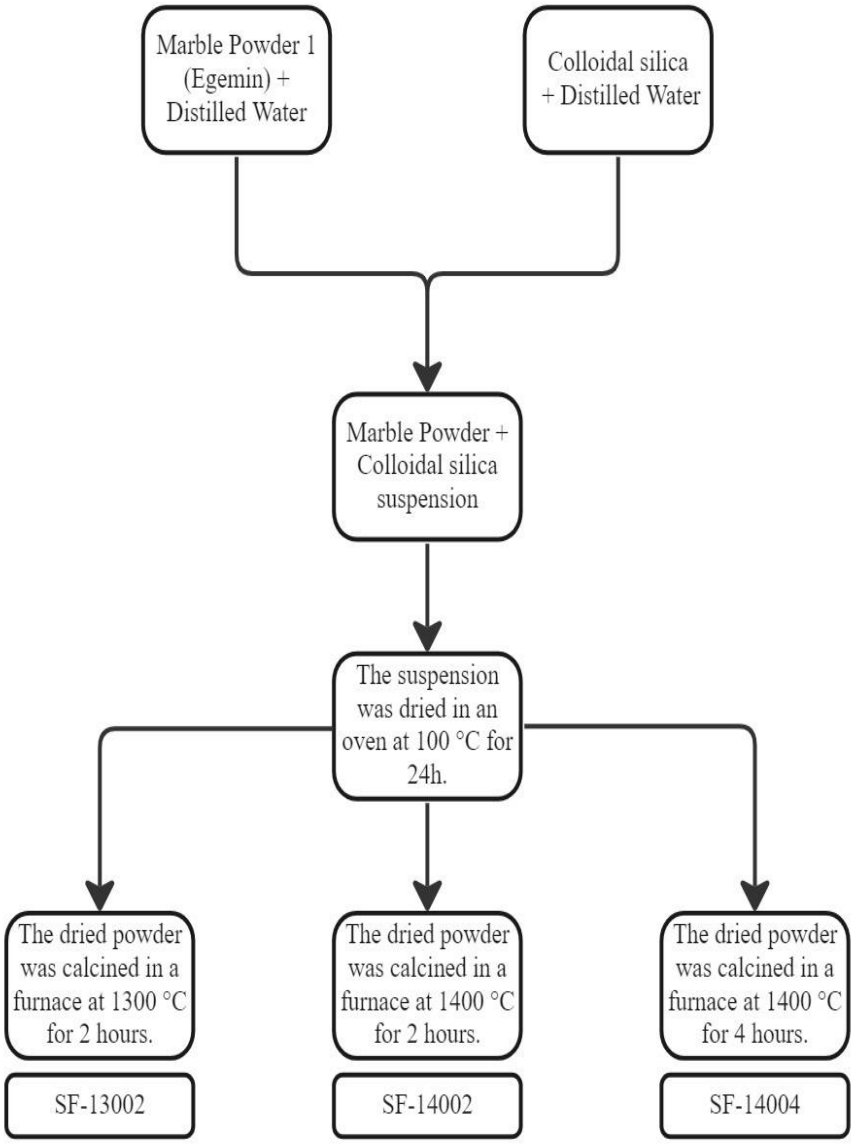

Figure 18. Processing flowsheet of SF-13002/14002/14004 powders.

3.2.2.3. C3SAFG-14004

Commercial marble powder 3 (AFG Bio) was mixed with colloidal silica and water by ball milling for 6 hours. The suspension was further dried in the oven overnight. The dried multiphase powder mixture was heat treated at 1400°C for 4 hours as schematically shown in Figure 19.

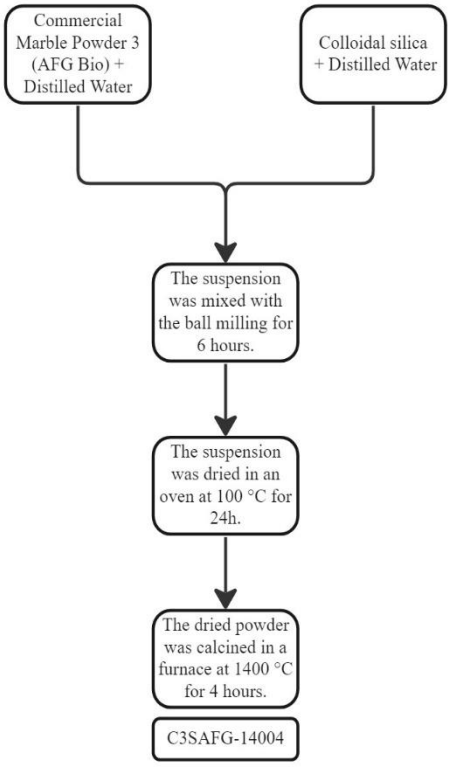

Figure 19. Processing flowsheet of C3SAFG-14004 powder.

3.3. Preparation of Cementitious Powder Suspensions

The sizes of the C3A and C3S powders were reduced by using a ball mill at 400 rpm for 5 minutes to obtain fine powders necessary for suspension preparation. Suspensions were formed by mixing in a mortar at the ratios specified in Tables 2 and 3 for 2.5 minutes which was quickly followed by oscillation testing.

Table 2. Amounts of additives used to obtain C3A cementitious suspensions.

Formulation	C3A (g)	Marble Powder(g)	Quartz (g)	MgSO4 (M/g)	HEC (%3.17) (g)	PEG 400 (g)	DW (g)	P/L
%60-DW	2	x	x	x	x	x	3	40/60
%50-DW	2	x	x	x	x	x	2	50/50
%55-DW	2	x	x	x	x	x	1.63	55/45
%60-0.5M MgSO4	2	x	x	0.5M/3g	x	x	x	40/60

Cont. on the next page

Cont. of Table 2.

%60-1M MgSO4	2	x	x	1M/3g	x	x	x	40/60
%60-1.5M MgSO4	2	x	x	1.5M/3g	x	x	x	40/60
%60-2M MgSO4	2	x	x	2M/3g	x	x	x	40/60
%60-4M MgSO4	2	x	x	4M/3g	x	x	x	40/60
%60-1M MgSO4-%2HEC	2	x	x	4M/1.17g	1.83	x	x	40/60
%60-1M MgSO4-%1PEG	2	x	x	4M/1.5g	x	1.5	x	40/60
%60-1M MgSO4-%2HEC-%1PEG	2	x	x	4M/1g	1	1	x	40/60
%60-1M MgSO4-%2HEC-%1PEG-%10CaCO3	1.8	0.2	x	4M/1g	1	1	x	40/60
%60-1M MgSO4-%2HEC-%1PEG-%20CaCO3	1.6	0.4	x	4M/1g	1	1	x	40/60
%60-1M MgSO4-%2HEC-%1PEG-%10CaCO3-%10SiO2	1.6	0.2	0.2	4M/1g	1	1	x	40/60

Table 3. Amounts of additives used to obtain C3S cementitious suspensions.

Formulation	**C3S(g)**	**Marble Powder(g)**	**GA (M/g)**	**HEC (%2.5) (g)**	**PEG 400 (g)**	**DW (g)**	**SDS (M/g)**	**TSC (M/g)**	**P/L**
%50-DW	4.5	x	x	x	x	4.5	x	x	50/50
%40-DW	4.5	x	x	x	x	3	x	x	60/40
%40-0.5M GA	4.5	x	0.5M/3g	x	x	x	x	x	60/40

Cont. on the next page

Cont. of Table 3.

%40-1M GA	4.5	x	1M/ 3g	x	x	x	x	x	60/40
%40-2M GA	4.5	x	2M/ 3g	x	x	x	x	x	60/40
%40-1M GA- %2.5HEC	4.5	x	1M/ 1.6g	1.4	x	x	x	x	60/40
%40-1M GA- %2.5HEC- %10CaCO3	4.05	0.45	1M/ 1.6g	1.4	x	x	x	x	60/40
%40-1M GA-PEG	4.5	x	1M/ 2.9g	x	0.1	x	x	x	60/40
%40-1M GA-PEG- %10CaCO3	4.05	0.45	1M/ 2.9g	x	0.1	x	x	x	60/40
%40-1M GA- %2.5HEC- PEG	4.5	x	1M/ 1.6g	1.3	0.1	x	x	x	60/40
%40-1M GA-SDS	4.5	x	1M/ 2.5g	x	x	x	0.1M/ 0.5g	x	60/40
%40-1M GA- %2.5HEC- SDS	4.5	x	1M/ 1.1g	1.4	x	x	0.1M/ 0.5g	x	60/40
%40-1M GA-PEG-SDS	4.5	x	1M/ 2.4g	x	0.1	x	0.1M/ 0.5g	x	60/40
%40-1M GA-TSC	4.5	x	1M/ 1.5g	x	x	x	x	0.1M/ 1.5g	60/40
%40-1M GA- %2.5HEC- TSC	4.5	x	1M/ 0.8g	1.4	x	x	x	0.1M/ 0.8g	60/40
%40-1M GA-PEG-TSC	4.5	x	1M/ 1.45g	x	0.1	x	x	0.1M/ 1.45g	60/40

3.4. Characterization of the Powders and Suspensions

The phase structure characterization of the produced powders was conducted by using Philips X'pert Pro in the center for materials research of İzmir Institute of Technology. Cu-kα radiation was used and studied under voltage and current conditions

of 45 kV and 40 mA, respectively. Scanning speed was investigated in the range of 0.08 degrees/minute and 2 theta (10–80) degrees. Quantitative phase analyses were carried out using the Rietveld refinement method using Profex software.

X-ray fluorescence (XRF) was used to determine the elemental and chemical compositions of the raw materials. About 0.5 g powder samples were analyzed with the Spectro X-Lab Pro X-ray fluorescence spectroscopy device in order to determine the elemental ratio.

The particle size distribution of marble powder 1 obtained from Egemin was analyzed with the Mastersizer 3000 (Malvern Panalytical) laser granulometry. First, marble powder was suspended in distilled water for 5 minutes using an ultrasonicator. The resulting suspension was diluted and measured at an opacity level of 9.74 in a water-based measuring cell. The refractive index value of the marble powder was taken as 1,590. The same procedure was applied to silica taken from Muğla Yağatan quartz mine and colloidal silica. The refractive index value of quartz powders was taken as 1.470 and was measured at the laser opacity level of 11.14. Boehmite particle size distribution was measured using the nanoplus zeta device. Sedigraph was used to determine the particle size distribution of marble powders obtained from Tekkim and AFG Bio. Laser granulometry was also used for the particle size measurement of the produced C3A and C3S powders.

Density data is an important parameter for the flow stability of the suspension formed by the particles. The densities of cementitious powders produced with additive raw materials and Egemin marble powder which are intended to be used in aqueous cementitious suspensions were measured with the He pycnometer as three repetitions with the Ultrapycnometer 1000 density measuring device. The volumes and densities of the powders were measured under 21 psi helium gas pressure.

The surface area of the raw materials was determined by the Micromeritics Gemini V surface area measuring device. Each sample was added to the measuring chamber of the device with a density of 1 g/cm3, and then the surface area was calculated for each sample using the Brunauer, Emmet, and Teller (BET) nitrogen gas adsorption technique in a liquid nitrogen environment at 77 K.

A sample suitable for the zeta potential measurement was prepared by mixing 0.1 g of powder from the raw materials in 10 ml of distilled water by using a vortex shaker followed by treatment in an ultrasonic bath. The pH values of the prepared suspensions were measured. Zeta potential sample chamber was cleaned with distilled water where

pre-contaminated dust and residues were removed. The prepared suspension was injected with the help of a syringe in such a way that no air could enter the chamber.

Thermogravimetric analysis was performed with Perkin Elmer Diomand TGA/DTA in order to determine the weight loss of the precursors with temperature and the amount of raw material to be used in the synthesis of desired powder phases.

Cell toxicity effects of high purity synthesized C3A and C3S cementitious powders and the planned additives in suspension were investigated separately. Cytotoxicity testing was performed with human-derived SaoS-2 cells. The diluted material extract at 4 different concentrations (1:1, 1:2, 1:4, 1:8) was added to the cells seeded at a concentration of 1 x 105 cells/mL on 96-well microplates. Extracts were obtained by dissolving powdered materials in cell culture medium. The cytotoxic effect of the extracts applied for 24 and 72 hours (5.0% CO2 at 37°C and 95% humidity) was evaluated by reading the absorbances in the spectrophotometer (570 nm) with the MTT test (ISO 10993-5:2009).

Culture Medium: DMEM High Glucose (Capricorn CP 40-1309), 10% Fetal Bovine Serum (FBS, A0500-3010, Cegrogen Biotech, Germany), 0.5% Gentamicin 10 mg/mL (A2712 Merck, Germany), Sodium Pyruvate 100 mM (L0473 Merck, Germany)

Negative Control: Media containing 1% Dimethylsulfoxide (DMSO)

Blank: Culture prepared with cell culture medium without test substance.

CHAPTER 4

RESULTS AND DISCUSSION

4.1. Characterization of the Powders and Suspensions

4.1.1. Size distribution data

Egemin marble powder particle size analysis was conducted with Mastersizer. The average particle size (d50) value of marble powder was 2.10 μm, the (d90) value was 8.14 μm, and the (d10) value was 0.590 μm as shown in Figure 20.

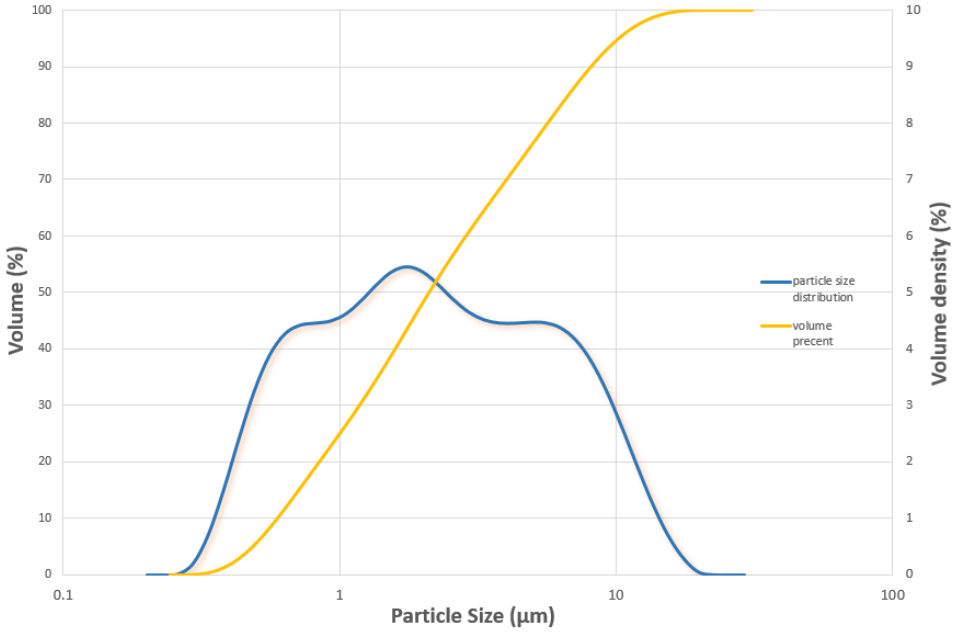

Figure 20. Particle size distribution of Egemin marble powder.

Sedigraph was used to examine the marble powder's particle size distribution that was obtained from Tekkim. The marble powder in distilled water was treated with an ultrasonicator for five minutes for the preparation of a stable suspension. The (d50) value was determined to be 4.8 μm, the (d90) value was 10.4 μm, and the (d10) value was 0.4 μm based on the sedimentation behavior of the diluted suspension in water as shown in

Figure 21. Same procedure was applied to the AFG Bio marble powder. The (d50) value was found to be 1.5 μm, the (d90) value was 4.1 μm, and the (d10) value was <0.4 μm based on the sedimentation behavior of the diluted suspension in water as shown in Figure 22.

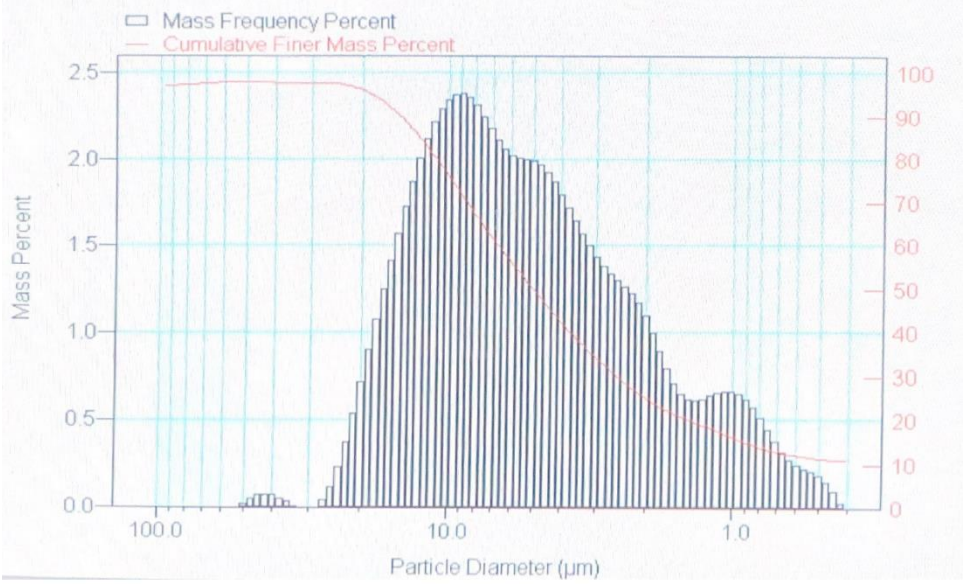

Figure 21. Particle size distribution of Tekkim marble powder.

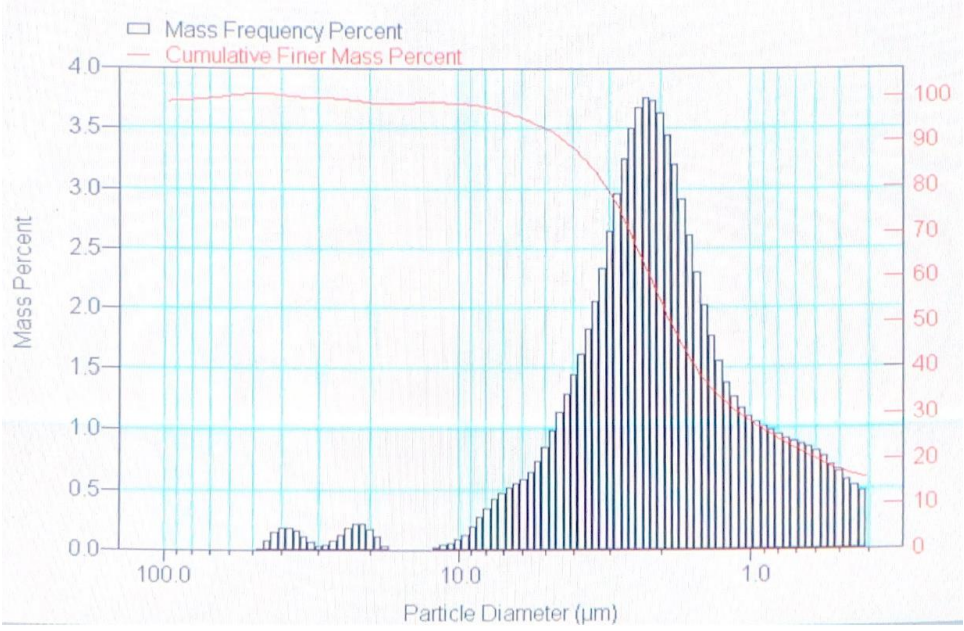

Figure 22. Particle size distribution of AFG Bio marble powder.

The 10-micron quartz powder sample obtained from the Muğla Yatağan quartz mine had a (d90) value of 9.15 μm, an average particle size of (d50) of 3.08 μm, and a final (d10) value of 0.829 μm as given in Figure 23.

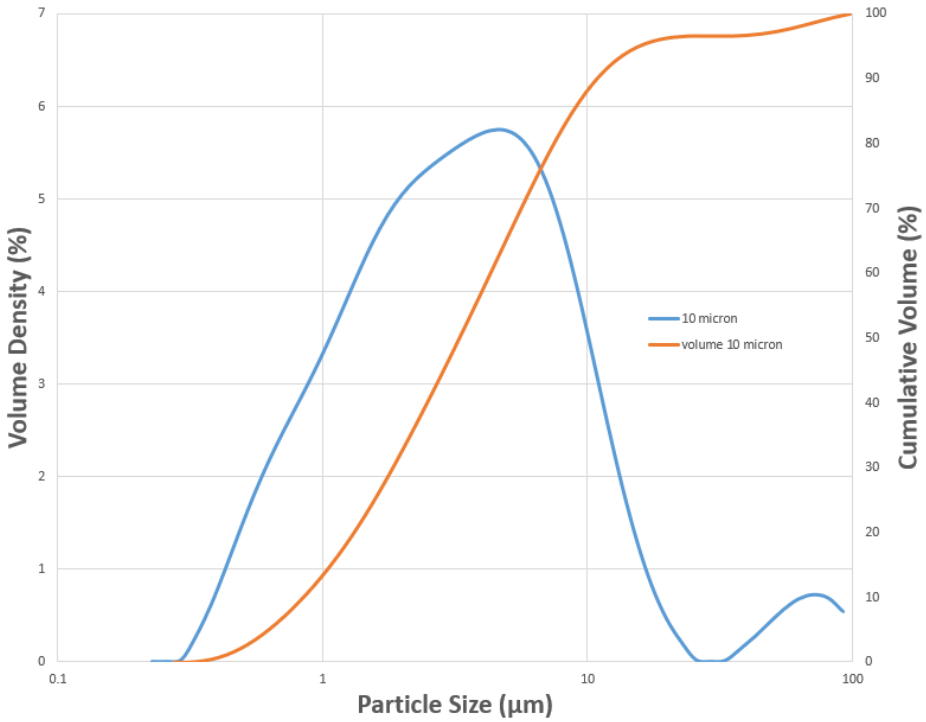

Figure 23. Particle size distribution of 10-micron quartz powder sample.

The particle size distribution of Aerosil 200 commercial colloidal silica was measured using the nanoplus zeta device. The mean particle size (d50) was determined as 254.2 nm, (d90) value as 496 nm, and (d10) value as 174.1 nm. The particle size distribution is given in Figure 24.

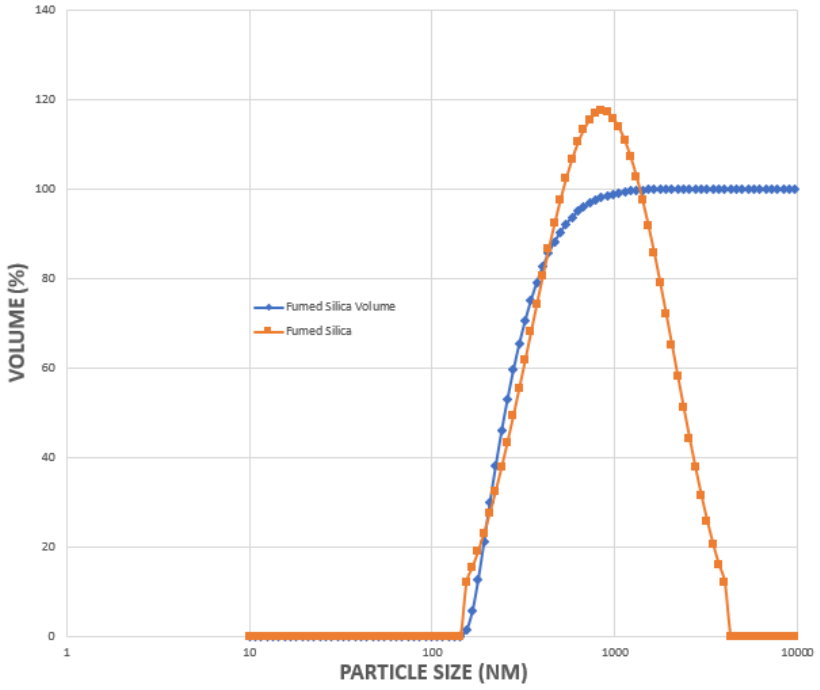

Figure 24. Particle size distribution of Aerosil 200 commercial colloidal silica.

The commercial boehmite particle size distribution which was used as a raw material in the production of tricalcium aluminate was measured using the nanoplus zeta device. The mean particle size (d50) was 22.7 nm, (d90) value was 44.7 nm, and (d10) value was 16 nm. The actual particle size distribution is as given in Figure 25.

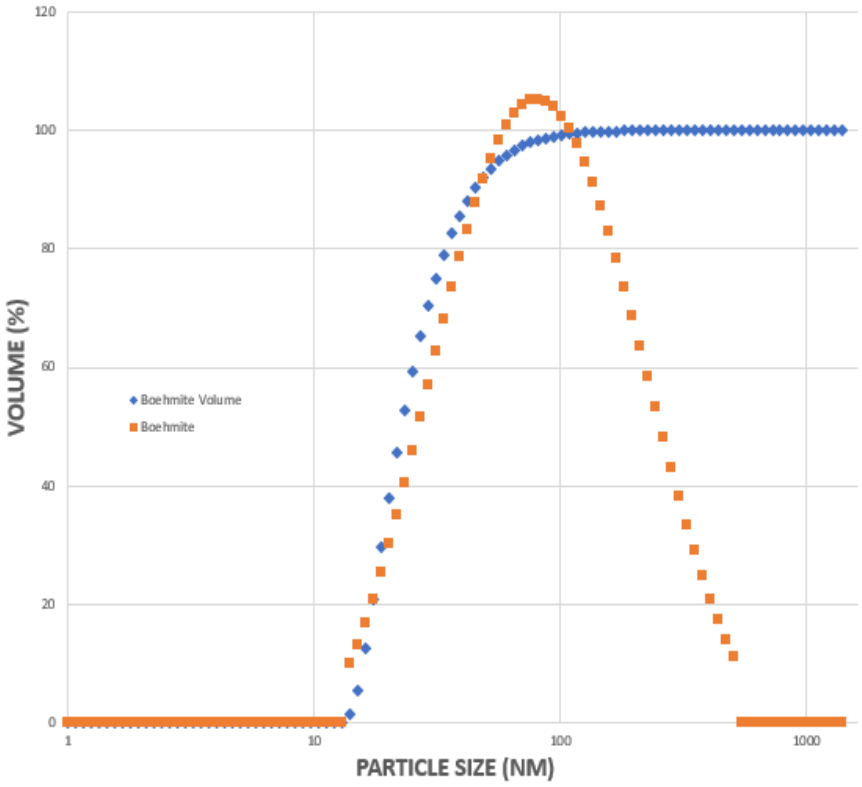

Figure 25. Particle size distribution of Boehmite.

The C3ATB-13002 coded calcium aluminate cementitious powder which was synthesized by using Tekkim marble powder and Boehmite raw materials was ground in a ball mill for 5 minutes. The (d50) value is 9.92 μm and the (d10) value is 1.16 μm and the particle size distribution can be seen in Figure 26. This particle size distribution is suitable for cement formation. C3S cementitious powder with the code of C3SAFG-14004 was ground for 5 minutes prior to the size determination. The average particle size (d50) value was 9.97 μm, (d90) value was 24.2 μm, and (d10) value was 1.49 μm as shown in Figure 27.

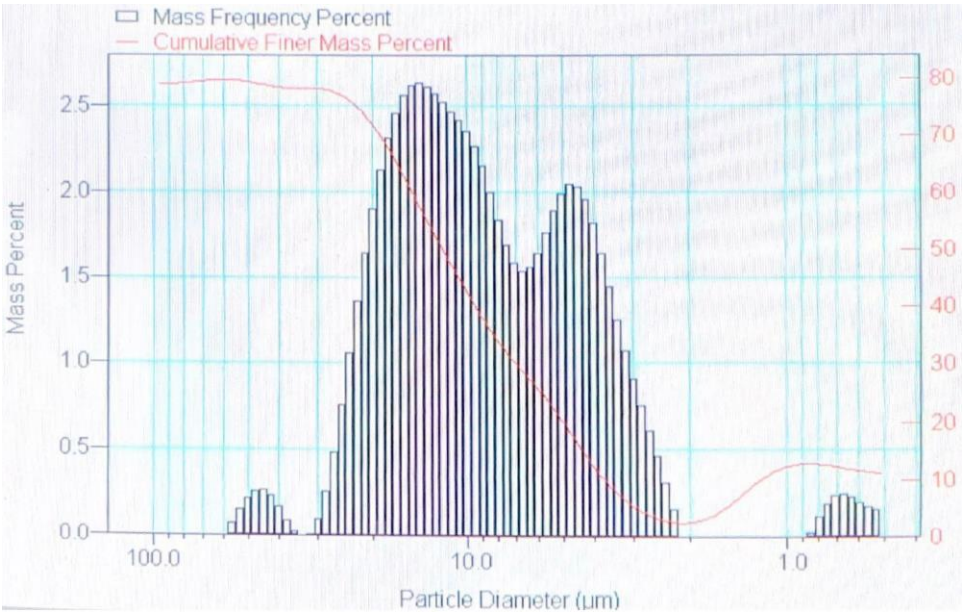

Figure 26. Particle size distribution of C3A cementitious powder.

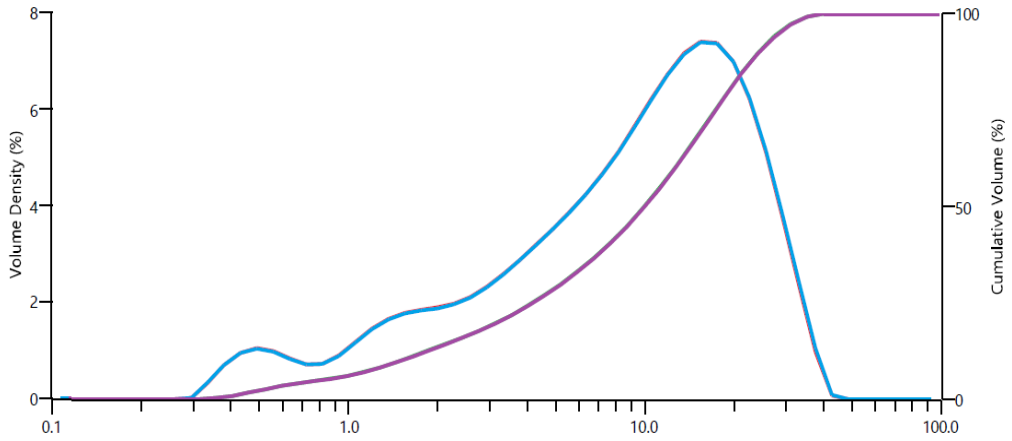

Figure 27. Particle size distribution of C3S cementitious powder.

4.1.2. Density Analysis

The density data of raw materials and cementitious powders are given in Table 4. The density values of Tekkim and AFG Bio marble powders were obtained from the companies and are 2.8 g/cc and 2.93 g/cc, respectively. Boehmite has a density of 3.07 g/cc and fumed silica has a density of 0.16 g/cc.

Table 4. Density, volume, and average density values of powder samples.

	Density(g/cc)				Volume(cc)			
	Trial 1	Trial 2	Trial 3	Average	Trial 1	Trial 2	Trial 3	Average
Egemin Marble Powder	2.6962	2.7183	2.7031	2.7058	2.9645	2.9404	2.9569	2.954
Yatağan quartz	2.7087	2.7125	2.7126	2.7113	2.3935	2.3947	2.3947	2.3958
Tekkim Marble Powder	2.8	2.8	2.8	2.8	-	-	-	-
AFG Bio Marble Powder	2.93	2.93	2.93	2.93	-	-	-	-
Boehmite	3.07	3.07	3.07	3.07	-	-	-	-
Fumed silica	0.16	0.16	0.16	0.16	-	-	-	-
C3S	3.1942	3.1959	3.2001	3.1967	2.4875	2.4862	2.483	2.4856
C3A	2.9053	2.9064	2.9097	2.9071	3.0608	3.0596	3.0561	3.0588

4.1.3. BET Surface Areas of the Powders

The determined BET surface areas of the precursor powders are given in Table 5.

Table 5. BET surface area characterization results of raw materials.

Raw materials	Surface Area(m^2/g)
Egemin marble powder	4.51
Fumed silica	239.27
Boehmite	281.91
Yatağan quartz	3.73

4.1.4. Surface Charges by Zeta Potential Measurements

The pH values of the obtained suspensions were measured as follows: quartz (pH = 4.5), Egemin (pH = 7.5), Boehmite (pH = 5.5), Tekkim calcium carbonate (pH = 6.5), and colloidal silica (pH = 3.5). According to the measurements given in Figures 28 to 32,

the quartz suspension sample zeta potential mean value was -15.62 mV, followed by Egemin (4.63 mV), Boehmite (38.24 mV), Tekkim calcium carbonate (4.72 mV), and colloidal silica (-15.74 mV).

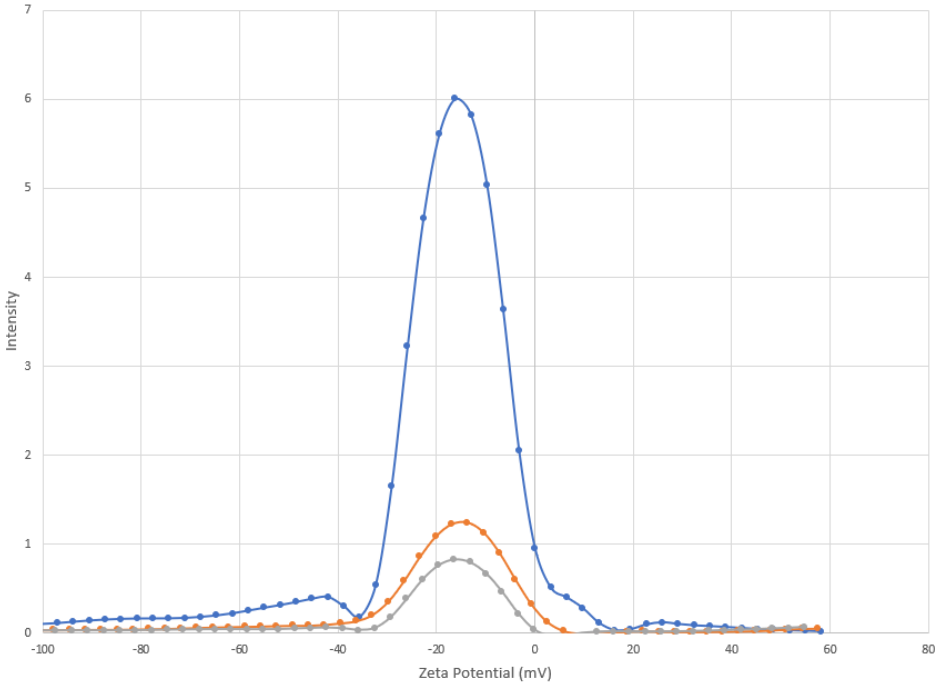

Figure 28. Surface charge of Yatağan quartz powder in water with a pH of 4.5.

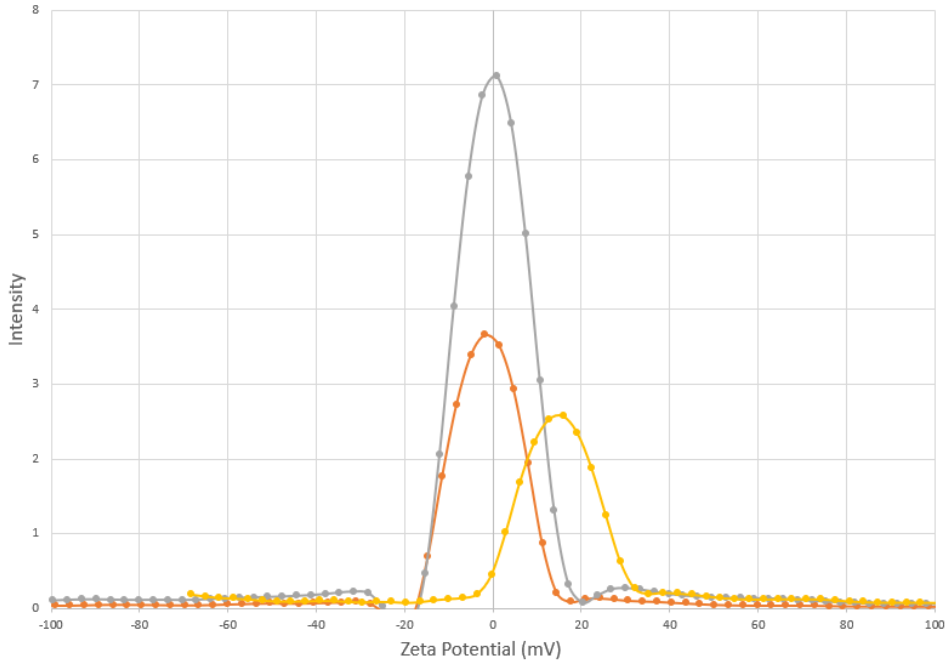

Figure 29. Surface charge of Egemin marble powder in water with a pH of 7.5.

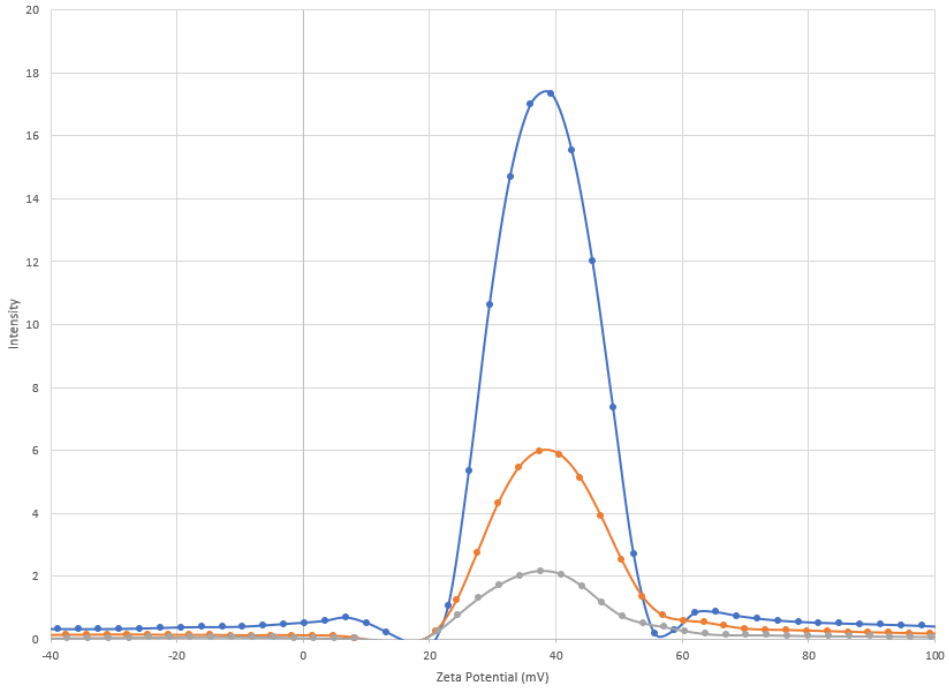

Figure 30. Surface charge of Boehmite in water with a pH of 5.5.

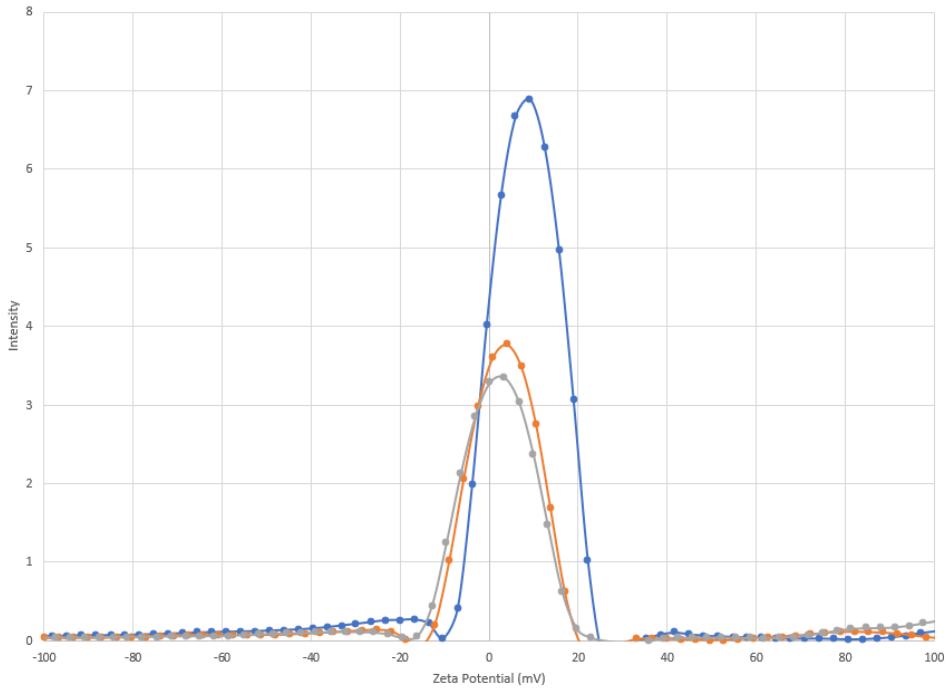

Figure 31. Surface charge of Tekkim marble powder in water with a pH of 6.5.

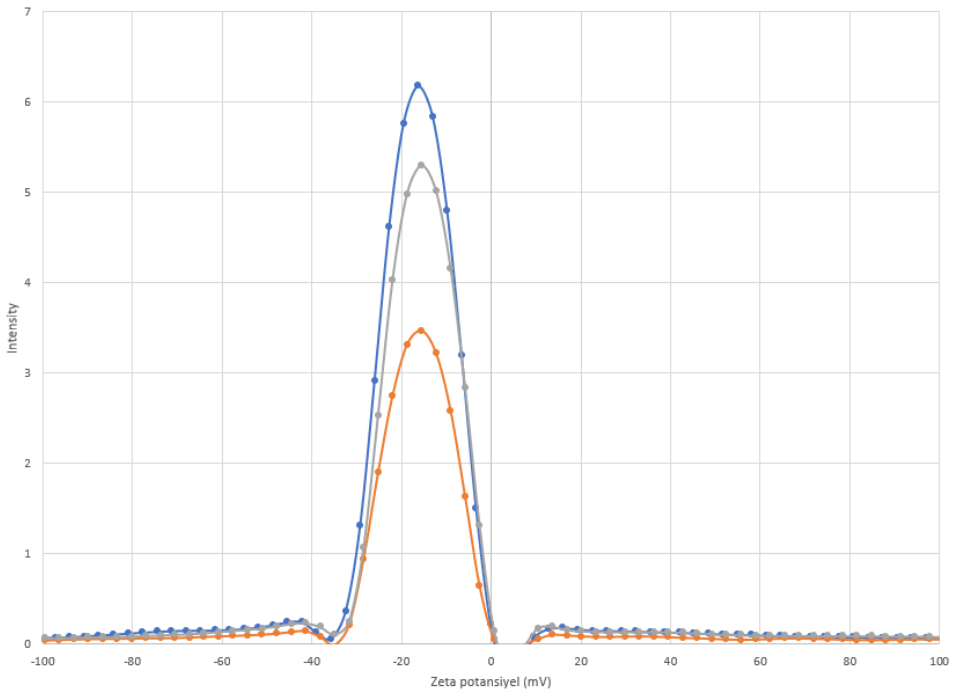

Figure 32. Surface charge of Fume colloidal silica in water with a pH of 3.5.

4.1.5. Thermogravimetric Analysis of Raw Materials

The decomposition of Egemin calcium carbonate into calcium oxide and carbon dioxide which was utilized to produce C3A and C3S starts at 573 °C and is completed at 780 °C as seen in Figure 33. Egemin marble dust had a 55.65% calcium oxide content (theoretical calcium oxide content of CaCO3 is 56%) which indicated that there is a low level of impurities in the marble powder. Tekkim and AFG Bio calcium carbonates also show the same thermal behavior according to the TGA results given in Figures 34 and 35. Quartz obtained from the Yatağan mine had almost no weight loss as seen in Figure 36. Fumed silica shows a similar thermal behaviour to quartz with a total weight loss of about 4% as seen in Figure 37. The weight loss at around 100 °C is due to the removal of adsorbed water and conversion of boehmite to Al_2O_3 starts at above 300°C and was completed at 550 °C as can be seen in Figure 38. C3A-hydrates are present in C3A suspensions. TGA results show a peak between 253 °C and 353 °C because of the dehydroxylation of C3A-hydrated-type products as seen in Figure 39. The hydration of C3S powders is commonly known to form Ca $(OH)_2$ and C3S hydrate gels. Three decomposition regions are therefore observed as seen in Figure 40. The removal of chemically bound water occurs in the first region between 100 °C and 400 °C. The

decomposition of $Ca(OH)_2$ most likely happens in between 417 °C and 477 °C. CS hydrate gel decomposition/dehydroxylation most likely happens in between 655 °C and 700 °C.

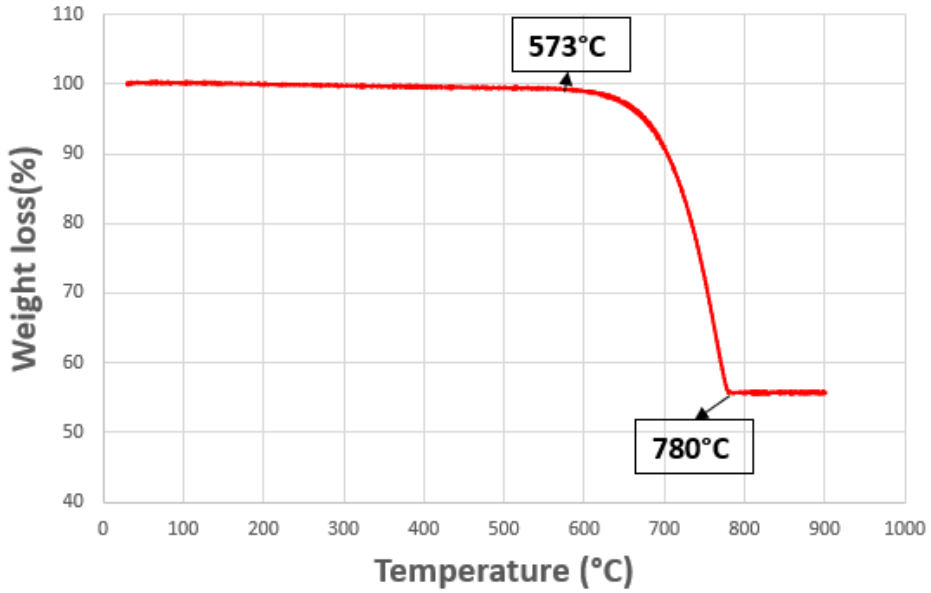

Figure 33. Thermal analysis of Egemin calcium carbonate in air atmosphere.

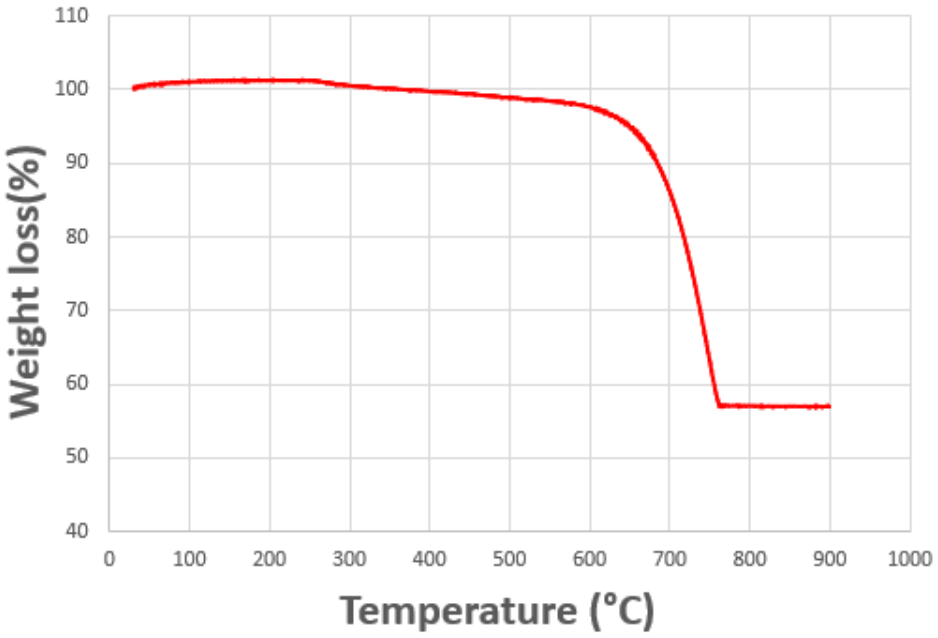

Figure 34. Thermal analysis of Tekkim calcium carbonate in air atmosphere.

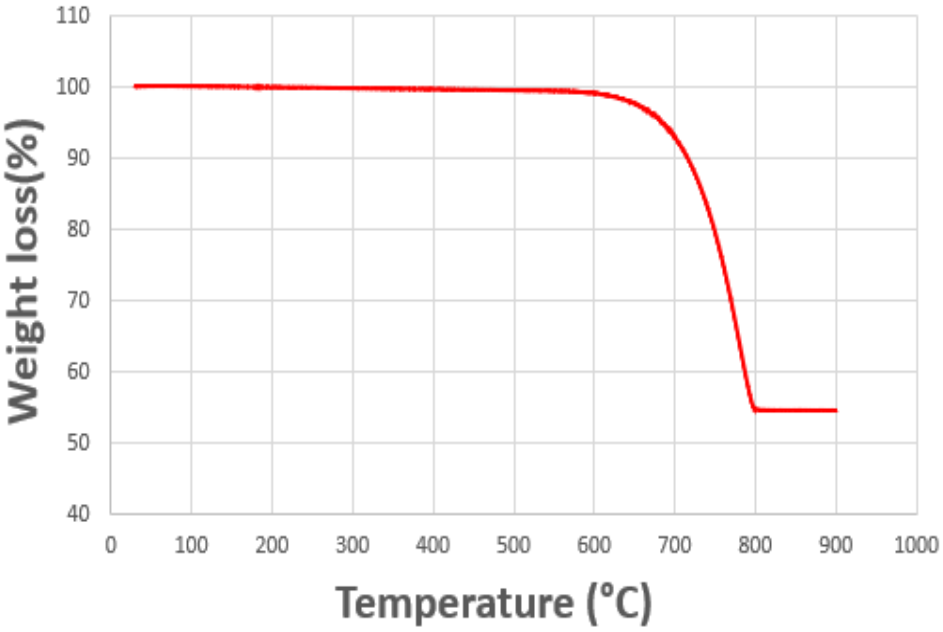

Figure 35. Thermal analysis of AFG Bio calcium carbonate in air atmosphere.

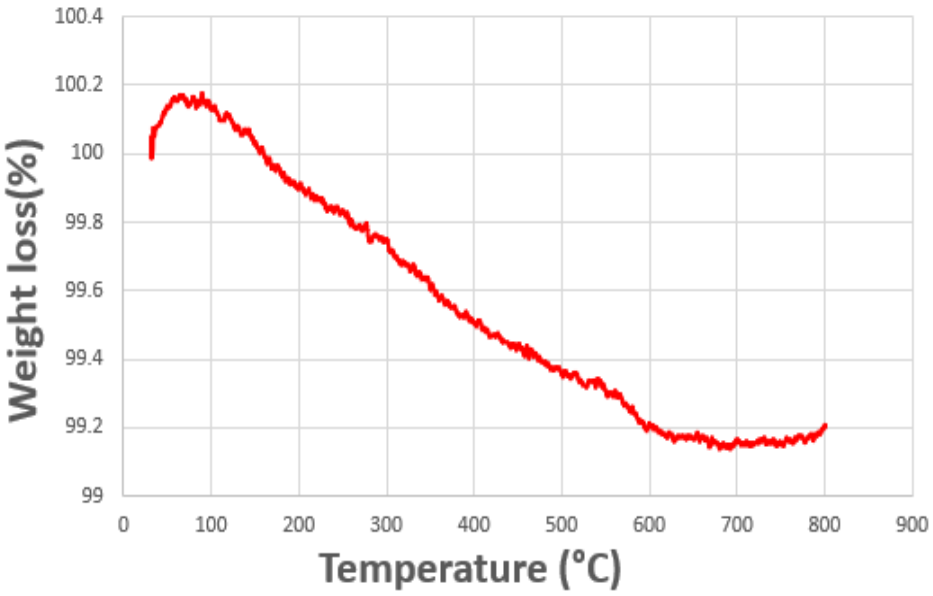

Figure 36. Thermal analysis of Yatağan quartz in air atmosphere.

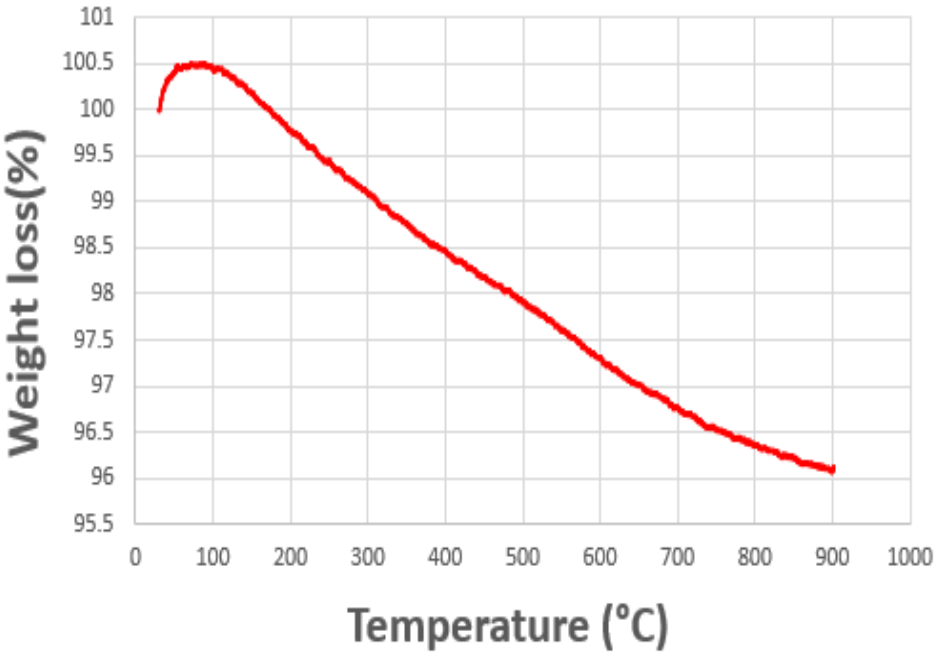

Figure 37. Thermal analysis of colloidal silica in air atmosphere.

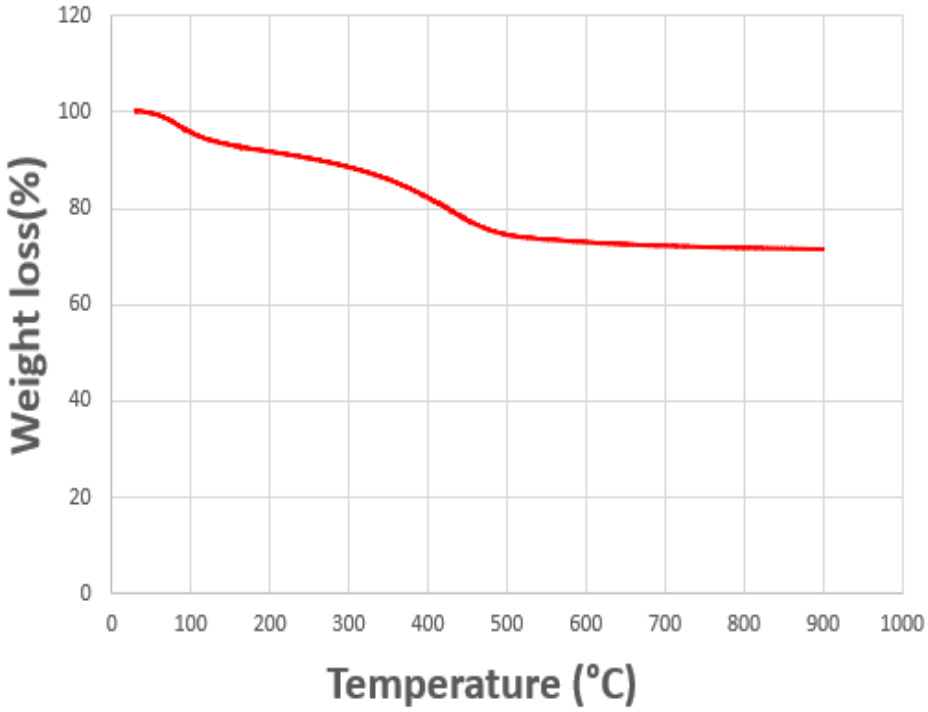

Figure 38. Thermal analysis of boehmite in air atmosphere.

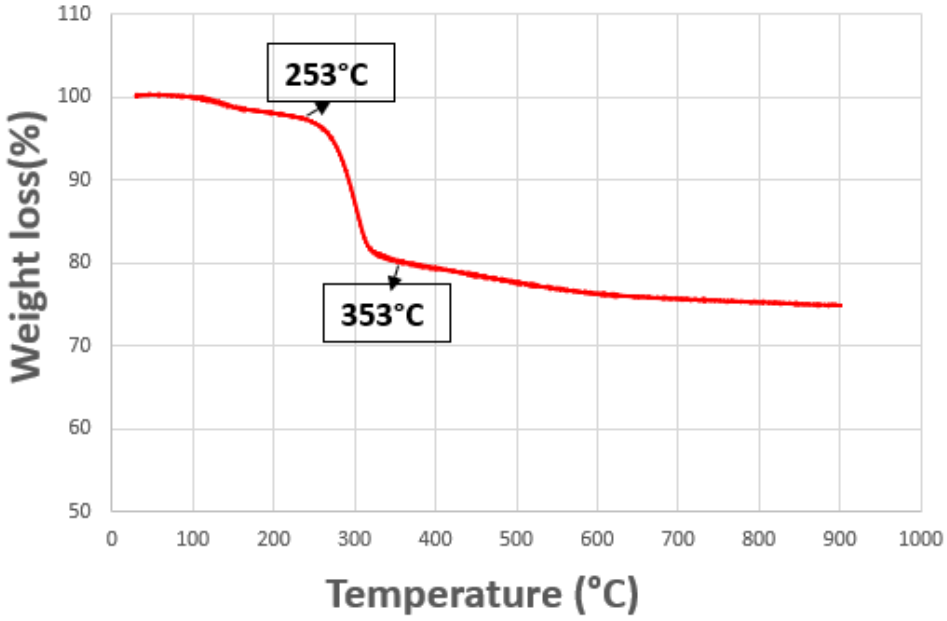

Figure 39. Thermal analysis of C3A-hydrates in air atmosphere.

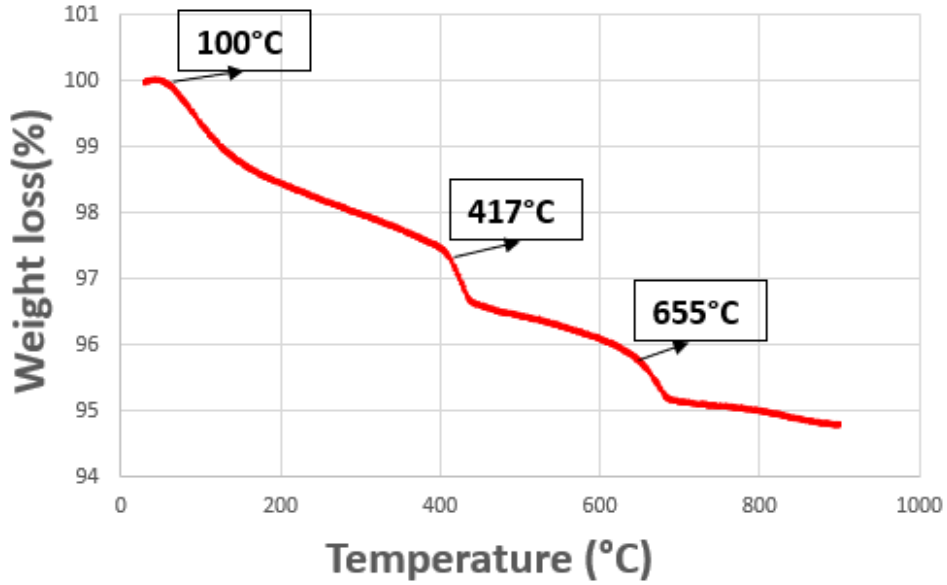

Figure 40. Thermal analysis of C3S-hydrates in air atmosphere.

4.1.6. XRD and XRF analysis

The phase structure characterization of the raw materials and produced C3A and C3S powders and their phase compositions were determined by using quantitative XRD analysis. The elemental compositions were determined by XRF.

The XRD patterns of Egemin marble powder, Tekkim, and AFG Bio commercial marble powders used for cementitious powder production are given in Figure 41. The only detected phase was calcium carbonate in two commercial marble powders while Egemin marble powder contains certain amounts of calcium oxide and dolomite ($CaMg(CO_3)_2$) phases.

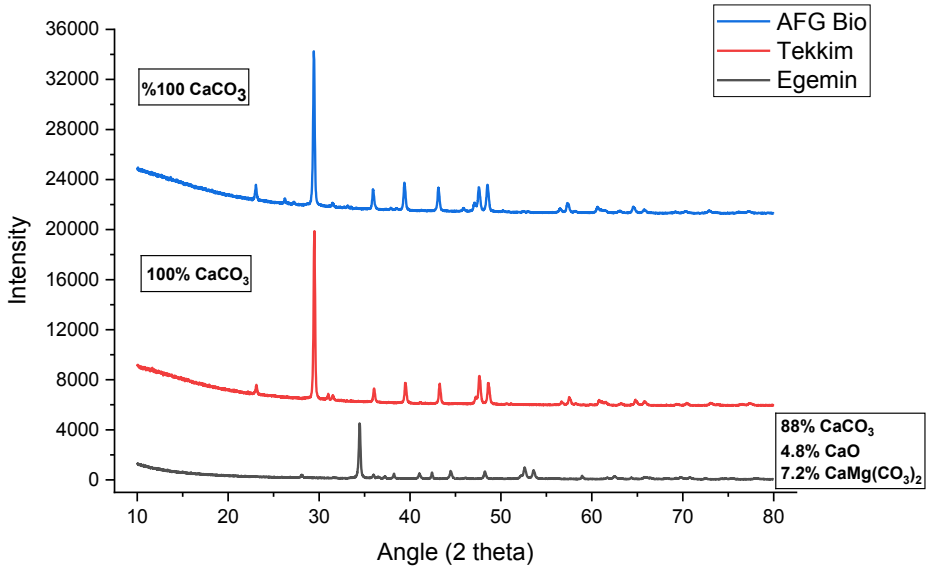

Figure 41. The XRD patterns of Egemin, Tekkim and AFG Bio marble powders.

XRF and ICP-OES chemical analysis of the Egemin marble powder was conducted to determine the nature of the impurities present in the powder. Egemin marble powder was dissolved in HCl solution for ICP-OES. XRF samples from three distinct powder packages were analyzed. The XRF and ICP-OES results of the powders from three different packages are tabulated respectively in Tables 6 and 7.

Table 6. XRF results of Egemin marble powder.

	Package 1		Package 2		Package 3	
Element	Elemental (%)	Oxide (%)	Elemental (%)	Oxide (%)	Elemental (%)	Oxide (%)
Sodium	3.600%	4.850%	3.860%	5.210%	3.490%	4.700%
Magnesium	1.547%	2.566%	1.528%	2.533%	1.496%	2.481%
Aluminum	0.148%	0.279%	0.158%	0.299%	0.158%	0.298%
Silicon	< 0.00051%	< 0.0011%	< 0.00051%	< 0.0011%	< 0.00051%	< 0.0011%
Phosphorus	0.048%	0.109%	0.051%	0.116%	0.050%	0.114%
Sulfur	0.019%	0.048%	0.021%	0.052%	0.018%	0.044%

Cont. on the next page

Cont. of Table 6.

Chlorine	0.004%	0.004%	0.005%	0.005%	0.005%	0.005%
Potassium	< 0.0010%	< 0.0012%	< 0.0010%	< 0.0012%	< 0.0010%	< 0.0012%
Calcium	65.320%	91.390%	65.010%	90.960%	65.450%	91.570%
Titanium	< 0.00051%	< 0.00084%	< 0.00051%	< 0.00084%	< 0.00051%	< 0.00084%
Vanadium	< 0.00051%	< 0.00090%	< 0.00051%	< 0.00090%	< 0.00051%	< 0.00090%
Chromium	< 0.00051%	< 0.00074%	< 0.00051%	< 0.00074%	< 0.00051%	< 0.00074%
Manganese	0.029%	0.038%	0.030%	0.039%	0.030%	0.039%
Iron	0.033%	0.047%	0.046%	0.066%	0.042%	0.060%
Cobalt	0.003%	0.004%	0.002%	0.002%	0.001%	0.001%
Nickel	< 0.00020%	< 0.00026%	< 0.00020%	< 0.00026%	< 0.00020%	< 0.00026%
Copper	0.149%	0.186%	0.111%	0.139%	0.145%	0.181%
Zinc	< 0.00010%	< 0.00012%	< 0.00010%	< 0.00012%	< 0.00010%	< 0.00012%
Germanium	0.005%	0.005%	< 0.00010%	< 0.00010%	< 0.00010%	< 0.00010%
Arsenic	< 0.00010%	< 0.00013%	< 0.00010%	< 0.00013%	< 0.00010%	< 0.00013%
Selenium	0.004%	0.004%	0.003%	0.003%	0.006%	0.006%
Bromine	0.000%	0.000%	< 0.00010%	< 0.00010%	0.000%	0.000%
Strontium	0.031%	0.037%	0.034%	0.041%	0.031%	0.036%
Yttrium	< 0.00071%	< 0.00071%	< 0.00071%	< 0.00071%	< 0.00071%	< 0.00071%
Zirconium	< 0.051%	< 0.068%	< 0.051%	< 0.068%	< 0.051%	< 0.068%
Niobium	< 0.0010%	< 0.0014%	< 0.0010%	< 0.0014%	0.000%	0.001%
Molybdenum	< 0.0010%	< 0.0010%	0.001%	0.001%	0.001%	0.001%
Silver	0.000%	0.000%	0.000%	0.000%	< 0.00051%	< 0.00051%
Cadmium	< 0.00051%	< 0.00051%	< 0.00051%	< 0.00051%	< 0.00051%	< 0.00051%
Indium	< 0.00051%	< 0.00051%	< 0.00051%	< 0.00051%	< 0.00051%	< 0.00051%
Tin	< 0.00061%	< 0.00077%	< 0.00061%	< 0.00077%	< 0.00061%	< 0.00077%
Antimony	< 0.00061%	< 0.00080%	< 0.00061%	< 0.00080%	< 0.00061%	< 0.00080%
Tellurium	< 0.018%	< 0.018%	< 0.00071%	< 0.00071%	< 0.016%	< 0.016%
Barium	0.425%	0.425%	0.540%	0.540%	0.445%	0.445%

Cont. on the next page

Cont. of Table 6.

Lanthanum	< 0.0010%	< 0.0010%	< 0.0010%	< 0.0010%	< 0.0010%	< 0.0010%
Tungsten	< 0.00020%	< 0.00025%	< 0.00020%	< 0.00025%	< 0.00020%	< 0.00025%
Mercury	< 0.00020%	< 0.00020%	< 0.00020%	< 0.00020%	< 0.00020%	< 0.00020%
Thallium	< 0.00020%	< 0.00020%	< 0.00020%	< 0.00020%	< 0.00020%	< 0.00020%
Lead	< 0.00020%	< 0.00022%	< 0.00020%	< 0.00022%	< 0.00020%	< 0.00022%
Bismuth	< 0.00020%	< 0.00020%	< 0.00020%	< 0.00020%	0.006%	0.006%

Table 7. ICP-OES result of Egemin marble powder.

Sample	**Al (mg/L)**	**Ba (mg/L)**	**Ca (mg/L)**	**Cu (mg/L)**	**Fe (mg/L)**
Concentration	0.8561	23.212	9840.3	0.0308	5.78
%	0.008425078	0.228435	96.84067	0.000303	0.056882
Sample	**Mg (mg/L)**	**Mn(mg/L)**	**Na(mg/L)**	**P (mg/L)**	**Sr(mg/L)**
Concentration	284.92	1.219	0.2037	1.1553	3.6483
%	2.803963654	0.011996	0.002005	0.01137	0.035904

XRD analysis of the quartz powder produced in the Yatağan mine had high purity and crystallinity as shown in Figure 42. The XRF analysis result indicated 98.6% silica as tabulated in Table 9 while about 99.5% silica was reported in the elemental analysis supplied by the company given in Table 8.

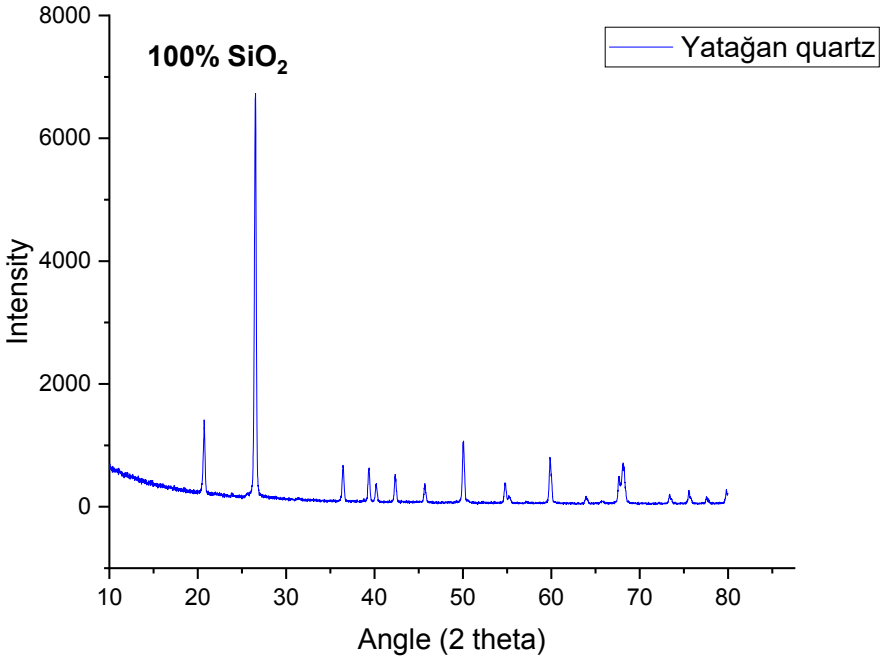

Figure 42. XRD pattern of Yatağan quartz.

Table 8. XRF results of quartz powder supplied by the company.

Element	Oxide (%)
Sodium	0.1096
Magnesium	0.0081
Aluminum	0.294
Silicon	99.555
Phosphorus	0.0024
Potassium	0.0026
Calcium	0.0076
Titanium	0.0012
Manganese	0.0002
Iron	0.0193
Total	100

Table 9. XRF results of quartz powder.

Element	Elemental (%)	Oxide (%)
Sodium	< 0,081%	< 0,11%
Magnesium	< 0,16%	< 0,27%
Aluminum	0,4235%	0,800%
Silicon	46,09%	98,60%
Phosphorus	0,1071%	0,2454%
Sulfur	0,00151%	0,00376%
Chlorine	0,00729%	0,00729%
Potassium	<0,0010%	< 0,0012%
Calcium	< 0,0010%	< 0,0014%
Titanium	< 0,00051%	< 0,00084%
Vanadium	< 0,00051%	< 0,00090%
Chromium	< 0,00051%	< 0,00074%
Manganese	< 0,0076%	< 0,0098%
Iron	0,01267%	0,0181%
Cobalt	< 0,00045%	< 0,00057%
Nickel	< 0,00020%	< 0,00026%
Copper	0,03483%	0,04359%
Zinc	< 0,00010%	< 0,00012%
Germanium	0,00157%	0,00157%
Arsenic	< 0,00010%	< 0,00013%
Selenium	0,00203%	0,00203%
Bromine	0,00048%	0,00048%
Strontium	0,00030%	0,00036%
Yttrium	< 0,00071%	< 0,00071%
Zirconium	< 0,051%	< 0,068%
Niobium	< 0,0010%	< 0,0014%
Molybdenum	< 0,0010%	< 0,0010%
Silver	< 0,00017%	< 0,00017%
Cadmium	< 0,00051%	< 0,00051%
Indium	< 0,00051%	< 0,00051%
Tin	< 0,00061%	< 0,00077%
Antimony	< 0,00061%	< 0,00080%
Tellurium	< 0,00071%	< 0,00071%
Barium	< 0,00081%	< 0,00081%
Lanthanum	< 0,0010%	< 0,0010%
Tungsten	< 0,00020%	< 0,00025%
Mercury	< 0,00020%	< 0,00020%
Thallium	< 0,00020%	< 0,00020%
Lead	< 0,00020%	< 0,00022%
Bismuth	< 0,00020%	< 0,00020%

The Aerosil 200 colloidal silica had an amorphous structure, and the quantitative analysis of the sample could not be performed. The powder was determined to contain 99.4% silica by XRF analysis as given in Table 10. These results indicate that the fume silica used in the powder synthesis in this work representing one of the most reactive silica sources due to its fine size, low crystallinity, and high purity.

Table 10. XRF results of colloidal silica.

Element	Elemental (%)	Oxide (%)
Sodium	< 0,081%	< 0,11%
Magnesium	< 0,17%	< 0,29%
Aluminum	0,0373%	0,071%
Silicon	46,45%	99,38%
Phosphorus	0,09141%	0,2094%
Sulfur	0,00128%	0,00319%
Chlorine	0,00494%	0,00494%
Potassium	< 0,0010%	< 0,0012%
Calcium	< 0,0010%	< 0,0014%
Titanium	< 0,00051%	< 0,00084%
Vanadium	< 0,00051%	< 0,00090%
Chromium	0,00261%	0,00382%
Manganese	0,02480%	0,0320%
Iron	< 0,00075%	< 0,0011%
Cobalt	0,00192%	0,00244%
Nickel	< 0,00020%	< 0,00026%
Copper	0,03359%	0,04204%
Zinc	< 0,00010%	< 0,00012%
Germanium	0,00157%	0,00157%
Arsenic	< 0,00010%	< 0,00013%
Selenium	0,00196%	0,00196%
Bromine	0,00012%	0,00012%
Strontium	< 0,00051%	< 0,00060%
Yttrium	< 0,00071%	< 0,00071%
Zirconium	< 0,051%	< 0,068%
Niobium	< 0,00010%	< 0,00014%
Molybdenum	< 0,0010%	< 0,0010%
Silver	< 0,00051%	< 0,00051%
Cadmium	< 0,00051%	< 0,00051%
Indium	< 0,00051%	< 0,00051%
Tin	< 0,00061%	< 0,00077%
Antimony	< 0,00061%	< 0,00080%
Tellurium	0,0080%	0,0080%

Boehmite powder also had an amorphous structure. It has an alumina content of 99.23% as shown by the elemental analysis results given in Table 11. These results indicate that the boehmite used in the powder synthesis in this work represents one of the most reactive alumina sources due to its fine size, low crystallinity, and high purity.

Table 11. XRF results of Boehmite powder.

Element	Elemental (%)	Oxide (%)
Sodium	< 0,081%	< 0,11%
Magnesium	0,18%	0,29%
Aluminum	52,52%	99,23%
Silicon	< 0,00051%	< 0,0011%
Phosphorus	0,1346%	0,3084%
Sulfur	0,00118%	0,00295%
Chlorine	0,00390%	0,00390%
Potassium	< 0,0010%	< 0,0012%
Calcium	< 0,0010%	< 0,0014%
Titanium	< 0,00051%	< 0,00084%
Vanadium	< 0,00051%	< 0,00090%
Chromium	< 0,00051%	< 0,00074%
Manganese	0,012%	0,016%
Iron	0,0114%	0,0163%
Cobalt	0,00148%	0,00188%
Nickel	< 0,00020%	< 0,00026%
Copper	0,0508%	0,0636%
Zinc	0,00454%	0,00566%
Germanium	0,00146%	0,00146%
Arsenic	< 0,00010%	< 0,00013%
Selenium	0,00186%	0,00186%
Bromine	0,00103%	0,00103%
Strontium	0,00093%	0,00110%
Yttrium	< 0,00071%	< 0,00071%
Zirconium	< 0,051%	< 0,068%
Niobium	0,00181%	0,00259%
Molybdenum	0,00346%	0,00346%
Silver	0,00233%	0,00233%
Cadmium	< 0,0019%	< 0,0019%
Indium	< 0,00051%	< 0,00051%
Tin	< 0,00061%	< 0,00077%
Antimony	< 0,00061%	< 0,00080%
Tellurium	< 0,019%	< 0,019%

The most suitable raw materials for the synthesis of highly pure cementitious powder phases were determined and listed in Table 12 based on physical and chemical characterization results. It is desired that the raw materials used in cementitious powder synthesis have high reactivities and purity ideally to complete the solid-state reactions at relatively low temperatures in short hold times. It is also important that the two phases are effectively mixed before the heat treatment. The mixed phases must have different size distributions for efficient packing in particle mixtures. It is also necessary to have a well dispersed system of the particles without strong agglomerates during wet mixing before heat treatment. It is important that the surface charges should be different for the effective mixing of the raw materials in the liquid medium. The most important properties that increase reactivity are crystallinity and high surface area besides effective mixing. Although the impurities contribute to the reactivity by increasing the disorder in the structure in general, they can also affect the thermodynamics besides the reaction kinetics and can change the stability of the reaction products. It has been revealed in clinker synthesis studies that raw material purity increases solid-state transformation rates. Reaction stoichiometry reflecting the ideal reaction at the molecular level and the theoretical energy amounts required are valid for pure reactants. The optimum temperature and time conditions for maximum conversion also change as the impurity contents increase. Different raw material compositions tested in the synthesis studies therefore yielded different conversion rates under similar conditions.

Table 12. The fundamental properties of raw materials for cementitious powder synthesis according to the characterization results.

	Particle size	Surface Area	Crystallinity	Surface Charge	Impurities
AFG-Bio	1.5μm (fine)	-	High	-	Low
Tekkim	4.8μm (fine)	-	High	4.72 mV	Low
Egemin Marble powder	2.1μm (fine)	4.51 m^2/g	High	4.63 mV	12%
Colloidal silica	0.254μm (fine)	239.27 m^2/g	Low	-15.74 mV	Low
Yatağan quartz	3.08μm (fine)	3.73 m^2/g	High	-15.62 mV	Low
Boehmite	0.0227μm (fine)	281.91 m^2/g	Low	38.24 mV	Low

The raw materials listed in Table 12 were mixed in several combinations for the preparation of highly pure C3A and C3S cementitious powder phases. Boehmite and Egemin marble powder were used for the production of C3A during the initial phases of the work. C3A formation occurs above 1200 °C according to the C3A phase diagram. The heat treatment temperature was initially set at 1200 °C and it was increased to 1300 °C along with a longer heat treatment period at the peak hold temperature. The maximum C3A phase content was about 79.6% in all three trials which was a relatively low value due most likely to the impurities present in the Egemin marble powder as shown in Figure 43.

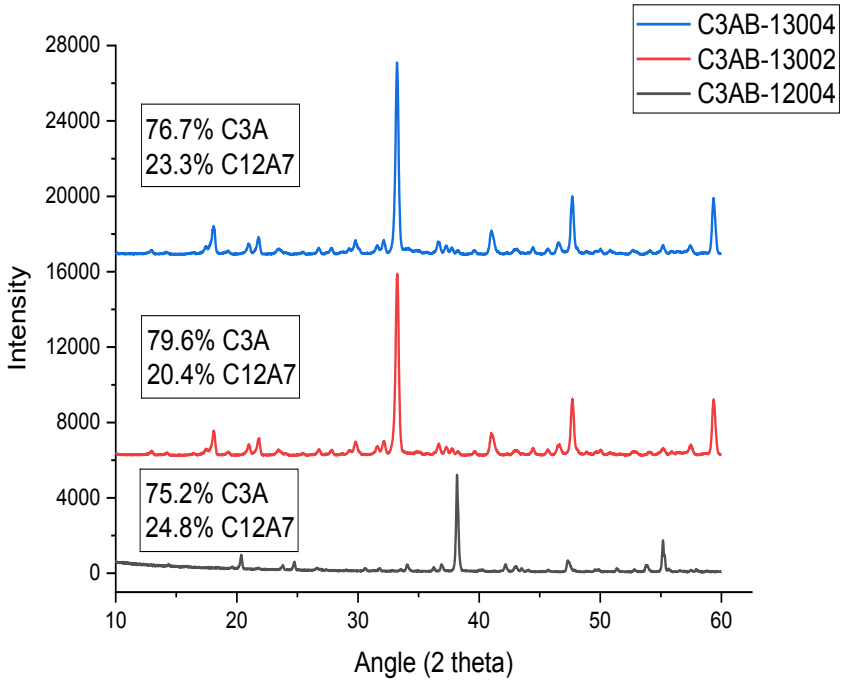

Figure 43. XRD results of C3AB-12004/13002/13004.

Egemin marble powder and boehmite suspensions prepared separately were mixed and heat treated to obtain a good dispersion and final high purity. As seen in Figure 44, although higher purities were obtained (max. 88.1%), the dolomite phase in Egemin marble dust prevented a higher (over 90%) purity.

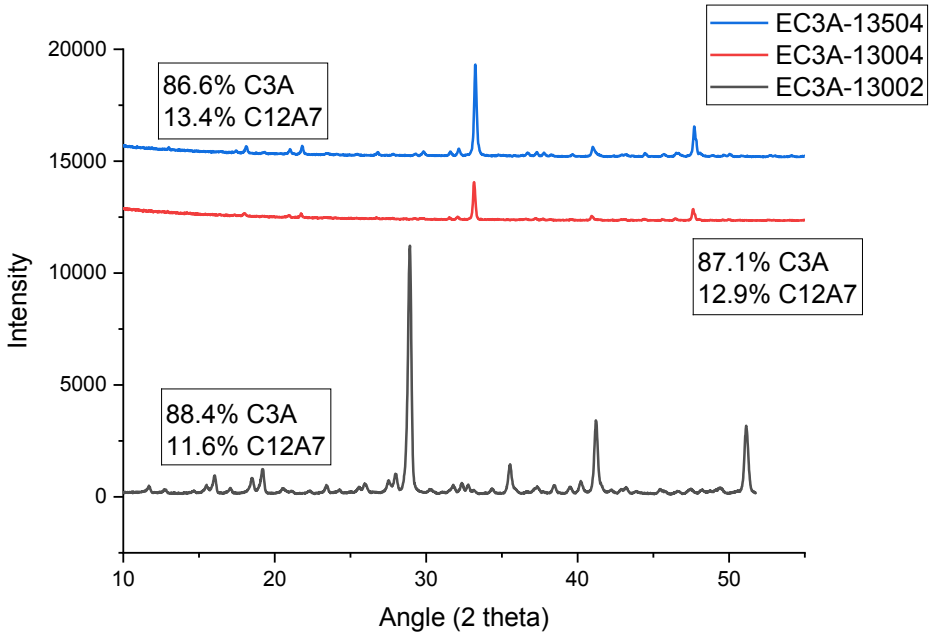

Figure 44. XRD results of EC3A-13002/13004/13504.

Since better mixtures provide greater purities, employing ethanol as a dispersant in place of water has been explored to produce a better mixture of starting phases. The results given in Figure 45 however have shown that mixtures obtained in water produces higher C3A purities most likely due to surface charge effects during the mixing of the precursor phases.

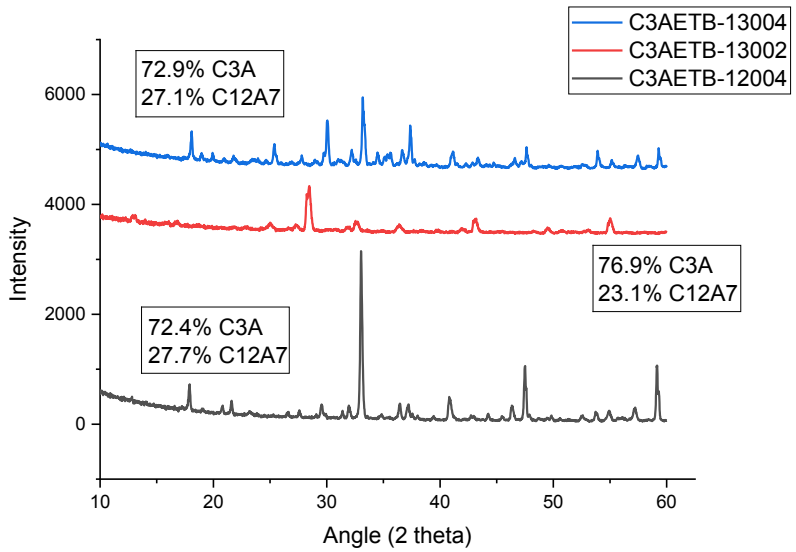

Figure 45. XRD results of C3AETB-12004/13002/13004.

The XRD results have shown that the most efficient temperature and heat treatment time for highly pure C3A preparation was 1300 °C for 2 hours. A high purity could not be obtained however due to the impurities in Egemin marble powder. Cementitious powders with 96.9% C3A phase purity was obtained when Tekkim marble powder which contains 100% CaCO3 was used in powder synthesis as shown in Figure 46.

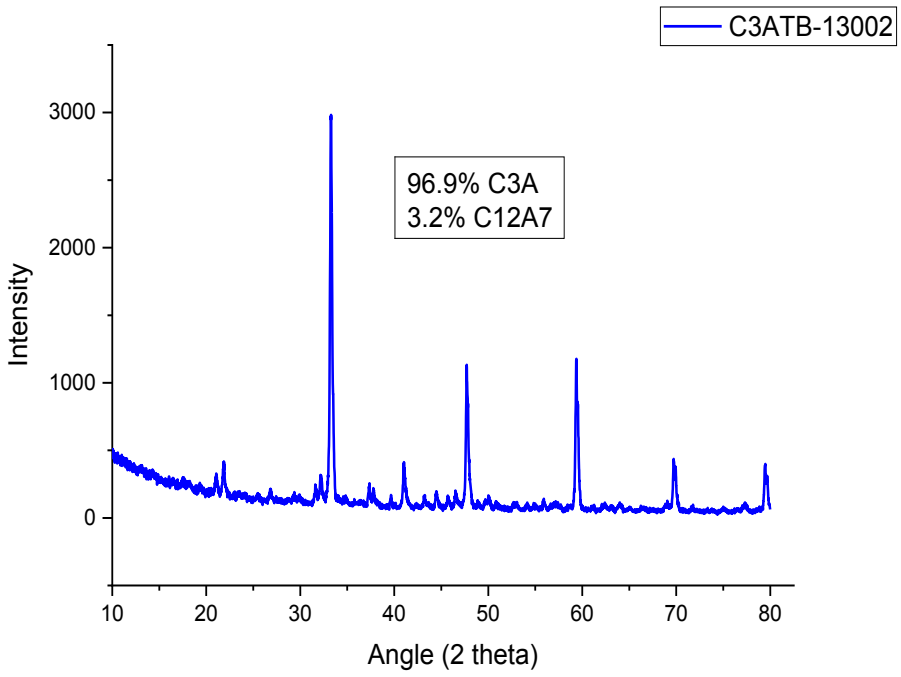

Figure 46. XRD result of C3ATB-13002.

Egemin marble powder and Yatağan quartz were initially combined to produce C3S. XRD data revealed that there was still unreacted calcium oxide after two hours of heat treatment at 1300 °C and a C2S rich powder was produced. The heat treatment period and the temperature were increased to 1400 °C and 85.5% C3S purity was obtained. A certain fraction part of the C3S phase however was converted back to the C2S phase since the cooling rate is crucial in the synthesis of C3S as shown in Figure 47.

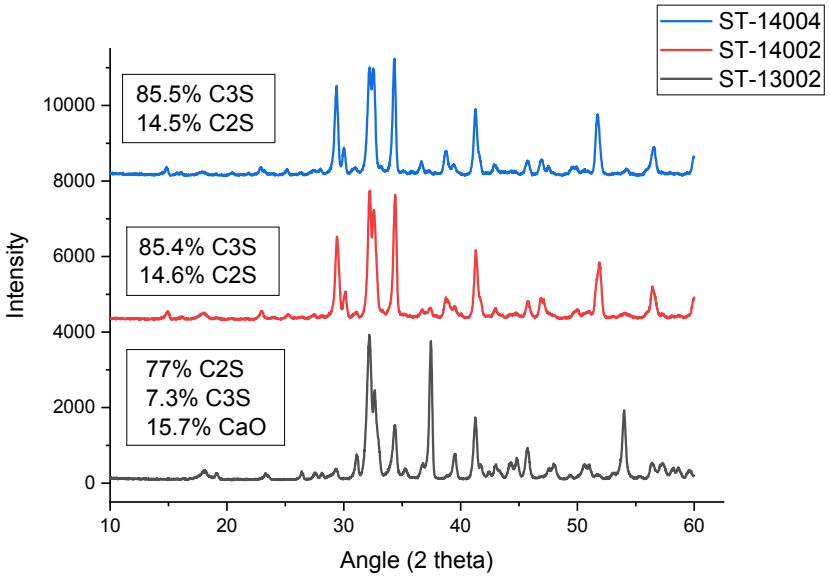

Figure 47. XRD results of ST-13002/14002/14004.

Fumed silica which is a much finer powder than Yatağan quartz was used to obtain a better mixture of precursor phases. The C2S phase formation was dominant at 1300 °C. The highest purity of 85.8% C3S was obtained for the sample coded SF-14004 as given in Figure 48.

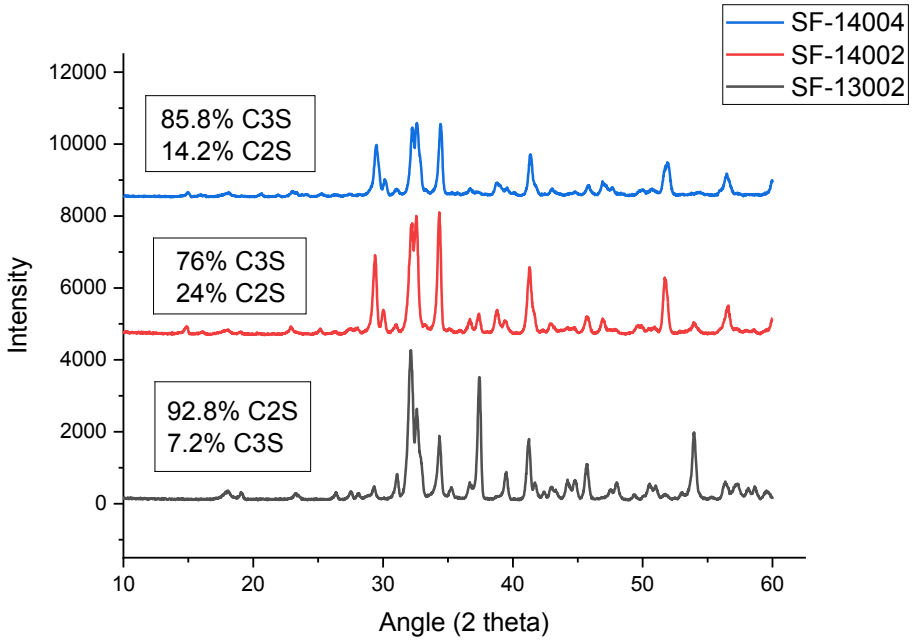

Figure 48. XRD results of SF-13002/14002/14004.

AFG Bio marble powder with a higher purity than Egemin marble powder was used to obtain purities over 90%. Temperature and heat treatment time were determined as 1400 °C and 4 hours. A cementitious powder with 100% C3S phase content with no other phases were synthesized as given in Figure 49.

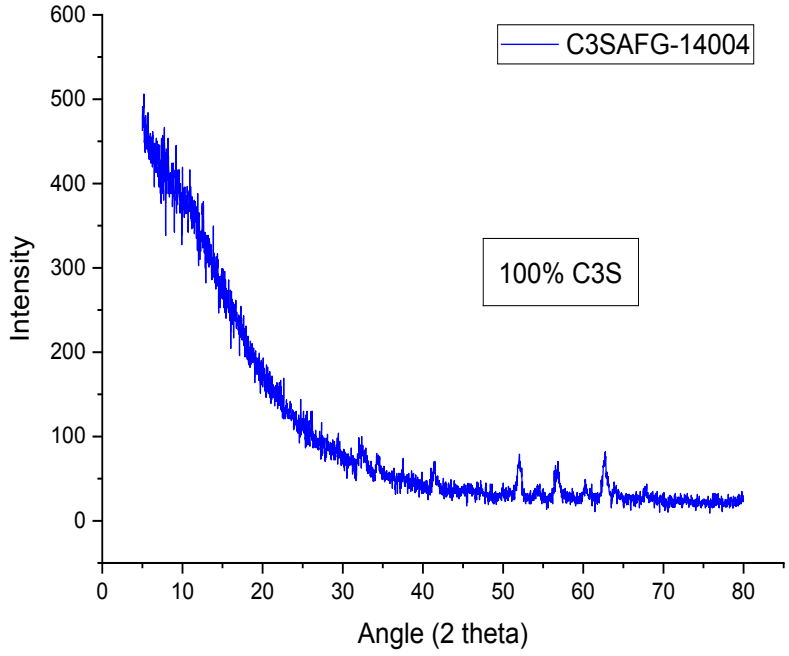

Figure 49. XRD result of C3SAFG-14004.

C3A cementitious powders synthesized with commercial Tekkim marble powder were mixed with deionized water at different solid/water ratios, which provided ease of mixing and processing, and were dehydrated and dried in an ethanol bath for certain periods. XRD analysis results given in Figures 50 and 51 conducted on dry products shows the phase transformation of cements within 15 minutes. C3A cementitious powder phase was converted to C3AH6 phase to a large extent. C3S cement characteristically hardens slowly compared to C3A. A small amount of calcium silicate hydrate was formed within15 minutes due to the phase transformations/hydration reactions.

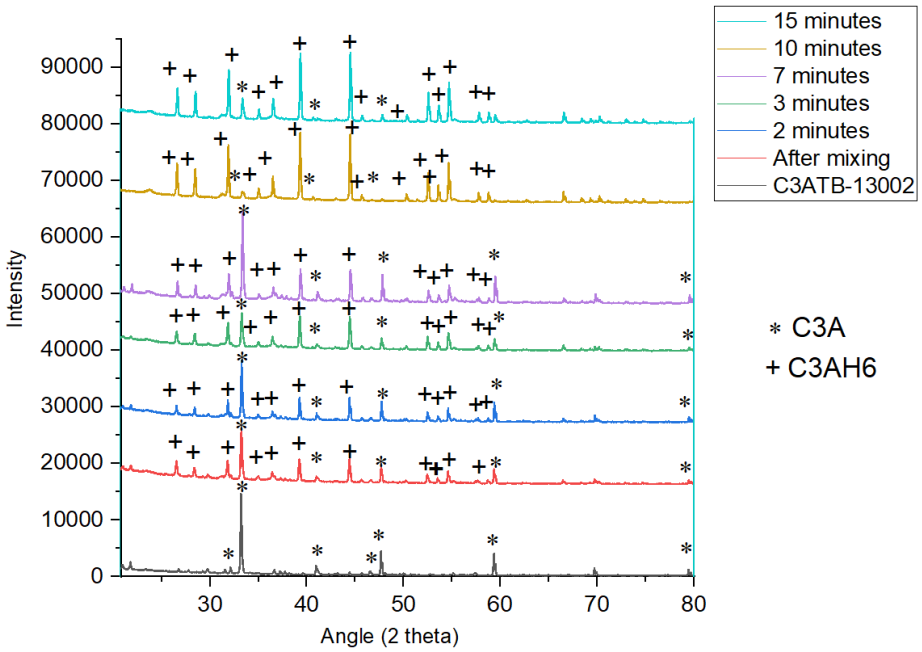

Figure 50. Time-dependent phase transformation of C3A cement.

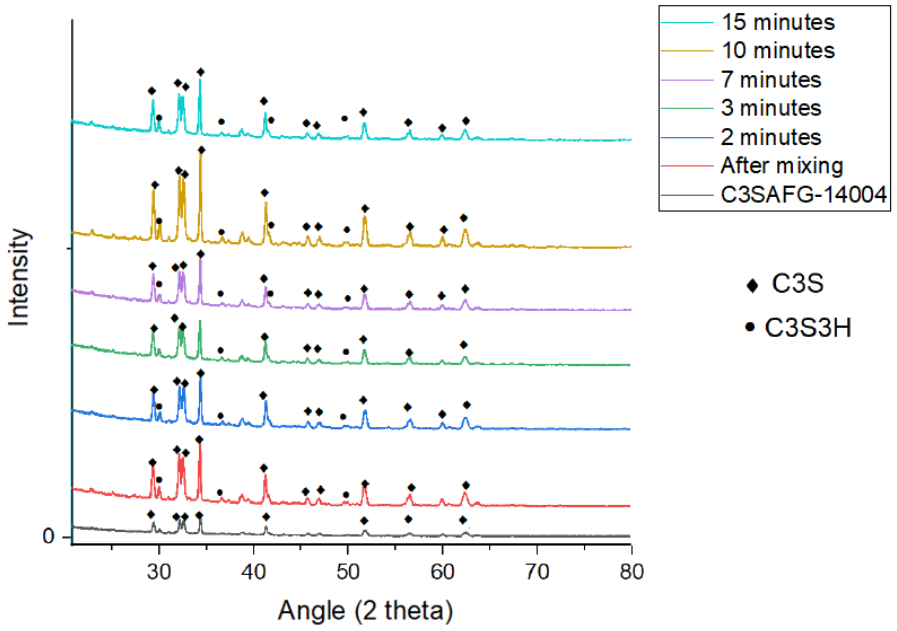

Figure 51. Time-dependent phase transformation of C3S cement.

4.1.7. Cell Toxicity Analysis

C3S cement prepared with the dissolution inhibitor 1M gluconic acid solution have indicated a higher biocompatibility than the one prepared with distilled water at low concentrations. Toxicity results obtained after 24 hours in Figure 52 and after 72 hours in Figure 53 show that the addition of gluconic acid caused differences in ion release. The toxicity of pure slurry appears to be more concentration-independent, while that of gluconic acid is much more toxic at higher concentrations which may be mostly due to the relatively low pH of the solution. The ability of the gluconate group to bind to the cations and adhere to the surface may also be another explanation for this behaviour. It is possible that the free release of heavy metals, which are thought to cause toxicity, may be inhibited by these groups. A lower toxicity therefore may occur due to lower ion release at low concentrations.

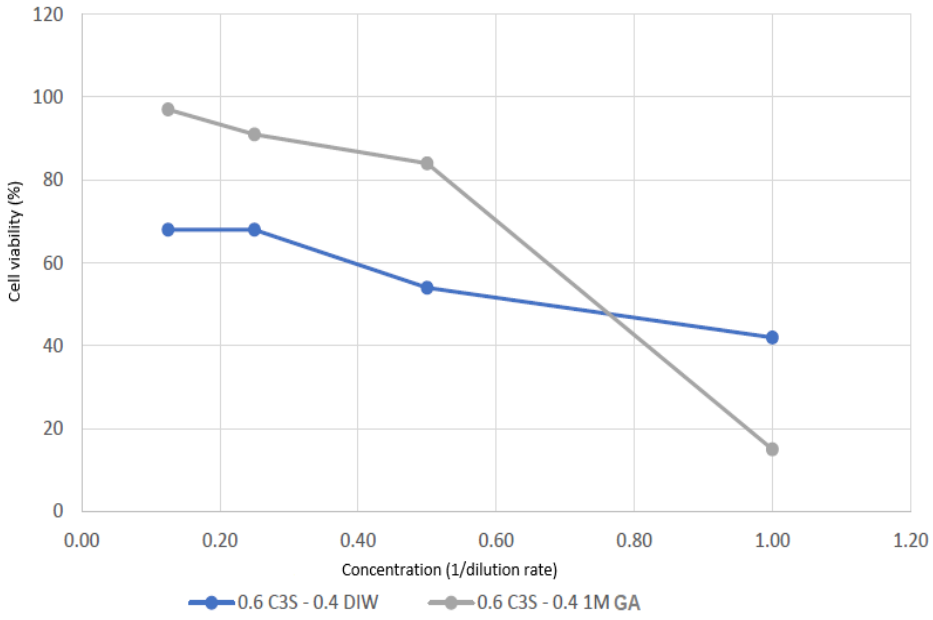

Figure 52. Viability rates of cells exposed to C3S cement extracts for 24 hours.

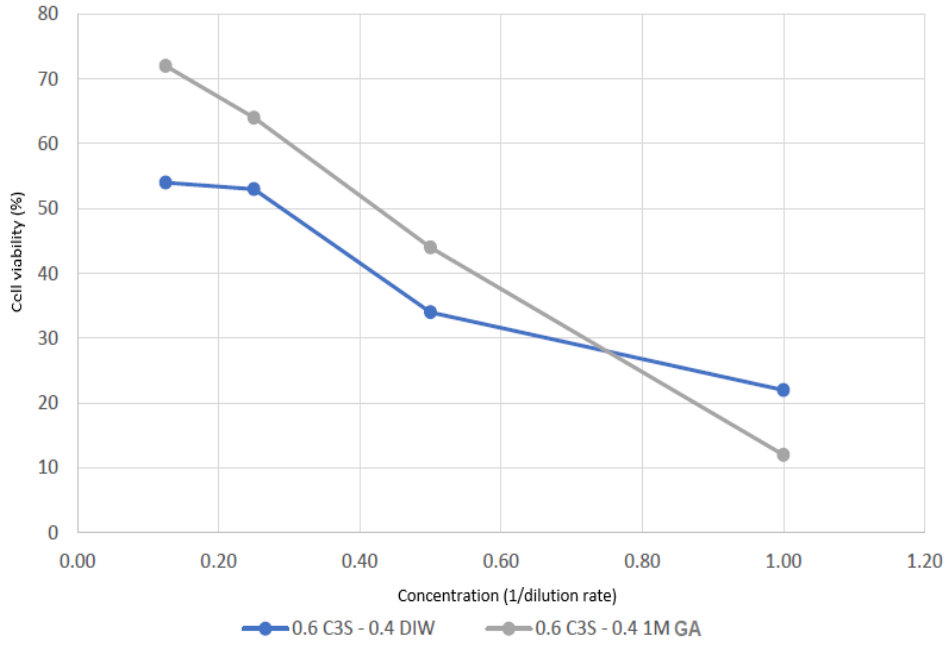

Figure 53. Viability rates of cells exposed to C3S cement extracts for 72 hours

The effects of various additives on the biocompatibility of C3A cement are shown in Figures 54 and 55. According to the results, hydroxyethyl cellulose (HEC) and trisodium citrate (TSC) additives caused toxic effects at high concentrations. Compared with the pure aqueous C3A cement, the 2M $MgSO_4$ solution showed similar biocompatibility. However, 1M $MgSO_4$ solution showed toxic effect in parallel with other additives. $MgSO_4$ is a compound known to be biocompatible and widely used as a food supplement. Therefore, it is thought that the resulting harmful effect may be due to the interaction of $MgSO_4$ with C3A and originates from C3A. As the ratios of HEC and MgSO4 adducts increase, the increase in their biocompatibility can be explained as follows: both additives slow down C3A release by different mechanisms. HEC reduces the mass transfer rate by increasing the solution viscosity with its hydrogel feature. $MgSO_4$ converts C3A to the more stable ettringite phase. Therefore, it is possible to reduce harmful emissions from alumina more effectively at higher concentrations.

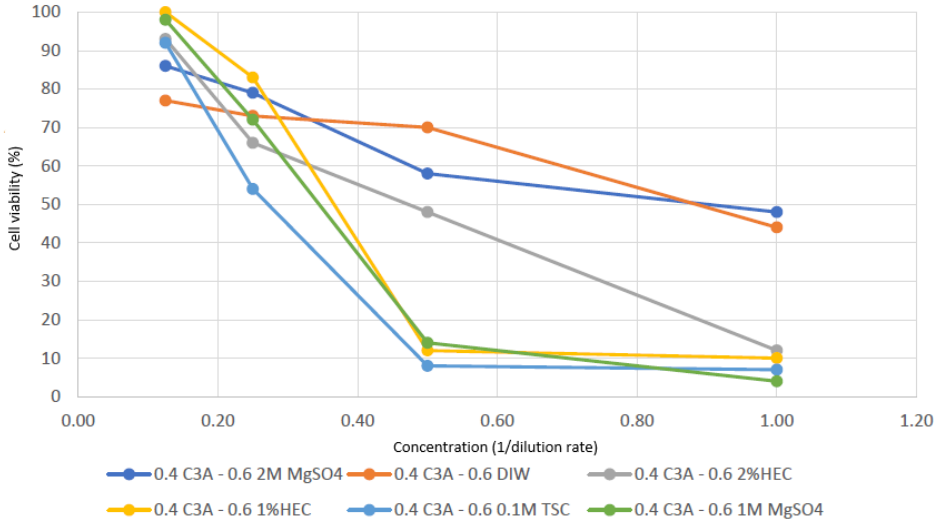

Figure 54. Viability rates of cells contacted with additive C3A cement extracts for 24 hours.

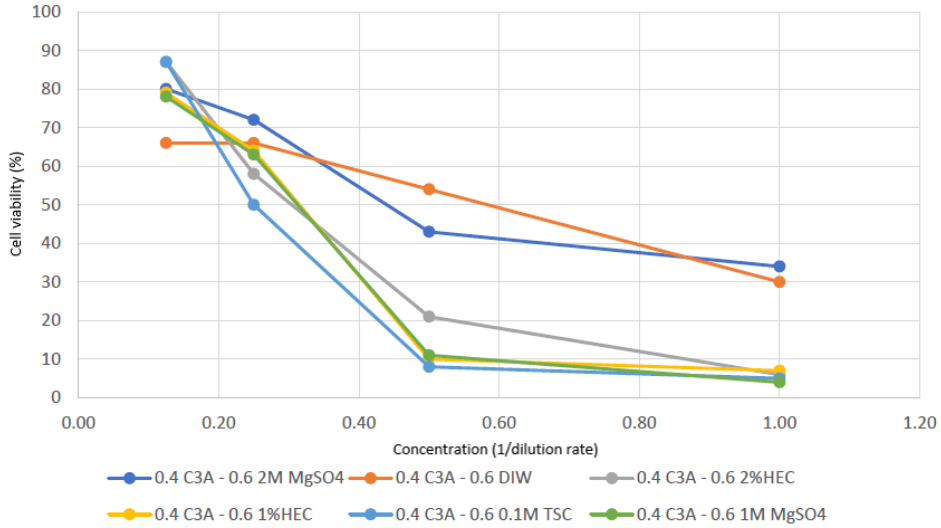

Figure 55. Viability rates of cells contacted with additive C3A cement extracts for 72 hours.

4.2. Rheological characterization of C3A and C3S powder

C3A cement is commonly known to the fastest hardening cement phase was mixed with water at a ratio of 40/60. The samples were mixed for 2 minutes and quickly transferred to the oscillating rheometer and the test was started. The strain amplitude was increased in a wide range (0.01%-100%) of deformation and the point where the microstructure became irregular was determined initially to determine the linear

viscoelastic strain limit (yield strength) of the cement. This point indicates the yield strength moment when the solid structure starts to collapse and shows the upper limit of the shear strain that can be applied constant in other measurements. The yield strength of the cementitious powder suspension was determined to be around 4400 Pa and the corresponding linear viscoelastic strain limit was around 0.25% as given in Figure 56 through this analysis.

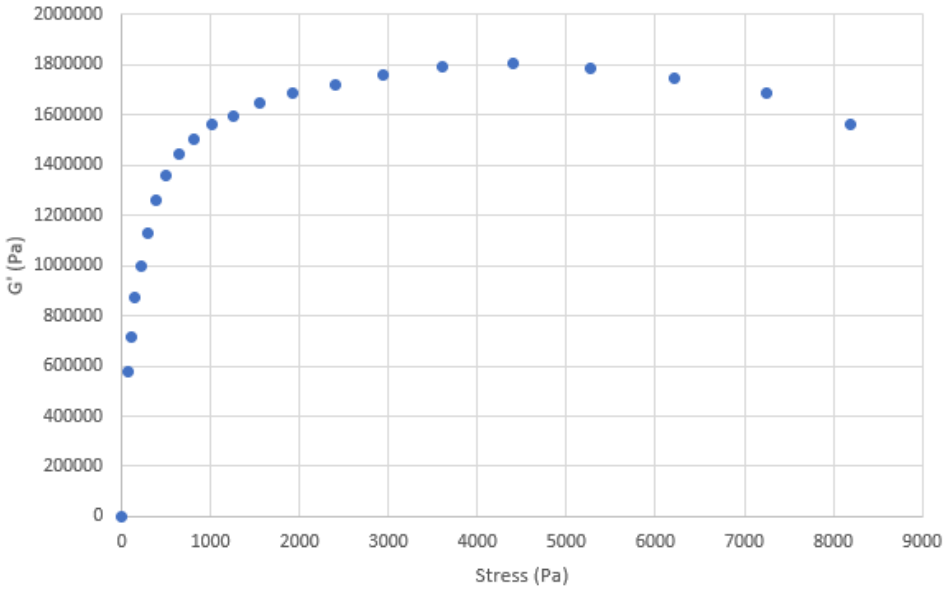

Figure 56. Variation of hardness of C3A cement (60% water-40% solids) with stress.

The setting kinetics determined by time-dependent measurements was determined by using three methods with different applied strain amplitudes. The wave mechanical energy can directly affect the internal structure and change the hardening kinetics with high strains and this phenomenon can be clearly seen in Figure 57. The three different strains used in this analysis each caused a different setting kinetics. During the ever-increasing oscillation the strain amplitude was increased from 0.01% to 100% and during the test the yield strength of the cement was exceeded which caused internal structure collapse. The strain amplitude was kept at the level of 0.1% so that the cement microstructure remained intact during continuous oscillation. The same strain value of 0.1% was used but the measurement took a few seconds during the short oscillation and the sample was removed. A new sample was prepared followed by the application of the same procedure for the next data point. The setting kinetics formed by the unaffected cement internal structure therefore may be observed when short oscillation method is

used. The actual setting kinetics of cement should be measured with this method where a lot of material and time may be wasted. Measurements can be made in one run without exceeding the linear viscoelastic strain limit with continuous oscillation method.

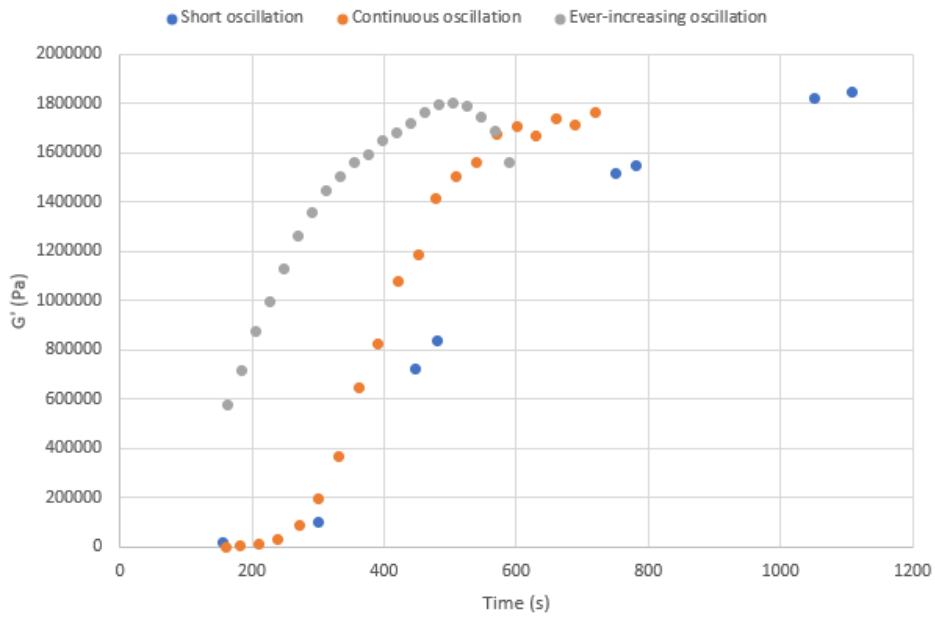

Figure 57. Setting kinetics of C3A cement (60% water-40% solids) measured by three different methods.

The advantage of the short oscillation method is that the complex viscosity value calculated from each data point can give the same value with the normal viscosity measurement with an oscillation-free normal rheometer. According to the Cox-Merz rule, the first data point (zero-shear viscosity or raw viscosity) in the viscosity measurements made by increasing the shear strain rate is equal to the complex viscosity value taken with short oscillation. The zero-shear viscosity which is a characteristic of the internal structure of fluids is determined by the short-release method in the characterization of cements. The zero-shear viscosity values of C3A cement taken at different times are given in Figure 58. The cementitious powder suspension without additives becomes a paste in about 5 minutes at the ratio of 40:60 water and fully hardens in about 20 minutes according to these results and the results are further tabulated in Table 13. This suspension/ink was therefore not suitable for 3D printing and further characterization by capillary rheometer for its injectability was not conducted. The setting rate must be reduced and thus the flow behavior under pressure should be balanced by using various additives.

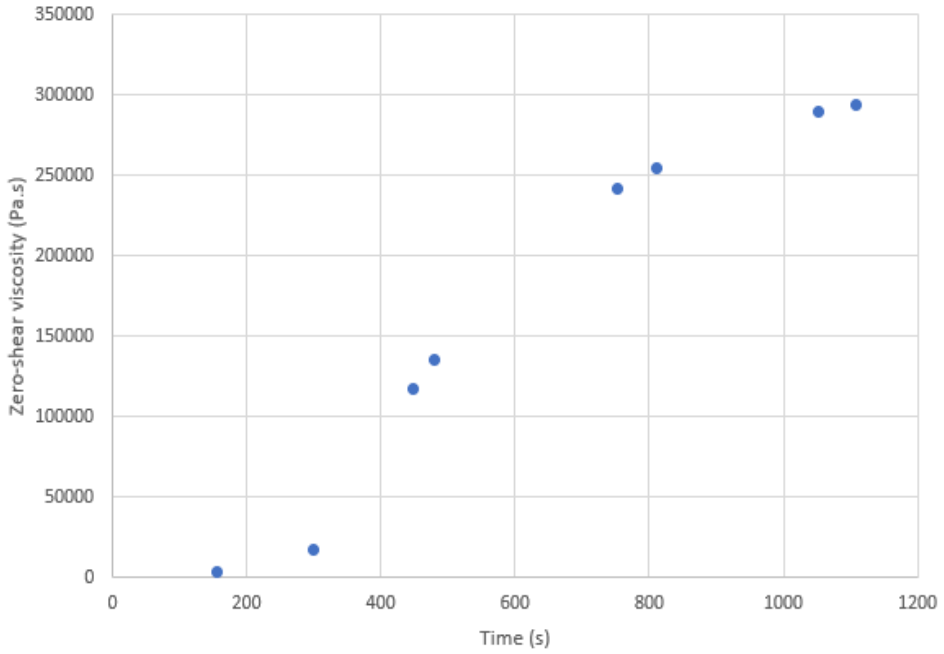

Figure 58. The variation of zero-shear viscosity of C3A cement (60% water-40% solids) as a function of time.

Table 13. Rheological properties of C3A cement (60% water-40% solids).

Cement	Max G' (Pa)	Max zero-shear viscosity (Pa.s)	Setting time (s)	Yield strength (Pa)	Viscosity at yield strength (Pa.s)	Yield strain	Flow time (s)
C3A (%60water)	1,848,086	293,973	1,109	4,401	287,176	0.00244	504

Detailed rheological analyses were carried out on the effect of $MgSO_4$ addition on the setting kinetics of C3A cement. It was first used at 0.5M concentration level and significantly reduced the setting rate. The data obtained with two different measurement methods shown in Figure 59 show that a paste forms in about 20 minutes. The aim of this analysis was to obtain test conditions close to the short oscillation conditions by using low strain amplitude and frequency.

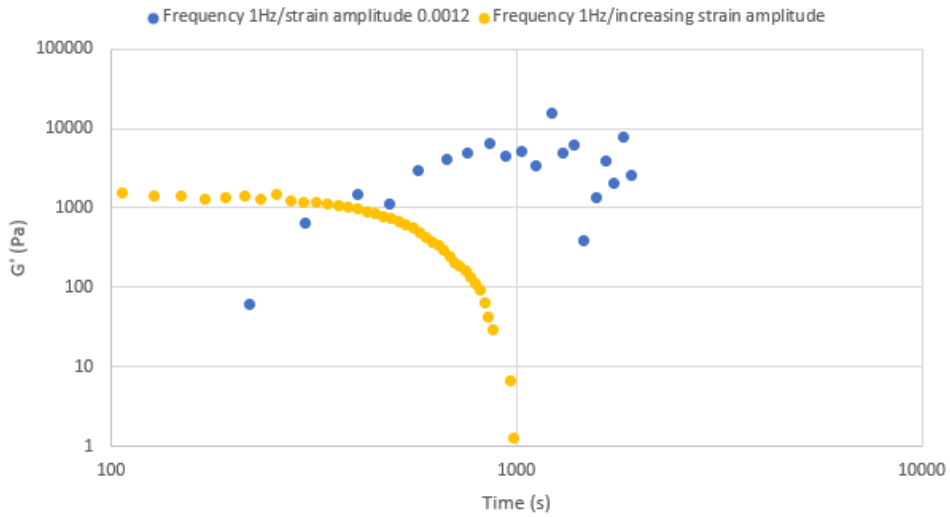

Figure 59. Setting kinetics of C3A cement (60% 0.5M MgSO4 aqueous solution-40% solids) by continuous oscillating measurement.

It was observed that the optimum concentration of $MgSO_4$ was around 1M when five different concentrations were investigated which also have shown a complex effect on C3A powder setting. The setting kinetics seen in Figure 60 remained at the lowest levels for 1M and 1.5M $MgSO_4$. Setting kinetics in the first 2000 seconds is especially important for the processing of 3D inks. The use of 4M MgSO4 solution unexpectedly accelerated setting kinetics of C3A. The reason for this was thought to be the increase in the formation of the ettringite phase as the sulfate concentration increases.

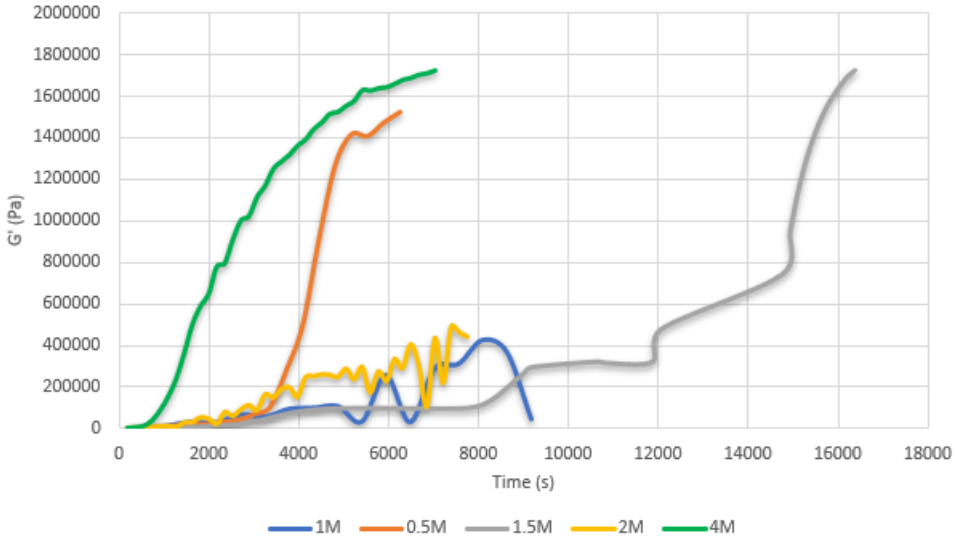

Figure 60. Setting kinetics of C3A cement (60% water-40% solids) at different MgSO4 concentrations.

The variation of the hardness of C3A cementitious powder suspensions containing different $MgSO_4$ contents with strain amplitude is given in Figure 61. It is understood that concentrations with low initial values slow down the hardening. In addition, it is seen that the horizontal length of the initial lines, the yield strength of cements, also changes with concentration, and the most stable microstructure is formed at the 2M. However, this structure collapses completely at the 2% strain amplitude level, and other cements show a more gradual failure. It is thought that the types and proportions of the formed phases have a direct effect on this behavior. According to the results, 1-1.5M $MgSO_4$ should be present in the inks as a standard. Other additives and rates will be tested with this additive.

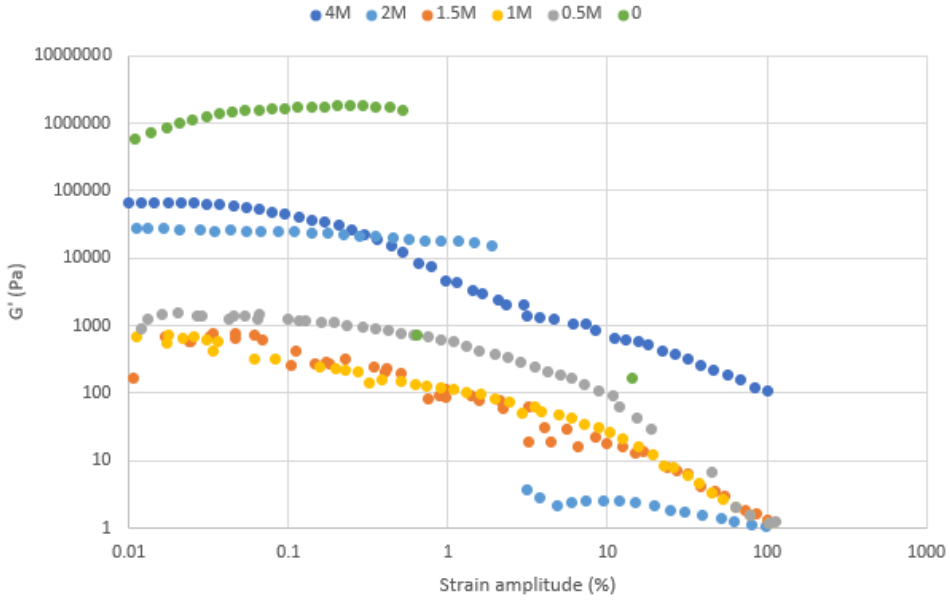

Figure 61. Variation of hardness of C3A cement (60% water-40% solids) with strain amplitude at different MgSO4 concentrations.

The effect of solid/water ratio was investigated in 1M $MgSO_4$ added cement. As seen in Figures 62 and 63, approximately every 5% solid increase increases the consistency of the wet cement 10 times. Ideal ink resistance levels for 3D printing are between 100 and 1000 Pa, this 40:60 ratio can stay at this level for a few minutes. It is aimed to extend this period with other add-ons and thus carry out capillary tests with a balanced flow. Hydroxyethyl cellulose (HEC) was tried as the first additive. HEC, which can reduce the activity of water and increase its viscosity due to its hydrogel feature, is expected to decrease mass transfer in cement. However, as seen in Figure 64, the 2% addition accelerated the cement setting. It is thought that the reason for this is the formation of a polymeric network structure parallel to the hardening of the inorganic cement. The significant increase in the setting rate indicates that more than one

mechanism may be active in the system. It can be seen from Figure 65 that the hydrogel addition increases the solid network structure similar to the particle addition.

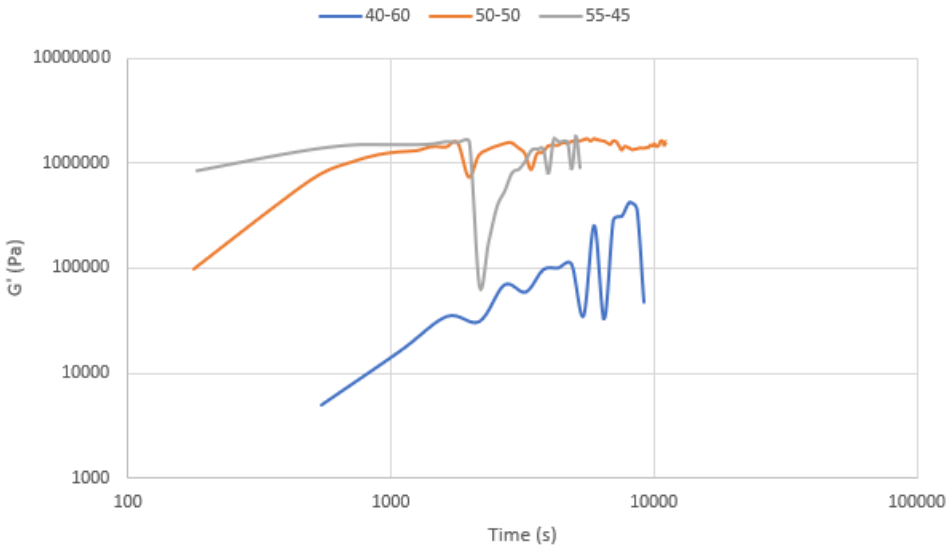

Figure 62. Setting kinetics of 1M MgSO4 added C3A cement by continuous oscillating measurement at different solid-water ratios.

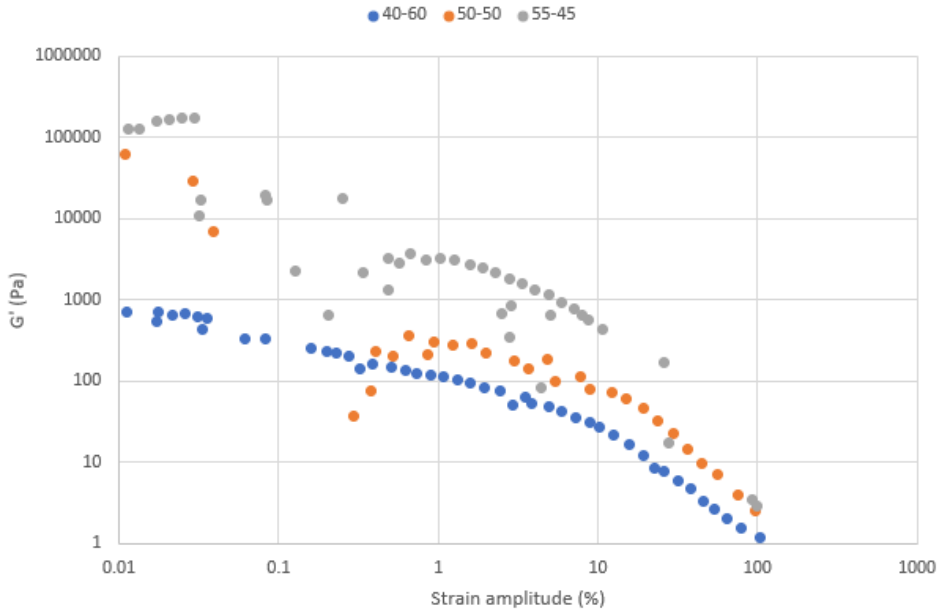

Figure 63. Variation of hardness of 1M MgSO4 added C3A cement with oscillation amplitude at different solid-water ratios.

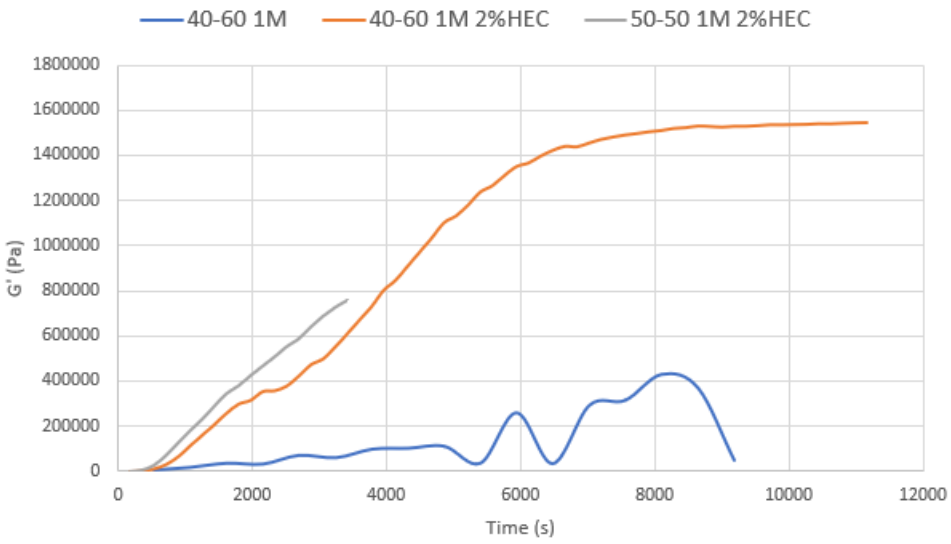

Figure 64. Change of setting kinetics of 1M MgSO4 added C3A cement at different solid-water ratios and HEC addition.

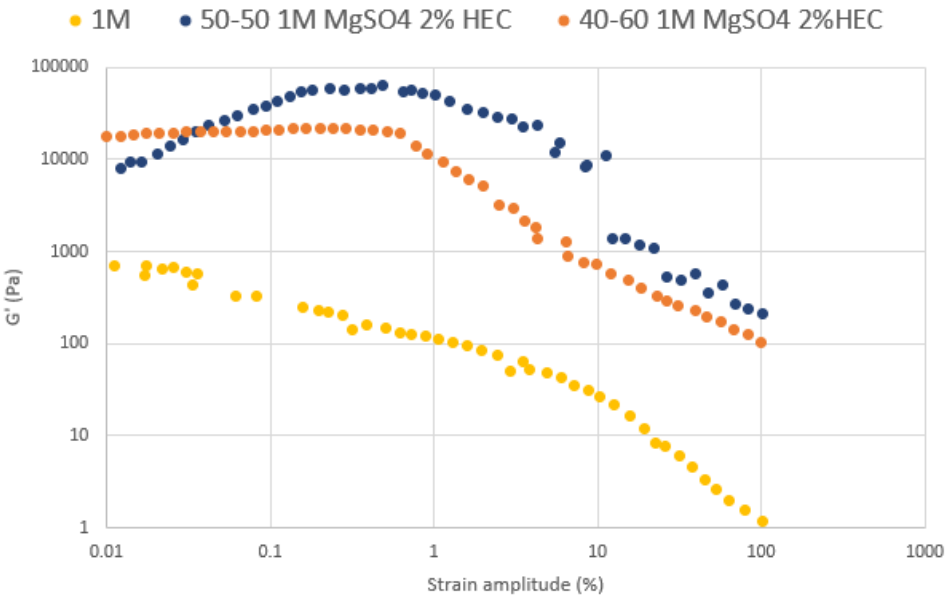

Figure 65. Variation of hardness of 1M MgSO4 added C3A cement with different solid-water ratios and HEC addition.

Polyethylene glycol-400 (PEG), marble powder ($CaCO_3$), and quartz (SiO_2) have also been tried as additives in C3A-based inks. Figures 66 and 67 show the effects of these additives on the setting kinetics and yield strength, respectively. 1% PEG slowed the hardening of the cement. Especially in the wet cement phase, it significantly reduced the consistency. This is thought to be because PEG acts as a lubricant to reduce particle friction and entanglement. Figure 67 shows that the combination of PEG with HEC is

more effective in reducing early hardening. Marble powder was used in addition to the cement, HEC, and PEG at rates of 10% and 20%. These two ratios provided very different set kinetics and flow stability. Marble powder provided an extremely fast setting at the level of 10%, while its yield strength remained low compared to this. At the 20% level, the overall setting rate decreased significantly, while the yield strength remained high at the level of the HEC and PEG combination. Quartz, the other particle additive tried, was added to the marble powder system at a rate of 10%. It was observed that it did not change the hardness much, but slowed down the initial increase. According to the data obtained, 1.5M $MgSO_4$ and 1% PEG should be present in C3A ink. 2% HEC and 20% marble dust have a positive effect when combined with PEG. The rheological properties of all additives are shown in Table 14.

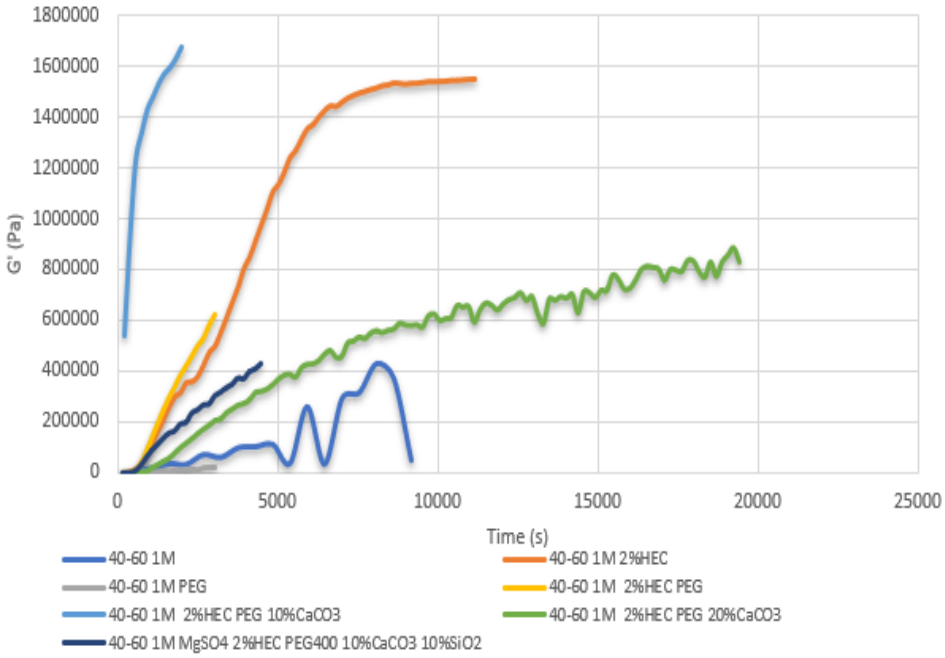

Figure 66. Change of setting kinetics of 1M MgSO4 retarded C3A cement (60% water-40% solids) with different additives.

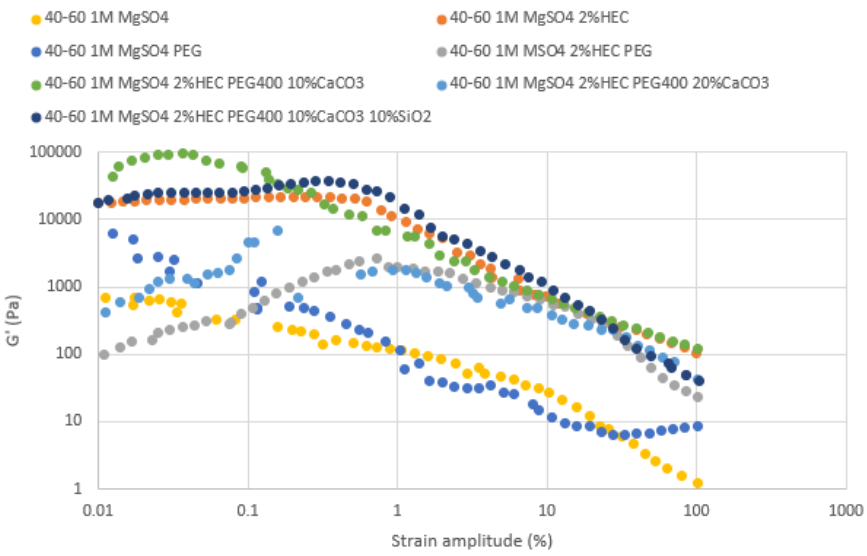

Figure 67. Variation of the hardness of 1M MgSO4 retarded C3A cement (60% water-40% solids) with different additives.

Table 14. Rheological properties of C3A cements modified with various additives

C3A additives	Max G' (Pa)	Max zero-shear viscosity (Pa.s)	Setting time (s)	Yield strength (Pa)	Viscosity at yield strength (Pa.s)	Yield strain	Flow time (s)
%60 0.5M MgSO4	1520641	242368	6241	1.12	273	0.00065	376
%60 1M MgSO4	47597	9650	9300	0.13	121	0.00017	205
%60 1.5M MgSO4	1726133	274839	16500	0.28	133	0.00034	290
%60 2M MgSO4	443776	73504	7861	3.72	4474	0.00013	376
%60 4M MgSO4	1726103	274761	7139	9.85	10787	0.00015	183
%50 1M MgSO4	1604725	255708	11280	8.5	12466	0.0001	355
%45 1M MgSO4	1797041	286221	5161	45.75	29170	0.00025	247
%60 1M MgSO4 %2HEC	1547787	246744	11282	52.64	3432	0.0024	504
%60 1M MgSO4 PEG	20895	3640	3181	0.99	1275	0.00012	162
%60 1M MgSO4 %2HEC PEG	624622	100051	3180	22.26	491	0.0072	624

Cont. on the next page

Cont. of Table 14.

%60 1M MgSO4 %2HEC PEG %10CaCO3	1676024	266819	2100	37.53	16267	0.00036	290
%60 1M MgSO4 %2HEC PEG %20CaCO3	828921	132937	19559	12.37	1241	0.0016	462
%60 1M MgSO4 %2HEC PEG %10CaCO3 %10SiO2	425964	75230	4620	134.31	6168	0.0035	543

The setting kinetics and yield strength of C3S cement are given in Figures 68 and 69. In the graph of variation of hardness with strain amplitude, it is seen that the most stable structure between 100-1000 Pa, which is the most suitable module range for 3D writing, is obtained at 60% solids-40% water. It is seen that the yield strength of cement is around 700 Pa. The linear viscoelastic strain limit corresponding to this value is 0.0003. Both values are approximately one-seventh compared to C3A cement. The amplitude value of the short oscillations applied to measure the hardening kinetics was set at the level of 0.0002. According to the measurements, the cement reached a low hardness of 24000 Pa within 20 minutes.

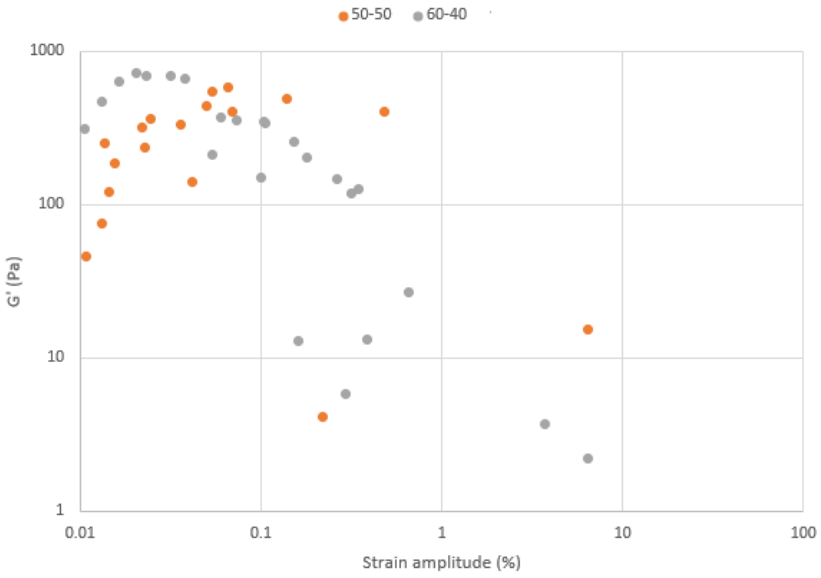

Figure 68. Variation of hardness values of C3S cement with strain amplitude at two different solid/water ratios.

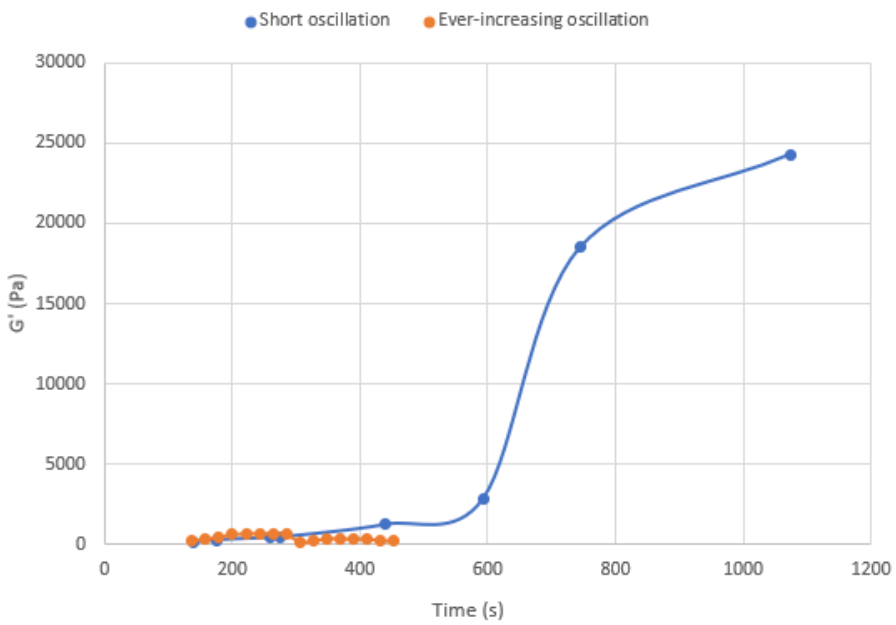

Figure 69. Measurement of setting kinetics of C3S cement (40% water - 60% solids) by two methods.

When the rheological behavior of C3S cement at three different gluconic acid concentrations was examined, it was observed that gluconic acid had a retarding effect on setting. However, 2M GA accelerated the setting kinetics (Figure 70). According to the results, 0.5M-1M Gluconic acid should be in the ink as a standard.

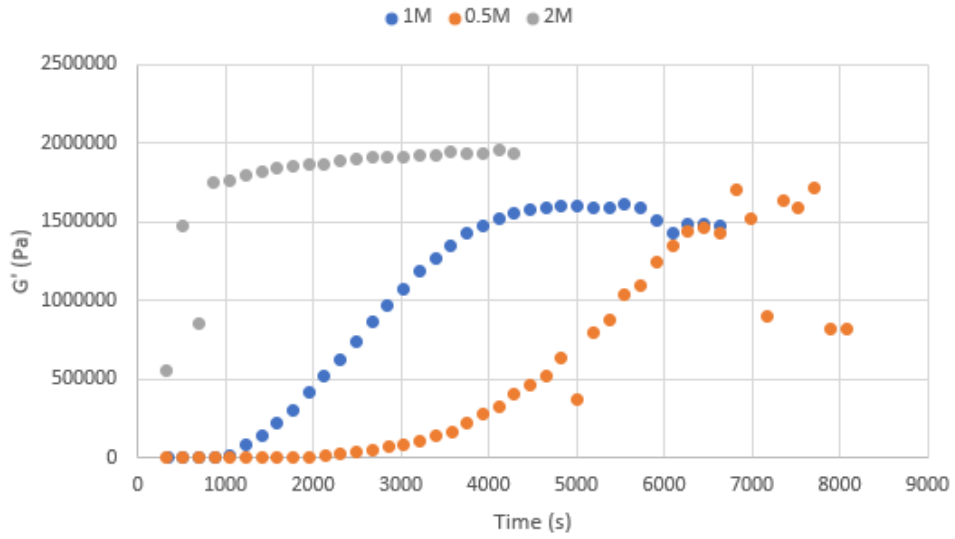

Figure 70. Setting kinetics of C3S cement (60% solids-40% water) at different Gluconic acid concentrations.

The addition of HEC to C3S showed the same effect as in C3A and accelerated the setting kinetics. In addition, it has increased the solid network structure and strength.

The addition of marble powder had a great effect on C3A, while it delayed the setting time of C3S a little (Figure 71). Therefore, only gluconic acid and different percentages of marble dust were also investigated. As seen in Figure 72, it was determined that marble powder increased the setting kinetics and strength.

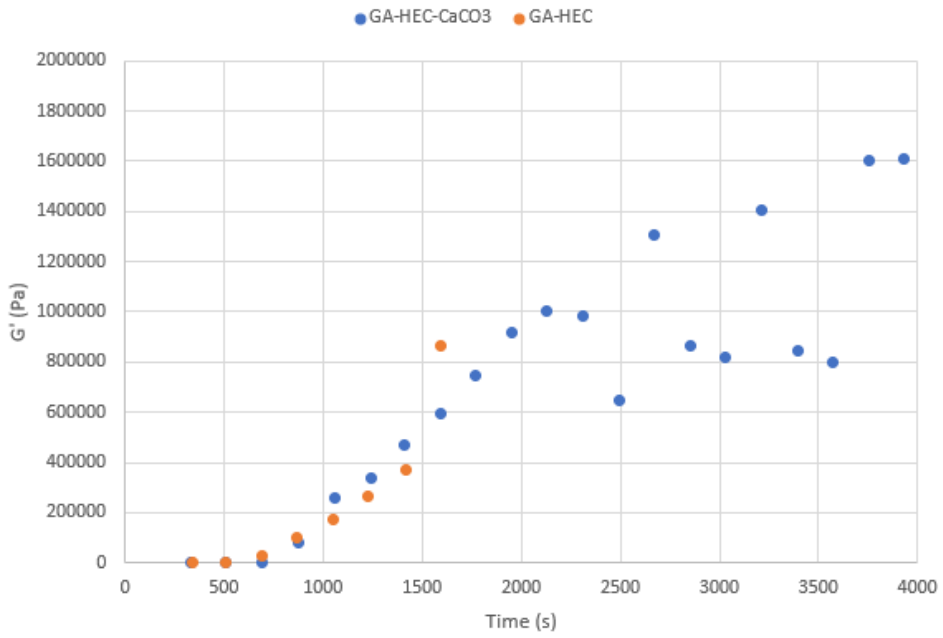

Figure 71. Setting kinetics of 1M GA C3S cement with HEC and 10% CaCO3.

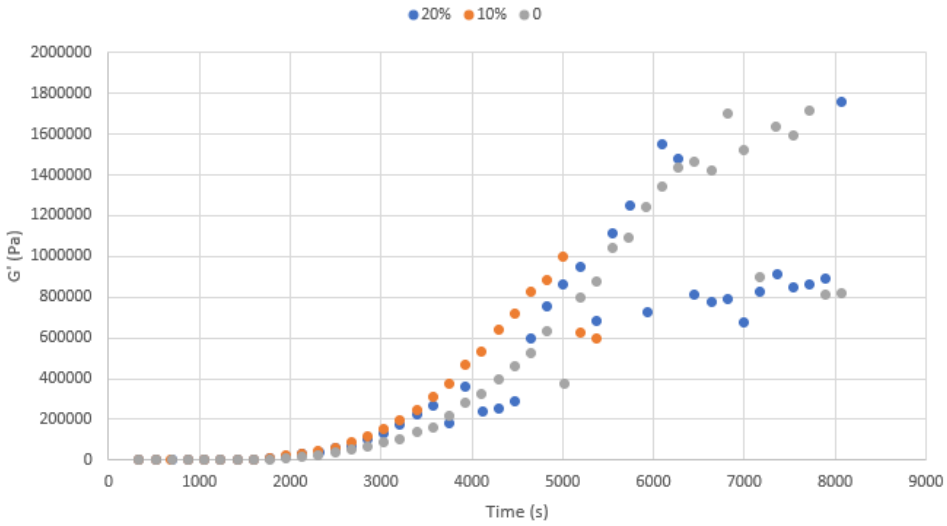

Figure 72. Setting kinetics of 1M GA C3S cement with 10% CaCO3, 20% CaCO3 and without CaCO3

Other additives tried are Polyethylene Glycol 400 (PEG), Trisodium Citrate (TSC), and Sodium Dodecyl Sulfate (SDS). Figure 73 shows the effect of PEG additive on C3S setting kinetics. In contrast to C3A, the addition of PEG accelerated the setting

kinetics of C3S cement. However, as it can be seen in Figure 74, the TSC additive has slowed the setting kinetics considerably since it acts as a lubricant. The SDS additive slowed the hardening kinetics and increased the strength in the same way as TSC (Figure 75). The SDS additive was studied separately with both HEC and PEG. C3S cement containing HEC and SDS showed more stable kinetics (Figure 76).

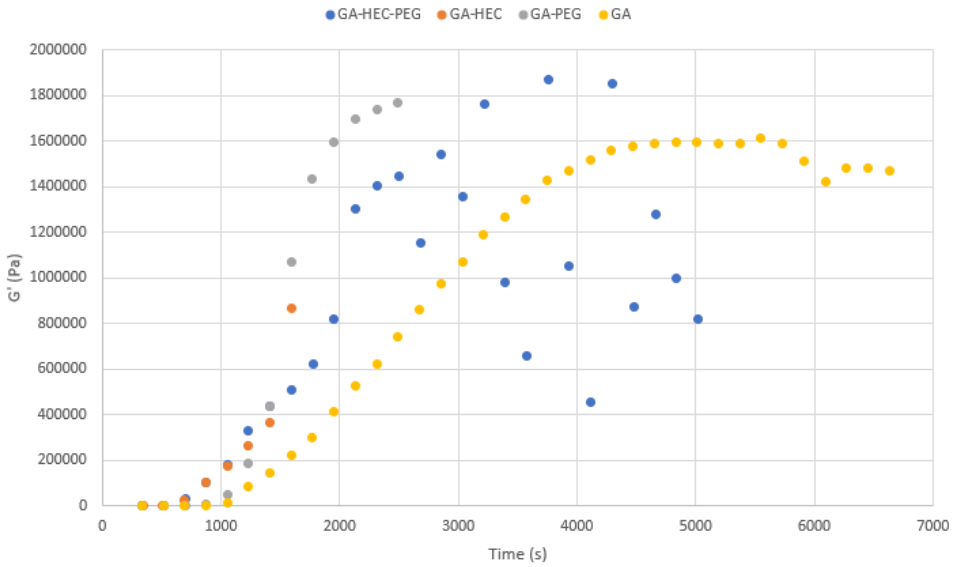

Figure 73. Setting kinetics of 1M GA, HEC C3S cement with PEG.

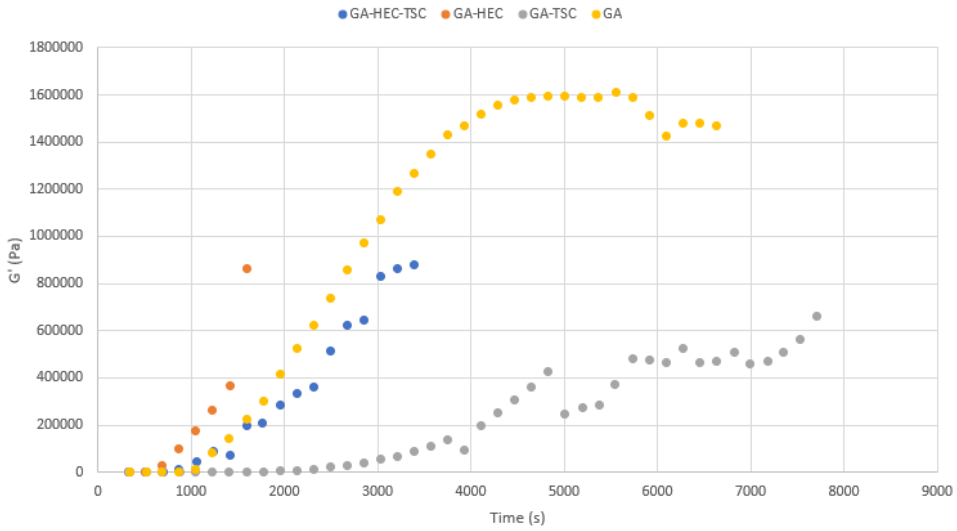

Figure 74. Setting kinetics of C3S cement with different additives and TSC effect.

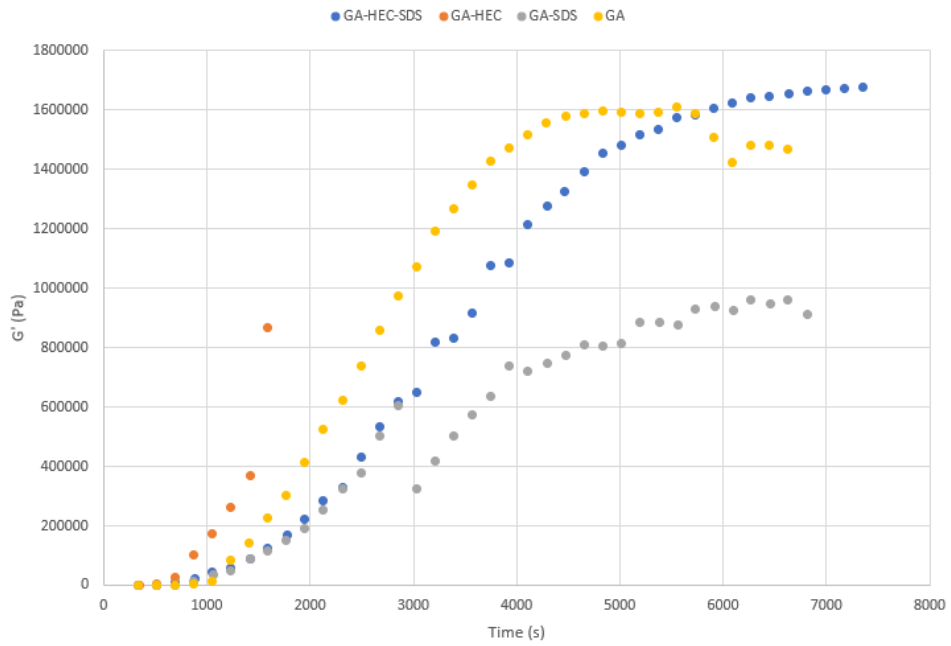

Figure 75. Setting kinetics of 1M GA, HEC and C3S cement with SDS.

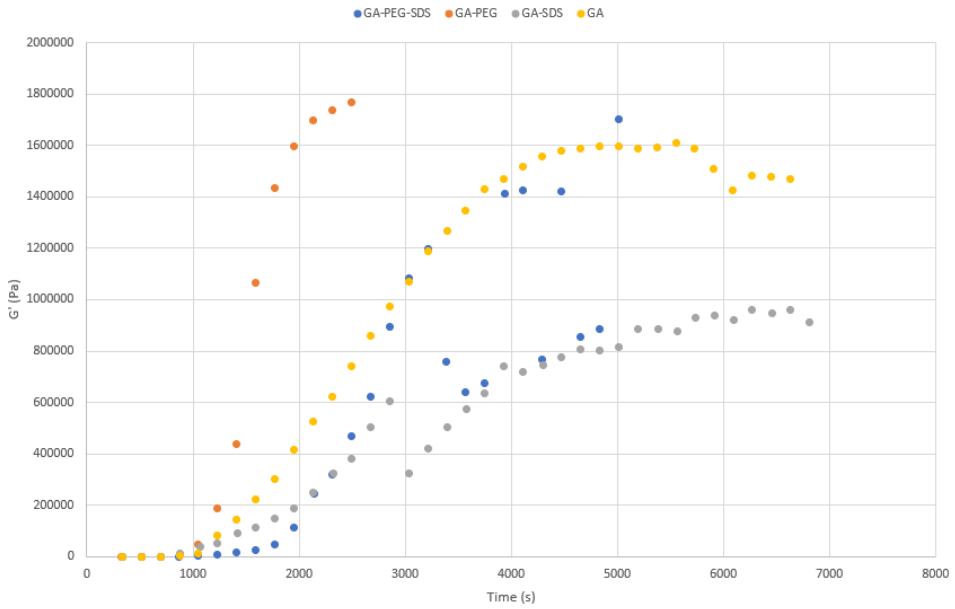

Figure 76. Setting kinetics of 1M GA, PEG and C3S cement with SDS.

Capillary rheometers basically work on the principle of pushing the fluid in a long pipe from the large chamber and removing it from the channel on the other side. The speed of the pushed piston determines the shear strain rate while the force applied to the piston determines the shear stress. It is possible to provide high-precision flow over a wide range of piston speeds and to measure the force exerted on the fluid with the

computer-controlled pusher. The data obtained from the capillary rheometer will determine the initial properties of the inks for 3D printing.

In addition to the C3A cement stabilized with HEC and PEG hydrogels and retarded with $MgSO_4$, 10% quartz powder was added for the diluent function. Flow tests under pressure performed under three different conditions are given in Figure 77. The flow was unbalanced because the forces applied at a high L/D ratio caused more stress in the internal structure. The resistance applied by the material to the piston as it advanced at a constant speed of 15 mm/min increased continuously and an irregular flow was observed. The presence of stable flow can be seen in Figure 77 for the tests conducted with D=2 mm. The flow behavior of the ink shown in Figure 78 was similar to the previous one where marble dust was added instead of quartz. The paste with this composition flowed through the high L/D ratio channel where the other was blocked. The cementitious powder suspensions/pastes generally flowed evenly under different conditions despite minor pressure fluctuations. The 10% $CaCO_3$ addition caused an increasing effect on the cement hardening rate according to the oscillating rheometer results which may be the reason for the force fluctuations observed in the capillary rheometer tests.

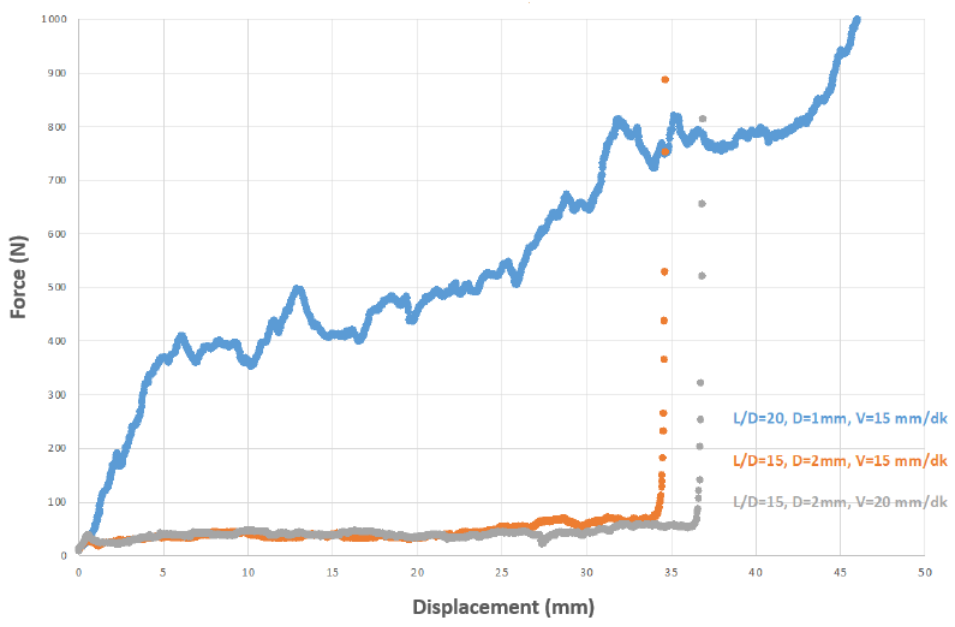

Figure 77. Flow behavior of C3A-based ink under pressure containing quartz powder, PEG, HEC and MgSO4.

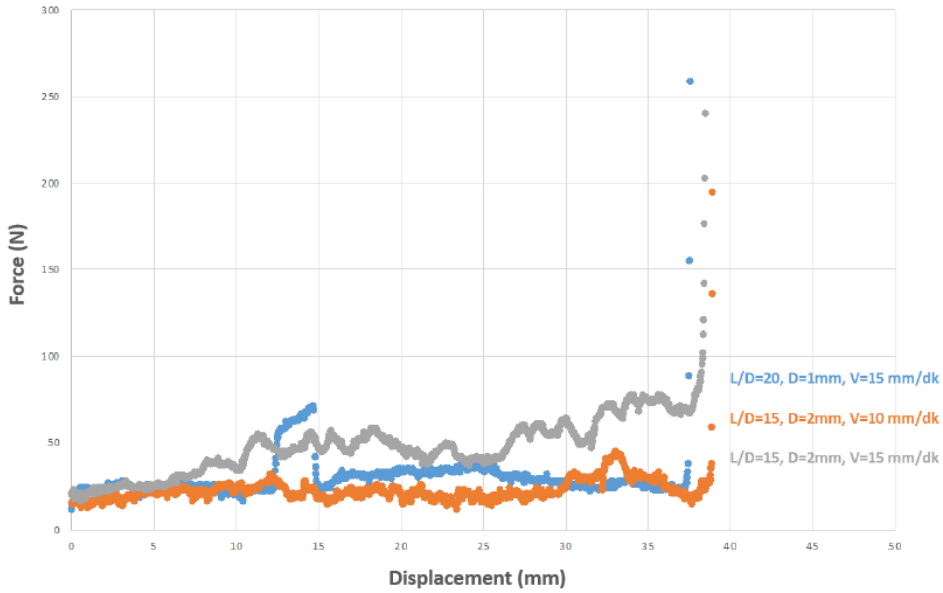

Figure 78. Flow behavior of C3A-based ink under pressure containing marble powder, PEG, HEC and MgSO4.

The effect of the addition of both solid additives together under similar conditions reduced the flow imbalance as clearly shown in Figure 79. The use of two additives at a total level of 20% caused the ink to behave more fluid like which can be supported by the decrease in the setting rate observed in the oscillating rheometer analysis. High L/D ratios and low flow rates are common conditions that make fluid flow difficult to maintain. The PEG-free version of the bi-solid ink showed uneven flow especially at high L/D ratios and low velocities as given in Figure 80. It can be concluded that it has a similar but more difficult-flowing internal structure compared to ink with only quartz particles. The use of trisodium citrate which is commonly used as an electrostatic stabilizer and dissolution inhibitor to provide more stable flow had an adverse effect on the C3A-based ink system injectability. The addition of trisodium citrate caused the highest loads and stresses as seen in Figure 81. The addition of silica gel to the C3A system containing HEC and PEG where marble powder is the only solid additive ensures that the polymeric network structure becomes stronger and therefore has a more stable internal structure. The flow behavior seen in Figure 82 shows low flow resistance despite the high polymer content.

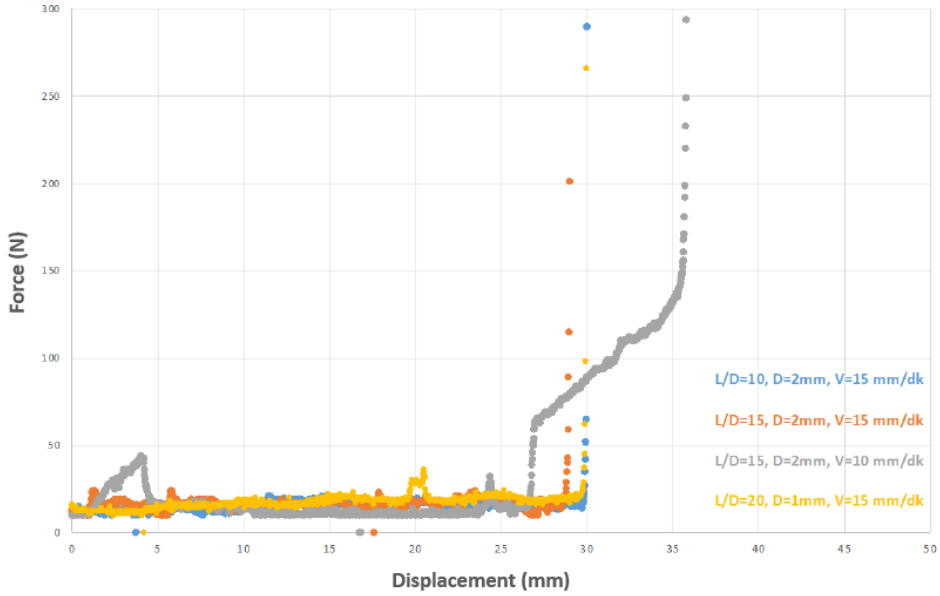

Figure 79. Flow behavior of C3A based ink under pressure containing marble powder, quartz powder, PEG, HEC and MgSO4.

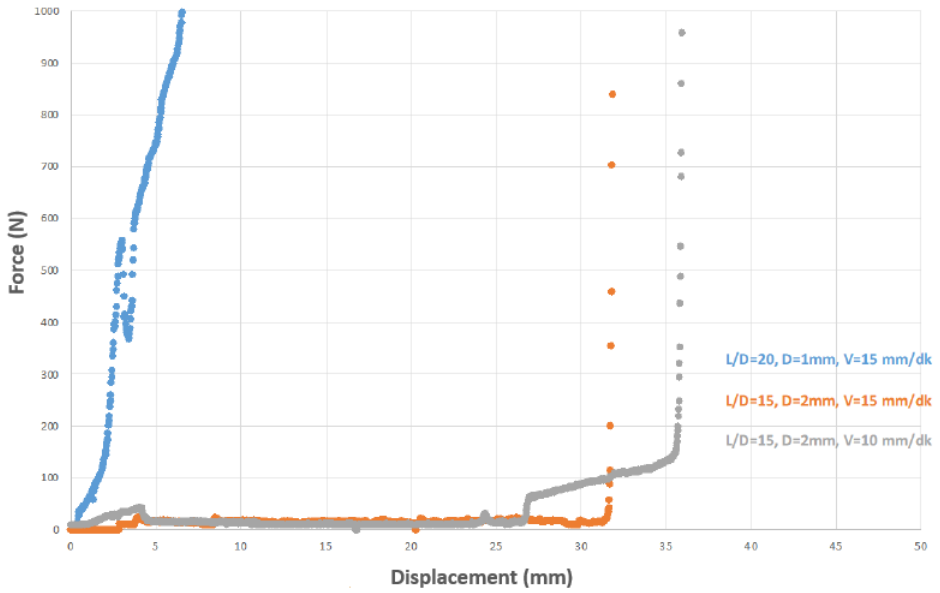

Figure 80. Flow behavior of C3A-based ink under pressure containing marble powder, quartz powder, HEC and MgSO4.

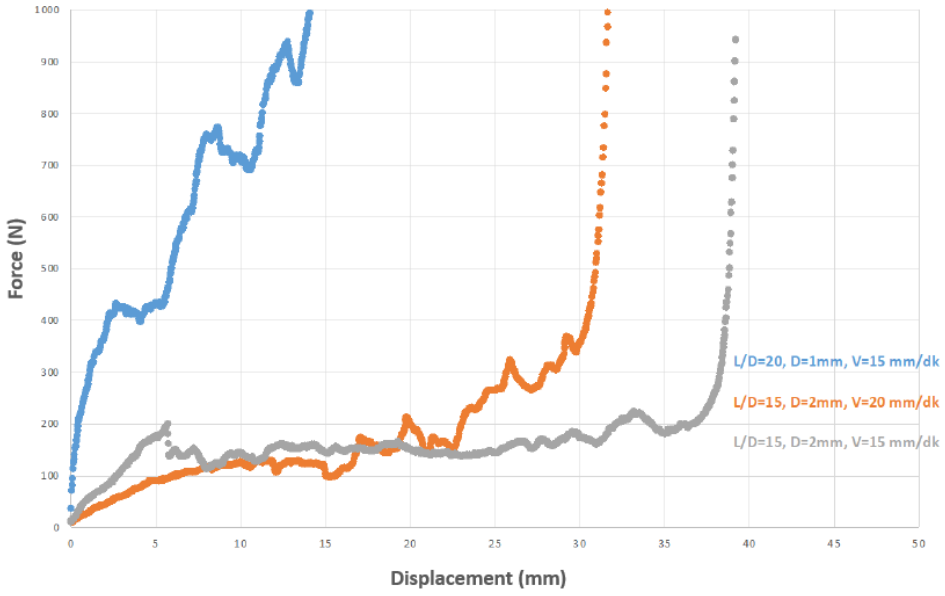

Figure 81. Flow behavior of C3A based ink under pressure containing marble powder, quartz powder, TSC, HEC and MgSO4.

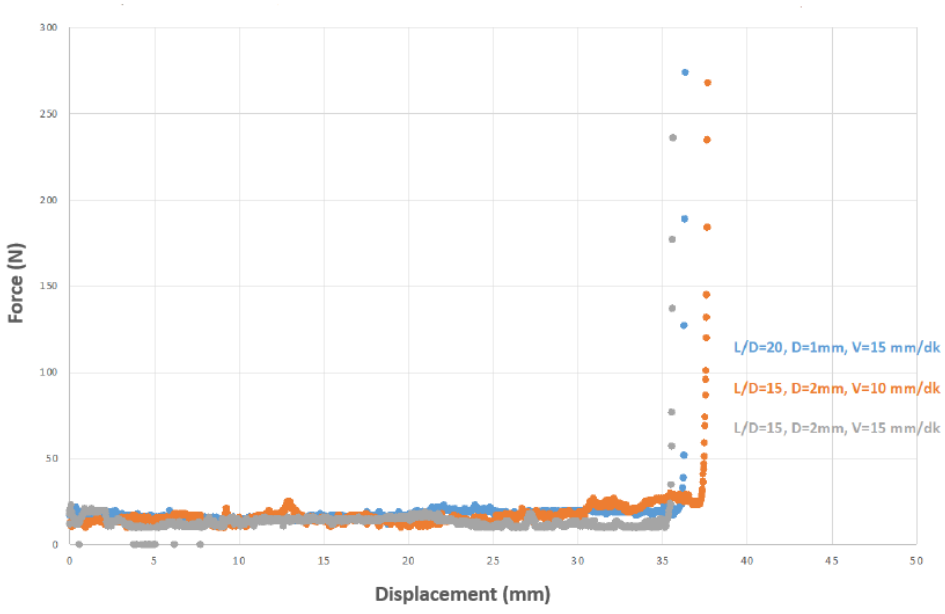

Figure 82. Flow behavior of C3A based ink under pressure containing marble powder, silica gel, PEG, HEC and MgSO4.

The same additives were mixed with C3S cementitious powder and their effects on flow behavior under pressure were tested under the same conditions. The effects of the gluconic acid use were initially investigated. The flow behavior shown in Figure 83 was completely unstable. The relatively stable flow curves given in Figure 84 show that C3S

can flow evenly only in HEC medium without the addition of any retarder. Ink can lose its balance at low speeds however causing a harder paste flow. It is important to add an optimum level of gluconic acid for C3S-based inks. The presence of relatively balanced flows by these two additions can be clearly seen in Figure 85. The most stable flow was achieved despite the high L/D and low velocity causing difficult flow conditions. Due to the positive effects of PEG in the C3A system, it was also added to the C3S system. HEC and PEG combinations were especially effective in maintaining flow balance in both systems. The flow behavior of the inks with the addition of PEG and marble powder to the previous sample is shown in Figure 86. The HEC-PEG combination provided stable flow under low flow rate and high L/D conditions. Flow without fluctuations were obtained under the most severe conditions for paste flow of L/D=20 and V=5mm/min. The combined use of marble powder and quartz generally had a positive effect on the tested cementitious powder suspensions. This was especially seen in fast-setting cementitious inks. The increased resistance to flow in HEC and GA containing C3S inks is shown in Figure 87. The highly stable flow behavior seen in Figure 88 was achieved by simply adding PEG to the previous sample. It was concluded that PEG should be present as a stabilizer in inks besides the beneficial effects of marble powder and quartz.

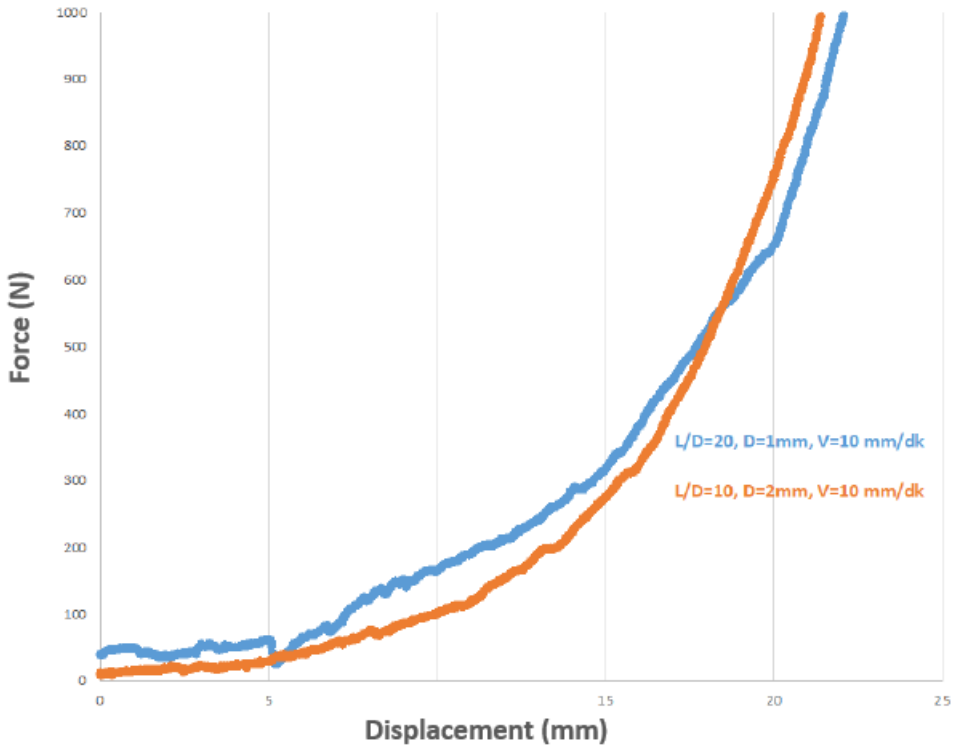

Figure 83. Flow behavior of 2M gluconic acid added C3S cement under pressure.

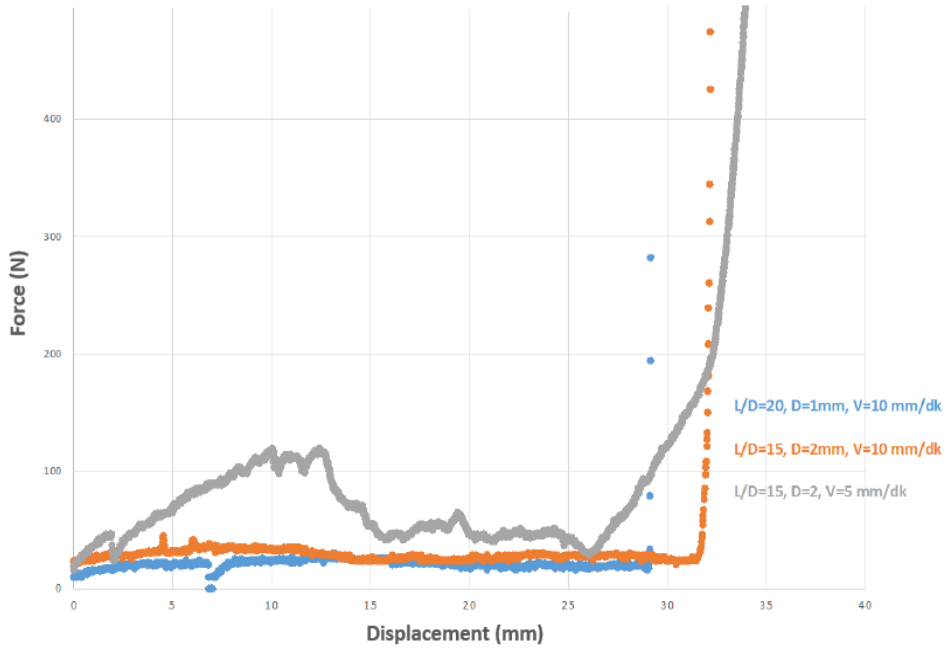

Figure 84. Flow behavior of C3S cement with 2.5% HEC additives under pressure.

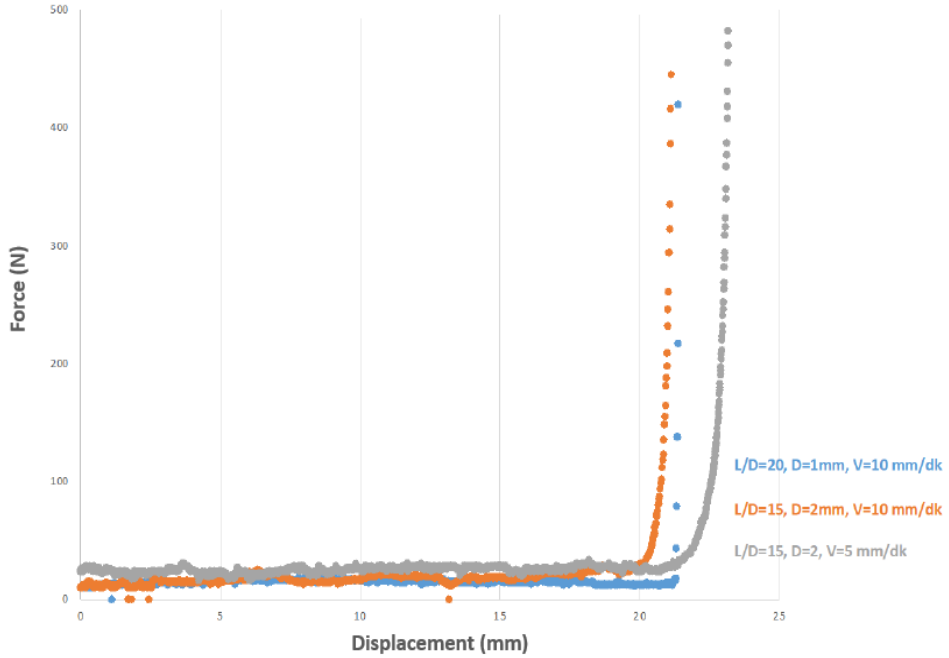

Figure 85. Flow behavior of HEC and Gluconic acid added C3S cement under pressure.

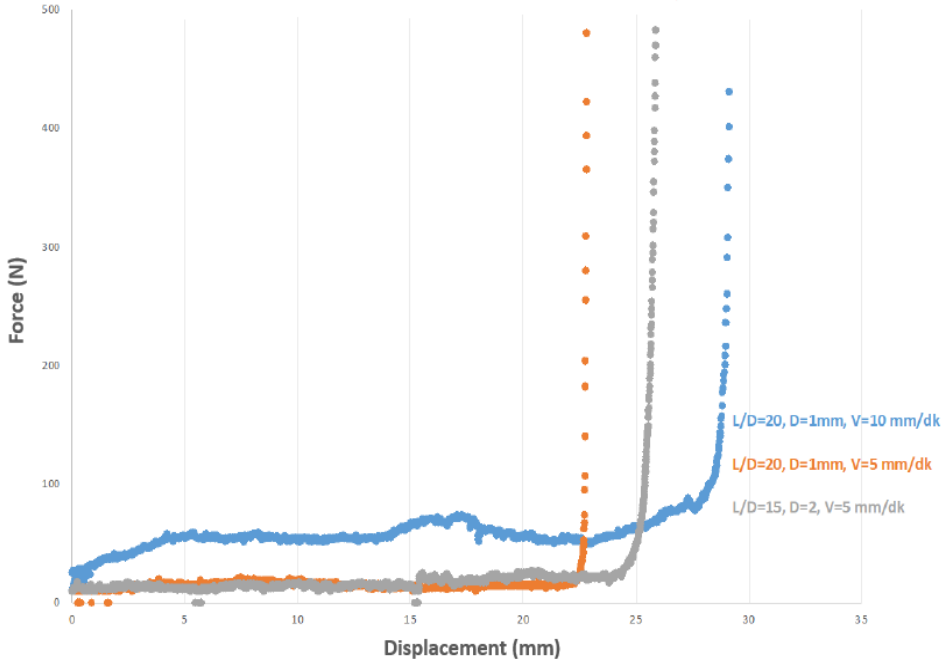

Figure 86. Flow behavior of C3S cement with HEC, Gluconic acid and marble powder additives under pressure.

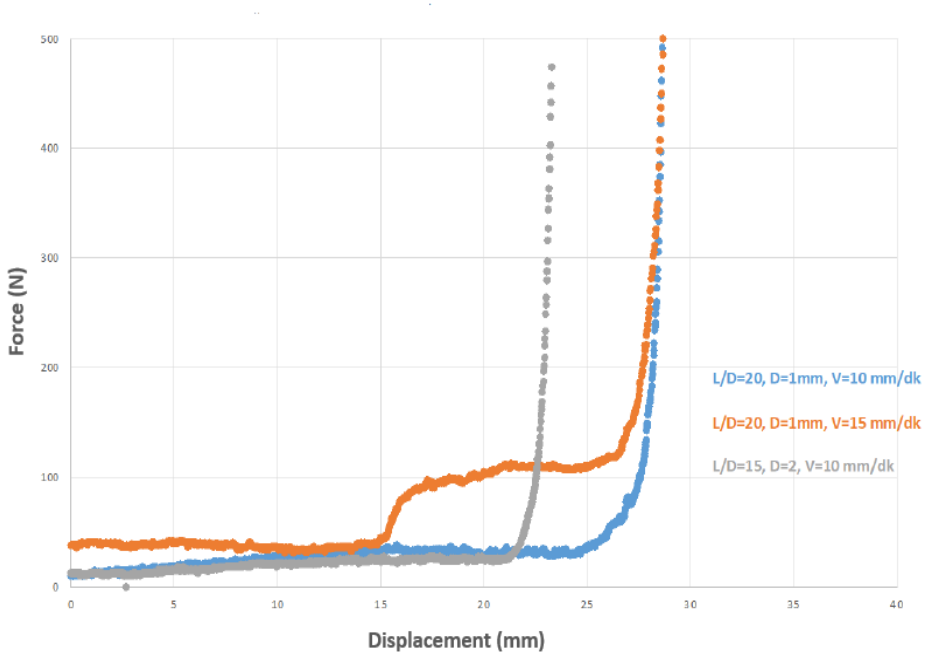

Figure 87. Flow behavior of C3S cement with HEC, Gluconic acid, marble powder and quartz powder additives under pressure.

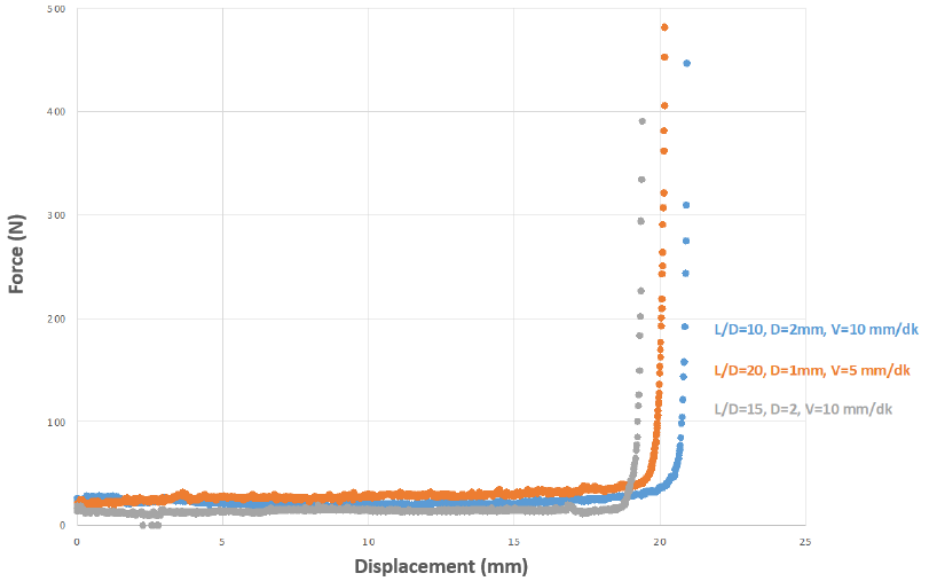

Figure 88. Flow behavior of C3S cement with HEC, PEG, Gluconic acid, marble powder and quartz powder additives under pressure.

Images of filaments produced from various inks are given in Figures 89-104.

Figure 89. The filament formed as a result of the extrusion test (12.2 gr c3a 1.525 gr marble powder 1.525 gr quartz 5 gr 3.17 hec 5 gr 4m MgSO4 L/D 15 2mm nozzle 10 mm/min).

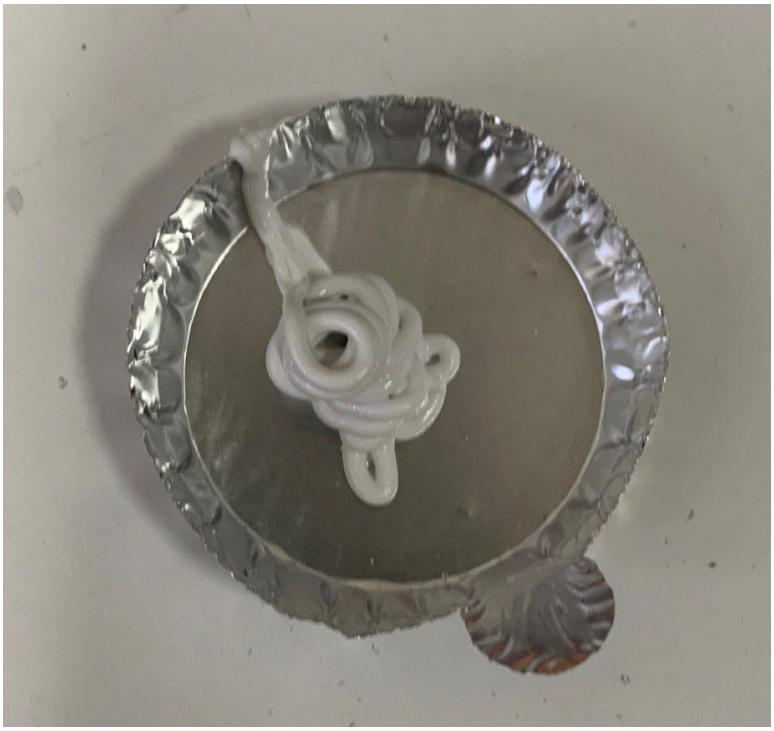

Figure 90. The filament formed as a result of the extrusion test (12.2 gr c3a 1.525 gr marble powder 1.525 gr quartz 5 gr 3.17 hec 5 gr 4m MgSO4 L/D 15 2mm nozzle 15 mm/min).

Figure 91. The filament formed as a result of the extrusion test (12.2 gr c3a 1.525 gr marble powder 1.525 gr quartz 5 gr 3.17 hec 5 gr 4m MgSO4 L/D 20 15 mm/min).

Figure 92. The filament formed as a result of the extrusion test (12.2 gr c3a 1.525 gr marble powder 1.525 gr quartz 2 gr 0.1 M trisodium citrate 4 gr 3.17 hec 4 gr 4m MgSO4 L/D 20 15 mm/min).

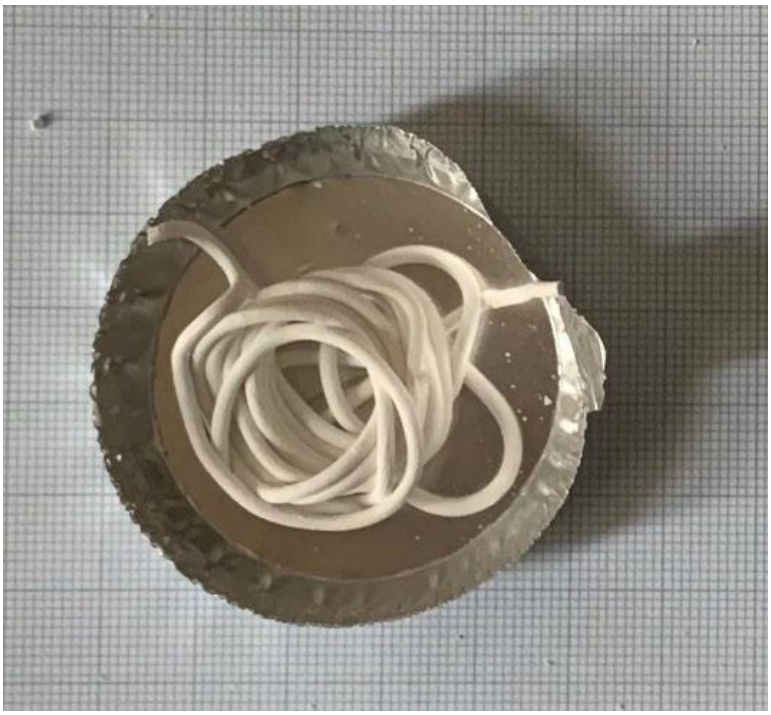

Figure 93. The filament formed as a result of the extrusion test (12.2 gr c3a 1.525 gr marble powder 1.525 gr quartz 2 gr 0.1 M trisodium citrate 4 gr 3.17 hec 4 gr 4m MgSO4 L/D 20 15 mm/min).

Figure 94. The filament formed as a result of the extrusion test (12.2 gr c3a 1.525 gr marble powder 1.525 gr silica gel 2 gr peg 400 4 gr 3.17 hec 4 gr 4m MgSO4 L/D 15 2mm nozzle 10 mm/min)

Figure 95. The filament formed as a result of the extrusion test (12.2 gr c3a 1.525 gr marble powder 1.525 gr silica gel 2 gr peg 400 4 gr 3.17 hec 4 gr 4m MgSO4 L/D 15 2mm nozzle 15 mm/min).

Figure 96. The filament formed as a result of the extrusion test (13.725 gr c3a 1.525 gr marble powder 2 gr peg 400 4 gr 3.17 hec 4 gr 4m MgSO4 L/D 15 2mm nozzle 10 mm/min).

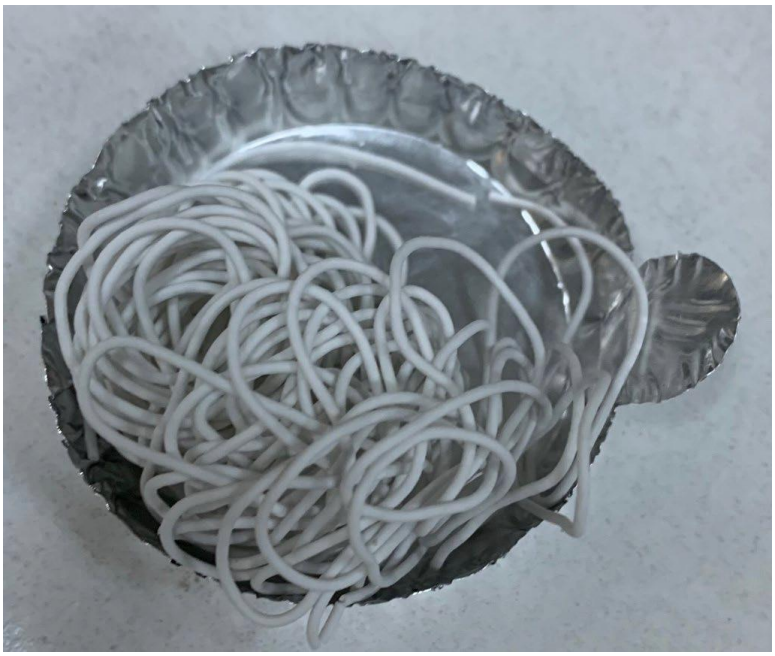

Figure 97. The filament formed as a result of the extrusion test (13.725 gr c3a 1.525 gr quartz 2 gr peg 400 4 gr 3.17 hec 4 gr 4m MgSO4 L/D 20 15 mm/min)

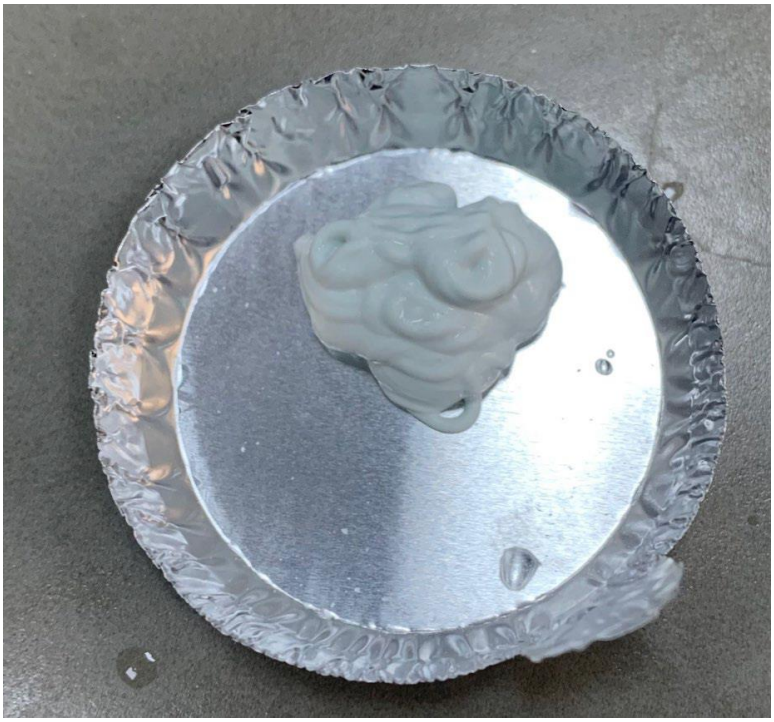

Figure 98. The filament formed as a result of the extrusion test (12gr c3s 6 gr 2.5 hec L/D 20 10 mm/min).

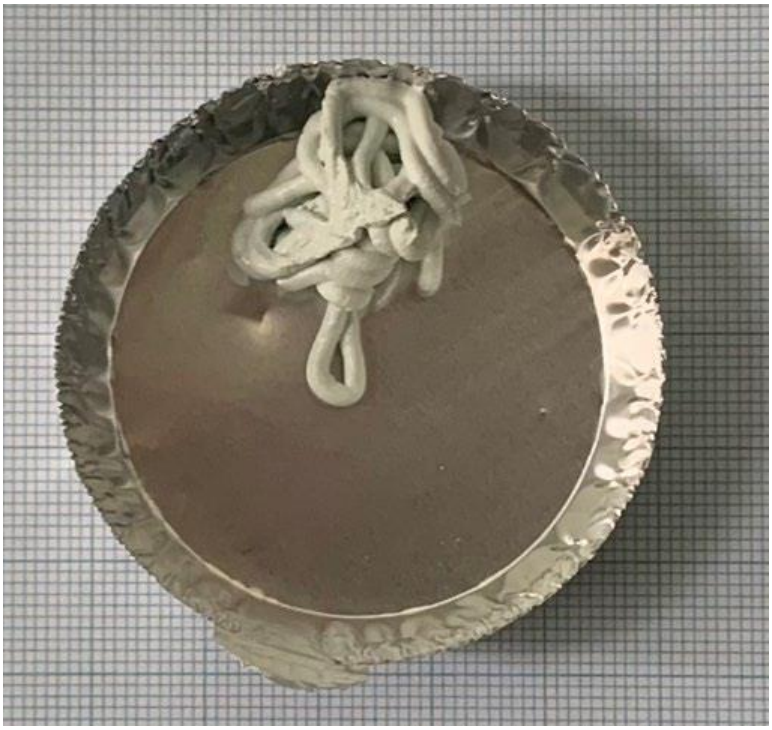

Figure 99. The filament formed as a result of the extrusion test (10.8 gr c3s 1.2 gr marble powder 3gr 2.5 wt hec 2gr 2M GA 1 gr peg 400 L/D 15 2mm nozzle 5 mm/min).

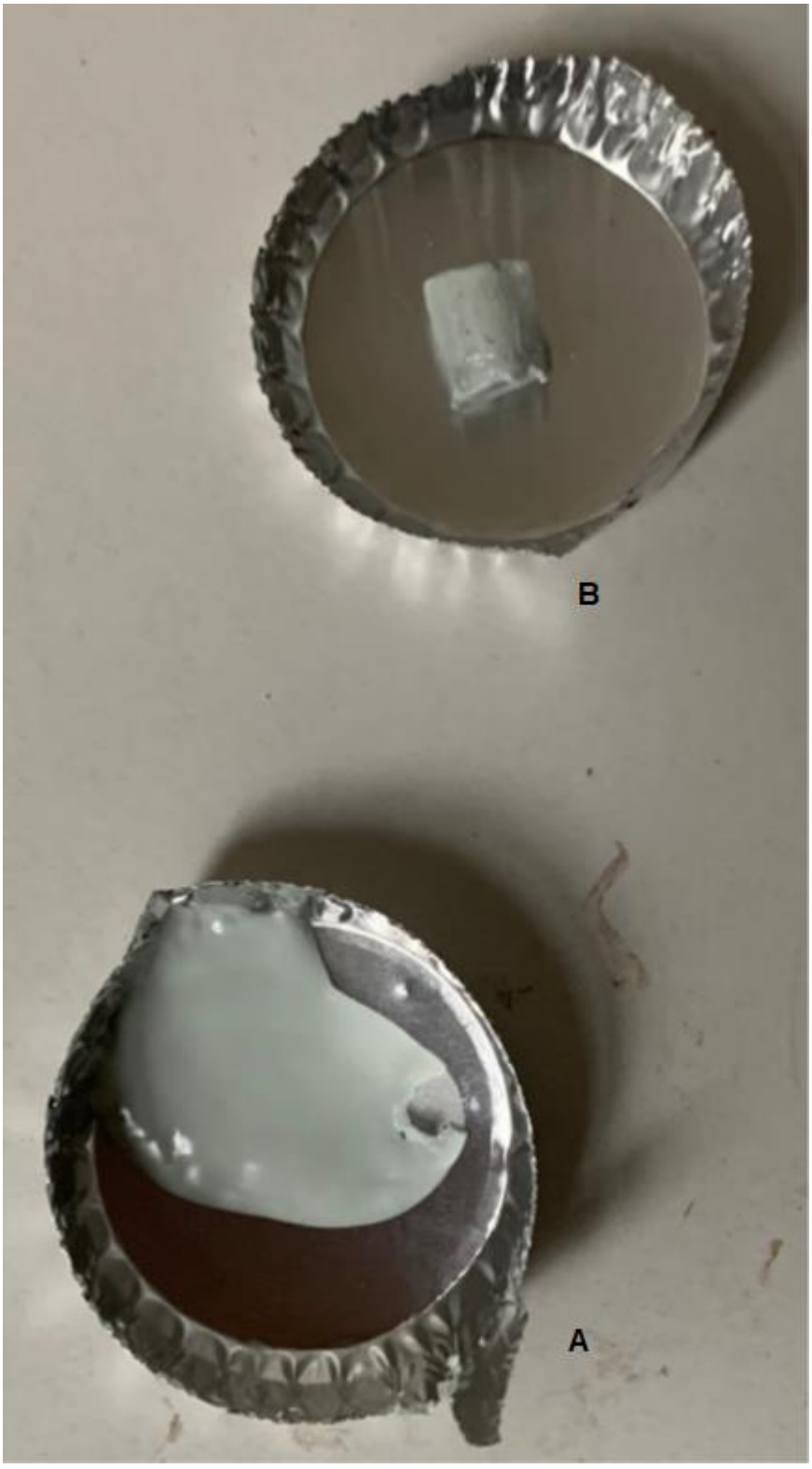

Figure 100. Extrusion test (9.6 gr c3s 5.4 gr 2M GA L/D 10 1mm nozzle speed 10 mm/min) as a result of extrusion product (A) and accumulated at the canal entrance (B).

Figure 101. The filament formed as a result of the extrusion test (9.6 gr c3s 1.2 gr quartz 1.2 gr marble powder 3gr 2.5 wt hec 3gr 2M GA L/D20 1mm 10 mm/min)

Figure 102. The filament formed as a result of the extrusion test (9.6 gr c3s 1.2 gr quartz 1.2 gr marble powder 3gr 2.5 wt hec 2gr 2M GA 1 gr peg 400 L/D 20 1mm 5 mm/min).

Figure 103. The filament formed as a result of the extrusion test (9.6 gr c3s 1.2 gr quartz 1.2 gr marble powder 3gr 2.5 wt hec 2gr 2M GA 1 gr peg 400 L/D 15 2mm nozzle 10 mm/min).

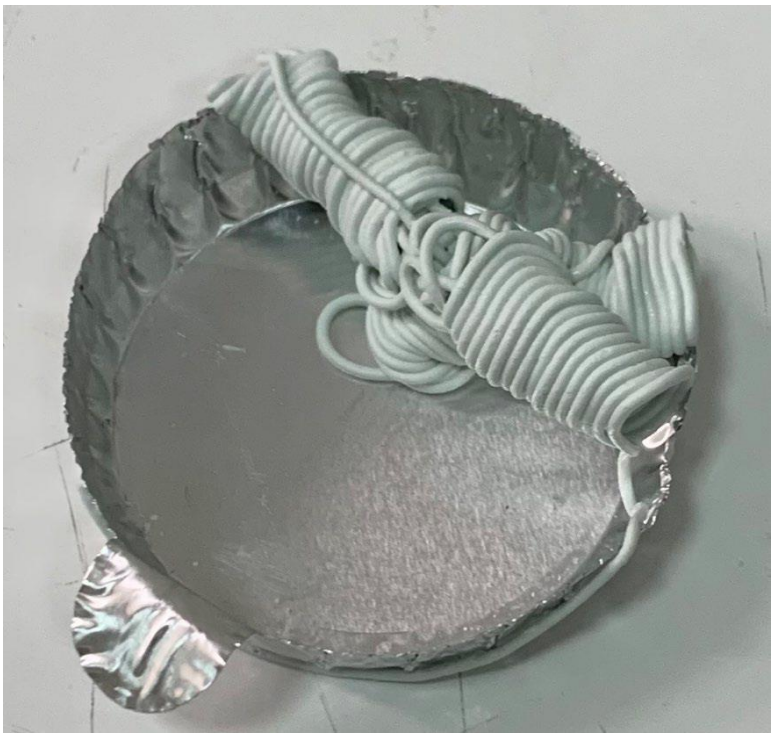

Figure 104. The filament formed as a result of the extrusion test (9.6 gr c3s 1.2 gr quartz 1.2 gr marble powder 3gr 2.5 wt hec 2gr 2M GA 1 gr peg 400 L/D 10 1mm 10 mm/min).

CHAPTER 5

CONCLUSIONS

Bone is a complex tissue composed mostly of hydroxyapatite, water, and organic components. In addition to their ability to heal themselves, they also have properties such as structural support and the ability to retain harmful chemicals. However, due to their inability to heal themselves in severe deformations, they are the world's second most transplanted tissue. Although there are different treatment methods, they have many disadvantages. Therefore, new studies have focused on 3D scaffolds.

The most suitable material for 3D scaffolds is ceramic, which has a composition similar to bone. However, there are rheological limits to the use of ceramics for 3D writing. Therefore, it is necessary to understand the hardening kinetics of cements and make them suitable for 3D printers.

In this study, C3A and C3S cements were produced, and their rheological properties were investigated with various additives using an oscillating rheometer and a capillary rheometer. The highest purity in C3A production was obtained by using Tekkim marble powder and boehmite. The optimum temperature was determined as 1300 °C for 2 hours. In C3S production, the highest purity was obtained with AFG Bio marble powder and fumed silica. The optimum temperature was found to be 1400 °C for 4 hours. In rheological studies, the hardening kinetics of different additives and cements were investigated. According to the oscillating rheometer results, MgSO4, HEC, PEG, and marble dust must be present in order for C3A cement to be suitable for 3D writing. MgSO4 slows down the setting kinetics of C3A, giving a wider time range for 3D writing. It was observed that HEC and PEG increased the strength. C3S suspensions reacted differently to HEC and PEG mixtures than C3A. Gluconic acid was used as a retarder. It has been observed that additive materials such as TSC and SDS should be included in order to keep the strength in the range of 100–1000 Pa, which is suitable for 3D writing. The injectability of the inks was observed with the capillary rheometer, giving similar results with the oscillating rheometer. The results obtained from the capillary rheometer are preliminary studies for future 3D printer studies.

REFERENCES

Balani, S. B.; Ghaffar, S. H.; Chougan, M.; Pei, E.; Şahin, E. Processes and Materials Used for Direct Writing Technologies: A Review. *Results in Engineering* **2021**, *11*, 100257. https://doi.org/10.1016/j.rineng.2021.100257.

Brydone, A. S.; Meek, D.; Maclaine, S. Bone Grafting, Orthopaedic Biomaterials, and the Clinical Need for Bone Engineering. *Proceedings of the Institution of Mechanical Engineers, Part H: Journal of Engineering in Medicine* **2010**, *224* (12), 1329–1343. https://doi.org/10.1243/09544119jeim770.

Dehghani, F.; Annabi, N. Engineering Porous Scaffolds Using Gas-Based Techniques. *Current Opinion in Biotechnology* **2011**, *22* (5), 661–666. https://doi.org/10.1016/j.copbio.2011.04.005.

Ding, S.-J.; Shie, M.-Y.; Wang, C.-Y. Novel Fast-Setting Calcium Silicate Bone Cements with High Bioactivity and Enhanced Osteogenesis in Vitro. *Journal of Materials Chemistry* **2009**, *19* (8), 1183. https://doi.org/10.1039/b819033j.

Huang, Y.; Han, S.; Pang, X.; Ding, Q.; Yan, Y. Electrodeposition of Porous Hydroxyapatite/Calcium Silicate Composite Coating on Titanium for Biomedical Applications. *Applied Surface Science* **2013**, *271*, 299–302. https://doi.org/10.1016/j.apsusc.2013.01.187.

Jamal, R.; Xu, F.; Shao, W.; Abdiryim, T. The Study on the Application of Solid-State Method for Synthesizing the Polyaniline/Noble Metal (Au or Pt) Hybrid Materials. *Nanoscale Research Letters* **2013**, *8* (1). https://doi.org/10.1186/1556-276x-8-117.

Kalfas, I. H. Principles of Bone Healing. *Neurosurgical Focus* **2001**, *10* (4), 1–4. https://doi.org/10.3171/foc.2001.10.4.2.

KARAGEORGIOU, V.; KAPLAN, D. Porosity of 3D Biomaterial Scaffolds and Osteogenesis. *Biomaterials* **2005**, *26* (27), 5474–5491. https://doi.org/10.1016/j.biomaterials.2005.02.002.

Kumar, A.; Kargozar, S.; Baino, F.; Han, S. S. Additive Manufacturing Methods for Producing Hydroxyapatite and Hydroxyapatite-Based Composite Scaffolds: A Review. *Frontiers in Materials* **2019**, *6*. https://doi.org/10.3389/fmats.2019.00313.

Li, W.; Ghazanfari, A.; Leu, M. C.; Landers, R. G. Extrusion-on-Demand Methods for High Solids Loading Ceramic Paste in Freeform Extrusion Fabrication. *Virtual and Physical Prototyping* **2017**, *12* (3), 193–205. https://doi.org/10.1080/17452759.2017.1312735.

Li, X.; Ouzia, A.; Scrivener, K. Laboratory Synthesis of C3S on the Kilogram Scale. *Cement and Concrete Research* **2018**, *108*, 201–207. https://doi.org/10.1016/j.cemconres.2018.03.019.

Liao, C.-J.; Chen, C.-F.; Chen, J.-H.; Chiang, S.-F.; Lin, Y.-J.; Chang, K.-Y. Fabrication of Porous Biodegradable Polymer Scaffolds Using a Solvent Merging/Particulate Leaching Method. *Journal of Biomedical Materials Research* **2001**, *59* (4), 676–681. https://doi.org/10.1002/jbm.10030.

Liu, C.; Shao, H.; Chen, F.; Zheng, H. Rheological Properties of Concentrated Aqueous Injectable Calcium Phosphate Cement Slurry. *Biomaterials* **2006**, *27* (29), 5003–5013. https://doi.org/10.1016/j.biomaterials.2006.05.043.

Liu, X.; Ma, P. X. Polymeric Scaffolds for Bone Tissue Engineering. *Annals of Biomedical Engineering* **2004**, *32* (3), 477–486. https://doi.org/10.1023/b:abme.0000017544.36001.8e.

Mansoutre, S.; Colombet, P.; Van Damme, H. Water Retention and Granular Rheological Behavior of Fresh C3S Paste as a Function of concentration11This Paper Was Originally Submitted to Advanced Cement Based Materials. It Was Received at the Editorial Office of Cement and Concrete Research on 27 August 1998 and Accepted in Final Form on 28 May 1999. *Cement and Concrete Research* **1999**, *29* (9), 1441–1453. https://doi.org/10.1016/s0008-8846(99)00129-5.

Matsuno, T.; Hashimoto, Y.; Adachi, S.; Omata, K.; Yoshitaka, Y.; Ozeki, Y.; Umezu, Y.; Tabata, Y.; Nakamura, M.; Satoh, T. Preparation of Injectable 3D-Formed .BETA.-Tricalcium Phosphate Bead/Alginate Composite for Bone Tissue Engineering. *Dental Materials Journal* **2008**, *27* (6), 827–834. https://doi.org/10.4012/dmj.27.827.

Mohamed, B. M.; Sharp, J. H. Kinetics and Mechanism of Formation of Tricalcium Aluminate, Ca3Al2O6. *Thermochimica Acta* **2002**, *388* (1–2), 105–114. https://doi.org/10.1016/s0040-6031(02)00035-7.

Oh, S. H.; Finones, R.; Jin, S.; Choi, S. Y.; Kim, K. N. Influence of Tricalcium Aluminate Phase on In Vitro Biocompatibility and Bioactivity of Calcium Aluminate Bone Cement. *Journal of Materials Research* **2004**, *19* (4), 1062–1067. https://doi.org/10.1557/jmr.2004.0139.

Şahin, E.; Kalyon, D. M. The Rheological Behavior of a Fast-Setting Calcium Phosphate Bone Cement and Its Dependence on Deformation Conditions. *Journal of the Mechanical Behavior of Biomedical Materials* **2017**, *72*, 252–260. https://doi.org/10.1016/j.jmbbm.2017.05.017.

Staiger, M. P.; Pietak, A. M.; Huadmai, J.; Dias, G. Magnesium and Its Alloys as Orthopedic Biomaterials: A Review. *Biomaterials* **2006**, *27* (9), 1728–1734. https://doi.org/10.1016/j.biomaterials.2005.10.003.

Turnbull, G.; Clarke, J.; Picard, F.; Riches, P.; Jia, L.; Han, F.; Li, B.; Shu, W. 3D Bioactive Composite Scaffolds for Bone Tissue Engineering. *Bioactive Materials* **2018**, *3* (3), 278–314. https://doi.org/10.1016/j.bioactmat.2017.10.001.

Whang, K.; Thomas, C. H.; Healy, K. E.; Nuber, G. A Novel Method to Fabricate Bioabsorbable Scaffolds. *Polymer* **1995**, *36* (4), 837–842. https://doi.org/10.1016/0032-3861(95)93115-3.

Zhu, J.; Marchant, R. E. Design Properties of Hydrogel Tissue-Engineering Scaffolds. *Expert Review of Medical Devices* **2011**, *8* (5), 607–626. https://doi.org/10.1586/erd.11.27.